NCAR/TN-398 + STR
NCAR TECHNICAL NOTE

December 1994

A Description of the Fifth-Generation Penn State/NCAR Mesoscale Model (MM5)

Georg A. Grell[1]
Jimy Dudhia[2]
David R. Stauffer[3]

MESOSCALE AND MICROSCALE METEOROLOGY DIVISION

[2]NATIONAL CENTER FOR ATMOSPHERIC RESEARCH
BOULDER, COLORADO

[1]FORECAST SYSTEMS LABORATORY,
NATIONAL OCEANIC AND ATMOSPHERIC ADMINISTRATION
BOULDER, COLORADO

[3]DEPARTMENT OF METEOROLOGY,
THE PENNSYLVANIA STATE UNIVERSITY
UNIVERSITY PARK, PENNSYLVANIA

Table of Contents

PREFACE

This technical report describes the fifth generation Penn State/NCAR Mesoscale Model, or MM5. It is intended to provide scientific and technical documentation of the model for users. Source code documentation is available as a separate Technical Note (NCAR/TN-392) by Haagenson et al. (1994). Comments and suggestions for improvements or corrections, are welcome and should be sent to the authors.

ACKNOWLEDGMENTS

A large number of scientists, students, and sponsors, too numerous to mention, have made significant contributions towards developing and improving this model. We would like to thank everyone who directly implemented changes and corrections into the code, as well as everyone who helped to identify errors and problems.

We would also like to extend our gratitude to the two reviewers (Prof. Tom Warner, and Dr. Jian-Wen Bao), whose comments improved the manuscript significantly.

Computing for this model development was undertaken on the CRAY YMP at NCAR, which is supported by the National Science Foundation.

The writing of this technical document was in part supported by the Department of Energy through grant DEA105-90ER61070, and the California Air Resouces Board through subcontract AG/990-TS05-S02 from Alpine Geophysics.

1. Introduction

This technical report is a description of the fifth-generation Penn State/NCAR Mesoscale Model (MM5). It is based on the original version described by Anthes and Warner (1978). Although a few of the following details of this model are well represented in Anthes *et al.* (1987), extensive changes and increases in options have occurred. For completeness, those parts that have changed little or none will also be represented here. The document structure is as follows. In section 2 we will describe the governing equations, algorithms, and boundary conditions. This will include the finite difference algorithms and time splitting techniques of both the hydrostatic and the nonhydrostatic equations of motion (hydrostatic and nonhydrostatic solver). All subsequent sections will describe features common to both solvers. Section 3 will discuss the mesh-refinement scheme, section 4 the four-dimensional data-assimilation technique, and section 5 will focus on the various physics options.

2. Governing equations and numerical algorithms

2.1 Hydrostatic model equations

The vertical σ-coordinate is defined in terms of pressure.

$$\sigma = \frac{p - p_t}{p_s - p_t},$$

where p_s and p_t are the surface and top pressures respectively of the model, where p_t is a constant.

The model equations are given by the following, where $p^* = p_s - p_t$.

Horizontal momentum;

$$\frac{\partial p^* u}{\partial t} = -m^2\left[\frac{\partial p^* uu/m}{\partial x} + \frac{\partial p^* vu/m}{\partial y}\right] - \frac{\partial p^* u\dot{\sigma}}{\partial \sigma}$$

$$- mp^*\left[\frac{\sigma}{\rho}\frac{\partial p^*}{\partial x} + \frac{\partial \phi}{\partial x}\right] + p^* fv + D_u \qquad (2.1.1)$$

$$\frac{\partial p^* v}{\partial t} = -m^2\left[\frac{\partial p^* uv/m}{\partial x} + \frac{\partial p^* vv/m}{\partial y}\right] - \frac{\partial p^* v\dot{\sigma}}{\partial \sigma}$$

$$- mp^*\left[\frac{\sigma}{\rho}\frac{\partial p^*}{\partial y} + \frac{\partial \phi}{\partial y}\right] - p^* fu + D_v \qquad (2.1.2)$$

Temperature;

$$\frac{\partial p^* T}{\partial t} = -m^2\left[\frac{\partial p^* uT/m}{\partial x} + \frac{\partial p^* vT/m}{\partial y}\right] - \frac{\partial p^* T\dot{\sigma}}{\partial \sigma}$$

$$+ p^*\frac{\omega}{\rho c_p} + p^*\frac{\dot{Q}}{c_p} + D_T, \tag{2.1.3}$$

where the D terms represent the vertical and horizontal diffusion terms and vertical mixing due to the planetary boundary layer turbulence or dry convective adjustment. The heat capacity for moist air at constant pressure is given by $c_p = c_{pd}(1 + 0.8q_v)$, where q_v is the mixing ratio for water vapor and c_{pd} is the heat capacity for dry air.

Surface pressure is computed from

$$\frac{\partial p^*}{\partial t} = -m^2\left[\frac{\partial p^* u/m}{\partial x} + \frac{\partial p^* v/m}{\partial y}\right] - \frac{\partial p^*\dot{\sigma}}{\partial \sigma}, \tag{2.1.4}$$

which is used in its vertically integrated form

$$\frac{\partial p^*}{\partial t} = -m^2\int_0^1\left[\frac{\partial p^* u/m}{\partial x} + \frac{\partial p^* v/m}{\partial y}\right]d\sigma. \tag{2.1.5}$$

Then the vertical velocity in σ-coordinates, $\dot{\sigma}$, is computed from (2.1.4) by vertical integration. Thus

$$\dot{\sigma} = -\frac{1}{p^*}\int_0^\sigma\left[\frac{\partial p^*}{\partial t} + m^2\left(\frac{\partial p^* u/m}{\partial x} + \frac{\partial p^* v/m}{\partial y}\right)\right]d\sigma', \tag{2.1.6}$$

where σ' is a dummy variable of integration and $\dot{\sigma}(\sigma = 0) = 0$.

In the thermodynamic equation, (2.1.3), $\omega = \frac{dp}{dt}$ and is calculated from

$$\omega = p^*\dot{\sigma} + \sigma\frac{dp^*}{dt}, \tag{2.1.7}$$

where

$$\frac{dp^*}{dt} = \frac{\partial p^*}{\partial t} + m\left[u\frac{\partial p^*}{\partial x} + v\frac{\partial p^*}{\partial y}\right]. \tag{2.1.8}$$

The hydrostatic equation is used to compute the geopotential heights from the virtual temperature, T_v:

$$\frac{\partial \phi}{\partial ln(\sigma + p_t/p^*)} = -RT_v\left[1 + \frac{q_c + q_r}{1 + q_v}\right]^{-1}, \tag{2.1.9}$$

where T_v is given by $T_v = T(1 + 0.608q_v)$, and q_c and q_r are the mixing ratios of cloud water and rain water.

2.2 Nonhydrostatic model equations

For the nonhydrostatic model we define a constant reference state and perturbations from it, as follows:

$$p(x,y,z,t) = p_0(z) + p'(x,y,z,t),$$

$$T(x,y,z,t) = T_0(z) + T'(x,y,z,t),$$

$$\rho(x,y,z,t) = \rho_0(z) + \rho'(x,y,z,t).$$

Typically the temperature profile for the reference state may be an analytic function that fits the mean tropospheric temperature profile.

The vertical σ-coordinate is then defined entirely from the reference pressure.

$$\sigma = \frac{p_0 - p_t}{p_s - p_t},$$

where p_s and p_t are the surface and top pressures respectively of the reference state and are independent of time. The total pressure at a grid point is therefore given by

$$p = p^*\sigma + p_t + p',$$

where $p^*(x,y) = p_s(x,y) - p_t$. The three-dimensional pressure perturbation, p', is a predicted quantity.

The model equations (Dudhia 1993) are then given by the following:
Horizontal momentum;

$$\frac{\partial p^* u}{\partial t} = -m^2\left[\frac{\partial p^* uu/m}{\partial x} + \frac{\partial p^* vu/m}{\partial y}\right] - \frac{\partial p^* u\dot{\sigma}}{\partial \sigma} + uDIV$$
$$- \frac{mp^*}{\rho}\left[\frac{\partial p'}{\partial x} - \frac{\sigma}{p^*}\frac{\partial p^*}{\partial x}\frac{\partial p'}{\partial \sigma}\right] + p^* fv + D_u \qquad (2.2.1)$$

$$\frac{\partial p^* v}{\partial t} = -m^2\left[\frac{\partial p^* uv/m}{\partial x} + \frac{\partial p^* vv/m}{\partial y}\right] - \frac{\partial p^* v\dot{\sigma}}{\partial \sigma} + vDIV$$
$$- \frac{mp^*}{\rho}\left[\frac{\partial p'}{\partial y} - \frac{\sigma}{p^*}\frac{\partial p^*}{\partial y}\frac{\partial p'}{\partial \sigma}\right] - p^* fu + D_v \qquad (2.2.2)$$

Vertical momentum;

$$\frac{\partial p^* w}{\partial t} = -m^2\left[\frac{\partial p^* uw/m}{\partial x} + \frac{\partial p^* vw/m}{\partial y}\right] - \frac{\partial p^* w\dot{\sigma}}{\partial \sigma} + wDIV$$

$$+ p^* g\frac{\rho_0}{\rho}\left[\frac{1}{p^*}\frac{\partial p'}{\partial \sigma} + \frac{T_v'}{T} - \frac{T_0 p'}{T p_0}\right] - p^* g\left[(q_c + q_r)\right] + D_w \qquad (2.2.3)$$

Pressure;

$$\frac{\partial p^* p'}{\partial t} = -m^2\left[\frac{\partial p^* up'/m}{\partial x} + \frac{\partial p^* vp'/m}{\partial y}\right] - \frac{\partial p^* p'\dot{\sigma}}{\partial \sigma} + p'DIV$$

$$- m^2 p^* \gamma p\left[\frac{\partial u/m}{\partial x} - \frac{\sigma}{mp^*}\frac{\partial p^*}{\partial x}\frac{\partial u}{\partial \sigma} + \frac{\partial v/m}{\partial y} - \frac{\sigma}{mp^*}\frac{\partial p^*}{\partial y}\frac{\partial v}{\partial \sigma}\right]$$

$$+ \rho_0 g\gamma p\frac{\partial w}{\partial \sigma} + p^*\rho_0 g w \qquad (2.2.4)$$

Temperature;

$$\frac{\partial p^* T}{\partial t} = -m^2\left[\frac{\partial p^* uT/m}{\partial x} + \frac{\partial p^* vT/m}{\partial y}\right] - \frac{\partial p^* T\dot{\sigma}}{\partial \sigma} + T\,DIV$$

$$+ \frac{1}{\rho c_p}\left[p^*\frac{Dp'}{Dt} - \rho_0 g p^* w - D_{p'}\right] + p^*\frac{\dot{Q}}{c_p} + D_T, \qquad (2.2.5)$$

where

$$DIV = m^2\left[\frac{\partial p^* u/m}{\partial x} + \frac{\partial p^* v/m}{\partial y}\right] + \frac{\partial p^*\dot{\sigma}}{\partial \sigma}, \qquad (2.2.6)$$

and

$$\dot{\sigma} = -\frac{\rho_0 g}{p^*}w - \frac{m\sigma}{p^*}\frac{\partial p^*}{\partial x}u - \frac{m\sigma}{p^*}\frac{\partial p^*}{\partial y}v. \qquad (2.2.7)$$

The DIV terms are not in the hydrostatic equations and arise because p^* is now constant in time. Thus the hydrostatic continuity equation no longer applies, leaving the right hand side terms in (2.2.6) uncancelled by the surface pressure tendency. The equations are thus in advective form.

Equation (2.2.4) can be derived from the fully compressible mass continuity relation and the perfect gas law. The only term neglected in equations (2.2.1)-(2.2.5) is a diabatic term contributing to the perturbation pressure tendency in (2.2.4). This term is negligible in normal meteorological regimes since it only forces a small divergence (i.e. expansion) in regions of heating.

2.3 Nonhydrostatic Finite Difference Algorithms

The B-grid staggering of horizontal velocity variables with respect to the other fields is shown in Fig. 2.1. Vertical velocity is staggered vertically. Noting that the j index increments in the x direction, and i in the y direction, the conventional notation will be as follows.

$$a_x = (a_{i,j+\frac{1}{2}} - a_{i,j-\frac{1}{2}})/\Delta x. \tag{2.3.1}$$

$$\overline{a}^x = \frac{1}{2}(a_{i,j+\frac{1}{2}} + a_{i,j-\frac{1}{2}}), \tag{2.3.2a}$$

Multiple averaging terms such as $\overline{a}^{xyy}$ can also be defined as successive averages where the order of superscripts does not matter, e.g.,

$$\overline{a}^{xyy} = \overline{\overline{a}^{x}}^{yy}.$$

Averaging vertically allows for non-uniform grid-lengths and nonlinearly varying fields, such as temperature and water vapor, by suitably weighting the values.

Thus for half-level fields averaged to full levels

$$\overline{a}^{\sigma} = \frac{a_{k+\frac{1}{2}}(\sigma_k - \sigma_{k-\frac{1}{2}}) + a_{k-\frac{1}{2}}(\sigma_{k+\frac{1}{2}} - \sigma_k)}{(\sigma_{k+\frac{1}{2}} - \sigma_{k-\frac{1}{2}})}, \tag{2.3.2b}$$

while averaging full-level fields to half levels uses an equation similar to (2.3.2a). For temperature, a is the potential temperature, and for water vapor, a is log q_v.

The spatial differencing of the terms in the horizontal momentum prediction equations is [including the map-scale factor $m(x,y)$],

$$\frac{\partial p_d^* u}{\partial t} = -m^2\left[\left(\overline{u}^x \overline{\frac{p_d^* u}{m}}^{xyy}\right)_x + \left(\overline{u}^y \overline{\frac{p_d^* v}{m}}^{xyx}\right)_y\right] - (\overline{p_d^* u}^{\sigma}\overline{\dot{\sigma}}^{xy})_{\sigma}$$

$$+ u\overline{DIV}^{xy} - \frac{m p_d^*}{\overline{\rho}^{xy}}\left[\overline{p_x'}^{y} - \overline{(\sigma p^*)_x}^{y}\overline{\frac{p_\sigma'}{p^*}}^{xy\sigma}\right]$$

$$+ p_d^* f v + D(p_d^* u), \tag{2.3.3}$$

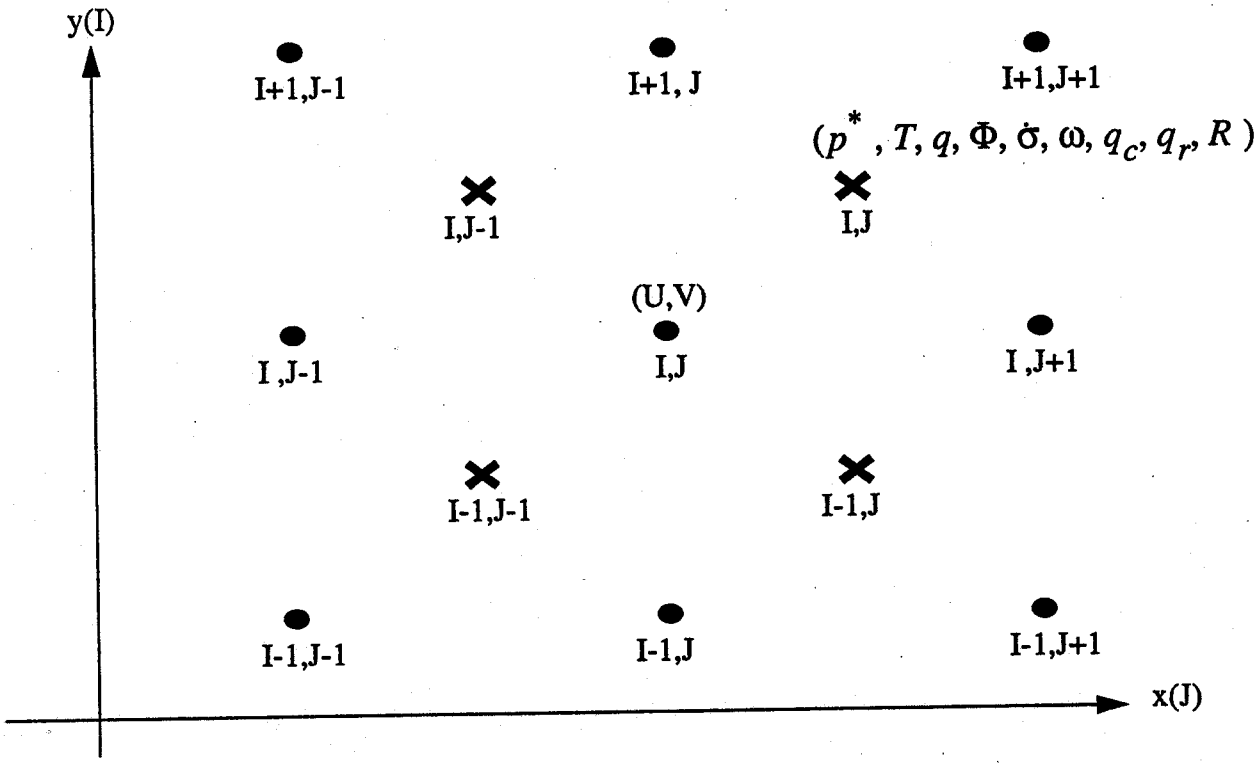

Fig. 2.1 Horizontal grid structure in the model.

$$\frac{\partial p_d^* v}{\partial t} = -m^2\left[\left(\overline{v}^x\overline{\frac{p_d^* u}{m}}^{xyy}\right)_x + \left(\overline{v}^y\overline{\frac{p_d^* v}{m}}^{xyx}\right)_y\right] - (\overline{p_d^* v}^{\sigma}\overline{\dot{\sigma}}^{xy})_\sigma$$
$$+ v\overline{DIV}^{xy} - \frac{mp_d^*}{\overline{\rho}^{xy}}\left[\overline{p_y'}^x - \overline{(\sigma p^*)_y}^x\overline{\frac{p_\sigma'}{p^*}}^{xy\sigma}\right]$$
$$- p_d^* f u + D(p_d^* v), \tag{2.3.4}$$

where $p_d^* = \overline{p^*}^{xy}$, and DIV, the mass divergence term, is given by

$$DIV = m^2\left[\left(\overline{\frac{p_d^* u}{m}}^{y}\right)_x + \left(\overline{\frac{p_d^* v}{m}}^{x}\right)_y\right] + p^*\dot{\sigma}_\sigma. \tag{2.3.5}$$

The triple averaging in the horizontal momentum advection terms follows that of the hydrostatic model as discussed by Anthes (1972). The subgrid-scale and diffusion operators are represented by $D(a) = K_h\Delta x^2(a_{xxxx} + a_{yyyy}) + (K_v a_z)_z +$ (PBL tendencies), where the fourth-order scheme is modified to second-order near the boundaries.

The coordinate vertical velocity, $\dot{\sigma}$, is obtained from

$$\dot{\sigma} = -\frac{\overline{\rho_0}^{\sigma} g}{p^*} w - \frac{m\sigma}{p^*}\overline{p^*}_x^x\overline{u}^{xy\sigma} - \frac{m\sigma}{p^*}\overline{p^*}_y^y\overline{v}^{xy\sigma}, \tag{2.3.6}$$

and the vertical momentum equation is

$$\frac{\partial p^* w}{\partial t} = -m^2\left[\left(\overline{w}^x\overline{\frac{p^* u}{m}}^{y\sigma}\right)_x + \left(\overline{w}^y\overline{\frac{p^* v}{m}}^{x\sigma}\right)_y\right] - (\overline{p^* w}^{\sigma}\overline{\dot{\sigma}}^{\sigma})_\sigma$$
$$+ w\overline{DIV}^{\sigma} + p^* g\overline{\frac{\rho_0}{\rho}}^{\sigma}\left[\frac{1}{p^*}p_\sigma' - \frac{1}{\gamma}\overline{\frac{p'T_0}{p_0 T}}^{\sigma}\right]$$
$$+ p^* g\overline{\frac{\rho_0}{\rho}}^{\sigma}\left[\overline{\frac{T_v'}{T}}^{\sigma} - \frac{R}{c_p}\overline{\frac{p'T_0}{p_0 T}}^{\sigma}\right] - p^* g\overline{(q_c + q_r)}^{\sigma} + D(p^* w). \tag{2.3.7}$$

The pressure tendency equation, neglecting diabatic terms, is given by

$$\frac{\partial p^* p'}{\partial t} = -m^2\left[\left(\overline{p'}^x\overline{\frac{p^* u}{m}}^{y}\right)_x + \left(\overline{p'}^y\overline{\frac{p^* v}{m}}^{x}\right)_y\right] - (\overline{p^* p'}^{\sigma}\dot{\sigma})_\sigma$$
$$+ p' DIV + p^*\rho_0 g\overline{w}^{\sigma} - m^2 p^*\gamma p\left[\left(\overline{\frac{u}{m}}^{y}\right)_x - (\sigma\overline{p^*}^x)_x\frac{1}{mp^*}\overline{u_\sigma}^{xy\sigma}\right.$$

$$+ \left(\frac{\overline{v}^{x}}{m}\right)_{y} - (\sigma\overline{p^*}^{y})_{y}\frac{1}{mp^*}\overline{v_\sigma}^{xy\sigma} - \frac{\rho_0 g}{m^2 p^*}w_\sigma\Bigg], \tag{2.3.8}$$

and temperature tendency is differenced as

$$\frac{\partial p^* T}{\partial t} = -m^2\left[\left(\overline{T}^{x}\frac{\overline{p^*u}^{y}}{m}\right)_{x} + \left(\overline{T}^{y}\frac{\overline{p^*v}^{x}}{m}\right)_{y}\right] - (\overline{p^*T}^{\sigma}\dot{\sigma})_\sigma$$

$$+ T\,DIV + \frac{1}{\rho c_p}\left[p^*\frac{Dp'}{Dt} - \rho_0 g\overline{p^*w}^{\sigma} - D(p^*p')\right]$$

$$+ p^*\frac{\dot{Q}}{c_p} + D(p^*T), \tag{2.3.9}$$

where Dp'/Dt is differenced like the corresponding terms in (2.3.8). Moisture variables have similar advection forms to those in (2.3.8) and (2.3.9) except when using the upstream option where $\overline{q}^{x}$ is replaced by the upstream value alone.

2.4 Hydrostatic Finite Difference Algorithms

The hydrostatic finite differencing of advection, Coriolis and heating follows (2.3.3), (2.3.4) and (2.3.9) without the *DIV* terms. The pressure gradient terms in (2.3.3) become

$$PG = -mp_d^*\overline{\phi_x}^y - \frac{mR\overline{T_v}^{xy}}{(1 + p_t/p_d^*)}\overline{p_x^*}^y, \tag{2.4.1}$$

and likewise for the y-gradient in (2.3.4). The surface pressure tendency is found from the integration over all ($KMAX$) layers of thickness $\delta\sigma(k)$,

$$\frac{\partial p^*}{\partial t} = -m^2 \sum_{k=1}^{KMAX} \left[\left(\frac{\overline{p_d^* u}^y}{m} \right)_x + \left(\frac{\overline{p_d^* v}^x}{m} \right)_y \right] \delta\sigma(k). \tag{2.4.2}$$

Then $\dot{\sigma}$ is found from downward integration,

$$\dot{\sigma}(k+1) = \dot{\sigma}(k) - \frac{\partial p^*}{\partial t}\frac{\delta\sigma(k)}{p^*} - m^2 \left[\left(\frac{\overline{p_d^* u}^y}{m} \right)_x + \left(\frac{\overline{p_d^* v}^x}{m} \right)_y \right] \frac{\delta\sigma(k)}{p^*}, \tag{2.4.3}$$

using the upper boundary condition that $\dot{\sigma}(k = 1) = 0$. The adiabatic term in (2.3.9), represented by the second set of terms in square brackets, becomes $p^*\omega$ in the hydrostatic model, where ω is defined by

$$\omega = \frac{dp}{dt} = p^*\overline{\dot{\sigma}}^\sigma + \sigma\left(\frac{\partial p^*}{\partial t} + m\overline{u}^{xy}\overline{p_x^*}^x + m\overline{v}^{xy}\overline{p_y^*}^y \right). \tag{2.4.4}$$

The integration of the hydrostatic equation to obtain geopotential height, ϕ, in the hydrostatic model is done as follows.

$$\delta\phi = -R\overline{T_v L}^\sigma \delta ln(\sigma + p_t/p^*), \tag{2.4.5}$$

where

$$L = \left[1 + \frac{q_c + q_r}{1 + q_v} \right]^{-1},$$

and allows for water loading when the explicit moisture scheme is used. Because ϕ is required on the velocity levels (half-levels), it has to be integrated first between the surface, where $\sigma = 1$ and $\phi = gh$ (h is the terrain height above sea-level), and the lowest half-level using (2.4.5) with just the lowest-level values T_v, q_v, q_c, q_r. At all other levels (2.4.5) uses vertical averaging between two levels.

The temporal differencing in the hydrostatic and nonhydrostatic models consists of leapfrog steps with an Asselin filter. With this time filter, splitting of the solution often associated with the leapfrog scheme is avoided. It is applied to all variables as

$$\hat{\alpha}^t = (1 - 2\nu)\alpha^t + \nu(\alpha^{t+1} + \hat{\alpha}^{t-1}), \tag{2.4.6}$$

where $\hat{\alpha}$ is the filtered variable. The coefficient ν in the model is 0.1 for all variables. For stability, diffusion terms are evaluated on the variables at time $t-1$, as are the terms associated with the moist physical processes.

2.5 Time splitting

In both the nonhydrostatic as well as the hydrostatic numerics, a time splitting scheme is applied to increase efficiency. Because the nonhydrostatic equations above are fully compressible, they permit sound waves. These are fast and require a short time step for numerical stability. For the hydrostatic equations, fast moving external gravity waves are the limiting factor. The techniques described next are designed to split these fast moving waves from the rest of the solution.

2.5.1 The nonhydrostatic semi-implicit scheme

For the nonhydrostatic equations it is possible to separate terms directly involved with acoustic waves from comparatively slowly varying terms, and to handle the former with shorter time steps while updating the slow terms less frequently. The reduced equation set for the short time step makes the model more efficient. The separated equations only contain interactions between momentum and pressure and can be written as:

Horizontal momentum;

$$\frac{\partial u}{\partial t} + \frac{m}{\rho}\left[\frac{\partial p'}{\partial x} - \frac{\sigma}{p^*}\frac{\partial p^*}{\partial x}\frac{\partial p'}{\partial \sigma}\right] = S_u \tag{2.5.1.1}$$

$$\frac{\partial v}{\partial t} + \frac{m}{\rho}\left[\frac{\partial p'}{\partial y} - \frac{\sigma}{p^*}\frac{\partial p^*}{\partial y}\frac{\partial p'}{\partial \sigma}\right] = S_v \tag{2.5.1.2}$$

Vertical momentum;

$$\frac{\partial w}{\partial t} - \frac{\rho_0}{\rho}\frac{g}{p^*}\frac{\partial p'}{\partial \sigma} + \frac{g}{\gamma}\frac{p'}{p} = S_w \tag{2.5.1.3}$$

Pressure;

$$\frac{\partial p'}{\partial t} + m^2\gamma p\left[\frac{\partial u/m}{\partial x} - \frac{\sigma}{mp^*}\frac{\partial p^*}{\partial x}\frac{\partial u}{\partial \sigma} + \frac{\partial v/m}{\partial y} - \frac{\sigma}{mp^*}\frac{\partial p^*}{\partial y}\frac{\partial v}{\partial \sigma}\right]$$

$$-\frac{\rho_0 g\gamma p}{p^*}\frac{\partial w}{\partial \sigma} - \rho_0 g w = S_{p'}, \qquad (2.5.1.4)$$

where the S terms contain advection, diffusion, buoyancy and Coriolis tendencies. These are kept constant during the sub-steps. Note that only part of the p'/p term is in (2.5.1.3), where the rest has been absorbed in the buoyancy term that contributes to S_w.

The method of solution follows the semi-implicit scheme of Klemp and Wilhelmson (1978) for the short time step. Starting with u, v, w, p' known at time τ, first the two horizontal momentum equations are stepped forward to give $u^{\tau+1}$ and $v^{\tau+1}$ which are then used in the pressure equation, giving a time-centered explicit treatment of horizontally propagating sound waves. Vertical propagation of sound waves is treated implicitly by making $w^{\tau+1}$ and $p'^{\tau+1}$ depend upon time-averaged values of p' and w respectively in (2.5.1.3) and (2.5.1.4). For instance, where p' appears in (2.5.1.3) it is represented by

$$\overline{p'}^{\beta} = \frac{1}{2}(1 + \beta)p'^{\tau+1} + \frac{1}{2}(1 - \beta)p'^{\tau},$$

and similarly for w in (2.5.1.4). The parameter β determines the time-weighting, where zero gives a time-centered average and positive values give a bias towards the future time step that can be used for acoustic damping. In practice, values of $\beta = 0.2 - 0.4$ are used.

With second-order vertical spatial derivatives the finite difference forms of equations (2.5.1.3) and (2.5.1.4) can be combined, eliminating $p'^{\tau+1}$, into a finite difference equation for $w^{\tau+1}$, which is solvable by direct recursion on a tri-diagonal matrix.

The implicit vertical differencing scheme allows the short time step to be independent of the vertical resolution of the model, which is important for efficiency, and thus the step only depends upon the horizontal grid length. Additionally, the divergence damping technique of Skamarock and Klemp (1992) is used to control horizontally propagating sound waves. This method is similar to using time-extrapolated pressure terms in (2.5.1.1) and (2.5.1.2), where in practice the extrapolation is about 0.1 $\Delta\tau$.

Temperature and moisture are predicted using the normal leapfrog step, Δt, because they have no high-frequency terms contributing to acoustic waves. The slow terms for momentum and pressure contained in the S-terms above are also evaluated on these leapfrog steps, but for these variables the march from $t - \Delta t$ to $t + \Delta t$ is split into typically four steps of length $\Delta\tau$ during which momentum and pressure are continually updated.

2.5.2 The hydrostatic split-explicit scheme

When numerically solving the hydrostatic equations of motion, the stability criterion is severely limited by external gravity waves. These are very fast moving gravity waves that are small in amplitude (quasi-linear) and contain only a small fraction of the total energy. Hence they change slowly over the time scale of the Rossby waves. Because of this, splitting methods have been developed to split these fast waves from the solution (similar also to the above method for the nonhydrostatic equations to split sound-waves). From all the existing different options, we have chosen a method developed by Madala (1981). This scheme separates the terms governing the gravity modes from those governing the Rossby modes. The term "split" here refers to the separation of the motion in terms of eigenmodes. Similar to the nonhydrostatic method, the equations are rewritten in finite difference form as

$$\frac{\partial P_s u}{\partial t} + \delta_x \Phi = A_u, \tag{2.5.2.1}$$

$$\frac{\partial P_s v}{\partial t} + \delta_y \Phi = A_v, \tag{2.5.2.2}$$

$$\frac{\partial P_s T}{\partial t} + M_2 \cdot D = A_T, \tag{2.5.2.3}$$

$$\frac{\partial P_s}{\partial t} + N_1 \cdot D = 0, and \tag{2.5.2.4}$$

$$\Phi = M_1 \cdot T. \tag{2.5.2.5}$$

where the right hand sides change slowly over the time scale of the Rossby-waves. Matrices M_1, M_2, and vector N_1 are independent of x, y, and t. Notice the similarity to the nonhydrostatic splitting method (equations 2.5.1-2.5.4). However, rather then integrating the "fast" terms on a small time-step directly, the method described below only computes correction terms to the equations, making this process extremely efficient. To illustrate this, we follow Madala (1981). From the governing equations he derives equations for the mass divergence D and the generalized geopotential Φ. They are

$$\frac{\partial D}{\partial t} + [\delta_x^2 + \delta_y^2]\Phi = \delta_x A_u + \delta_y A_v \tag{2.5.2.6}$$

and

$$\frac{\partial \Phi}{\partial t} + M_3 \cdot D = M_1 \cdot A_T. \tag{2.5.2.7}$$

Integrating equations (2.5.2.1-2.5.2.3) from $t-\Delta t$ to $t+\Delta t$, where Δt is the time step of the slow Rossby modes, one gets

$$p_s u(t+\Delta t) - p_s u(t-\Delta t) + 2\Delta t \delta_x \tilde{\Phi} = 2\Delta t A_u(t), \tag{2.5.2.8}$$

$$p_s v(t+\Delta t) - p_s v(t-\Delta t) + 2\Delta t \delta_y \tilde{\Phi} = 2\Delta t A_v(t), \tag{2.5.2.9}$$

$$p_s T(t+\Delta t) - p_s T(t-\Delta t) + 2\Delta t M_2 \tilde{\Phi} = 2\Delta t A_T(t), \tag{2.5.2.10}$$

where the operator $\tilde{()}$ for the split-explicit scheme is defined as

$$\tilde{\beta} = \frac{\Delta\tau}{\Delta t}\sum_{n=1}^{m} \beta(t-\Delta t + n\Delta\tau),$$

where $m = \frac{\Delta\tau}{\Delta t}$. Denoting with superscript ex solutions computed using only the explicit time integration over $2\Delta t$, equations (2.5.2.8-2.5.2.10) can be written as

$$p_s u(t+\Delta t) + 2\Delta t \delta_x[\tilde{\Phi} - \Phi(t)] = p_s u^{ex}(t+\Delta t), \tag{2.5.2.11}$$

$$p_s v(t+\Delta t) + 2\Delta t \delta_x[\tilde{\Phi} - \Phi(t)] = p_s v^{ex}(t+\Delta t), \tag{2.5.2.12}$$

$$p_s T(t+\Delta t) + 2\Delta t M_2[\tilde{D} - D(t)] = p_s T^{ex}(t+\Delta t). \tag{2.5.2.13}$$

Here $\Phi(t)$ and $D(t)$ have been computed using the explicit time integration over $2\Delta t$. Similar, for the pressure tendency we can write

$$P_s(t+\Delta t) + 2\Delta t N_1 \cdot [\tilde{D} - D(t)] = P^{ex}(t+\Delta t). \tag{2.5.2.14}$$

To find equations for the correction terms on the left hand side of equations (2.5.2.11-2.5.2.13), the divergence and geopotential equations (2.5.2.6-2.5.2.7) are then solved over the the small time-steps using

$$\begin{aligned} &[D(t+(n+1)\Delta\tau) - D(t)] - [D(t+(n-1)\Delta\tau) - D(t)] \\ &+ 2\Delta\tau(\delta_x^2 + \delta_y^2)[\Phi(t+n\Delta\tau) - \Phi(t)] \\ &= \frac{1}{m^i}[D_{ex}(t+\Delta t) - D(t-\Delta t)] \end{aligned} \tag{2.5.2.15}$$

and

$$[\Phi(t+(n+1)\Delta\tau)-\Phi(t)]-[\Phi(t+(n-1)\Delta\tau)-\Phi(t)]$$
$$+2\Delta\tau M_3[D(t+n\Delta\tau)-D(t)] \quad . \qquad (2.5.2.16)$$
$$=\frac{1}{m^i}[\Phi_{ex}(t+\Delta t)-\Phi(t-\Delta t)]$$

The correction terms themselves are integrated in equations (2.5.2.15)and (2.5.2.16), and then added to equations (2.5.2.11-2.5.2.14).

$\Delta\tau$, the timestep of the fast modes, of course varies with the mode. For a clean separation of the modes, a vertical normal mode initialization developed and applied to the MM4/MM5 system by Errico (1986) is used at the beginning of the model run to calculate the vertical modes. In MM5, only the external and the fastest internal mode are being considered with different time steps. This allows the time-steps of the slow tendencies to be twice as large as they were with the previously used Brown-Campana (1978) algorithm, and they are comparable to the ones used in the nonhydrostatic numerics.

2.6 Lateral Boundary conditions for the coarsest mesh domain

2.6.1 Sponge Boundary Conditions

The sponge boundary condition is given by

$$\left(\frac{\partial \alpha}{\partial t}\right)_n = w(n)\left(\frac{\partial \alpha}{\partial t}\right)_{MC} + (1 - w(n))\left(\frac{\partial \alpha}{\partial t}\right)_{LS}, \tag{2.6.1}$$

where $n = 1, 2, 3, 4$ for cross-point variables, $n = 1, 2, 3, 4, 5$ for dot-point variables, α represents any variable, MC denotes the model calculated tendency, LS the large-scale tendency which is obtained either from observations or large-scale model simulations (one-way nesting), and n is the displacement in grid-points from the nearest boundary ($n = 1$ on the boundary). The weighting coefficients $w(n)$ for cross point variables (counting from the boundary points inward) are 0.0, 0.4, 0.7, and 0.9, while for dot-point variables they are equal to 0.0, 0.2, 0.55, 0.8, and 0.95. All other points in the coarse domain have $w(n) = 1$.

The above method cannot be used for the nonhydrostatic part of the model.

2.6.2 Nudging Boundary Conditions

The relaxation boundary condition involves "relaxing" or "nudging" the model-predicted variables toward a large-scale analysis. The method includes Newtonian and diffusion terms

$$\left(\frac{\partial \alpha}{\partial t}\right)_n = F(n)F_1(\alpha_{LS} - \alpha_{MC}) - F(n)F_2\Delta_2(\alpha_{LS} - \alpha_{MC}). \qquad n = 2, 3, 4 \tag{2.6.2}$$

F decreases linearly from the lateral boundary, such that

$$F(n) = \left(\frac{5 - n}{3}\right) \qquad n = 2, 3, 4, \tag{2.6.3}$$

$$F(n) = 0 \qquad n > 4, \tag{2.6.4},$$

where F_1 and F_2 are given by

$$F_1 = \frac{1}{10\Delta t} \tag{2.6.5}$$

and

$$F_2 = \frac{\Delta s^2}{50\Delta t}. \tag{2.6.6}$$

This method is also used for the nonhydrostatic part of the model to nudge the pressure perturbation to the observations or larger-scale model simulations. However, for

the nonhydrostatic solver the vertical velocity is not nudged. It can vary freely, except for the outermost rows and columns, where zero gradient conditions are specified. For the velocity components, the values at the inflow points are specified in a manner similar to the specification of temperature and pressure. The values at the outflow boundaries are obtained by extrapolation from the interior points. These boundary values are required only in the computation of the nonlinear horizontal momentum flux divergence terms; They are not required in the computation of the horizontal divergence.

2.6.3 Moisture variables

Cloud water, rain water, snow, and ice are considered zero on inflow and zero gradient on outflow. There is an option to specify the boundary values in the same way as for the other variables (e.g., these variables may be known in a one-way nesting application).

2.7 Upper radiative boundary condition

An option in the nonhydrostatic model is the upper radiative boundary condition. Klemp and Durran (1983) and Bougeault (1983) have developed an upper boundary condition that allows wave energy to pass through unreflected. It can be expressed for hydrostatic waves as

$$\hat{p} = \frac{\rho N}{K}\hat{w}, \tag{2.7.1}$$

where $\hat{p}$ and $\hat{w}$ are horizontal Fourier components of pressure and vertical velocity respectively, ρ and N are the density and buoyancy frequency near the model top, and K is the total horizontal wavenumber of the Fourier component. This expression should be enforced for all components if the energy transport is to be purely upward with no reflection.

The upper boundary condition is combined with the implicit pressure/vertical momentum calculation. Before either value at time $n+1$ is known, the values at the top model level (w_1 is staggered half a grid length above p_1) can be expressed as

$$p_1^{n+1} = b + aw_1^{n+1}, \tag{2.7.2}$$

where the coefficient $a(x,y,t)$ is dependent upon the thermodynamic structure and the bottom boundary condition on w in the model column. It varies within only 5 per cent of a constant value even with high terrain, and is also not strongly time-dependent. The

value of $b(x,y,t)$ depends on pressure and most of the pressure tendency terms, and both a and b are known at this stage. So transforming, assuming a varies little about a non-zero constant and taking a mean value $\overline{a}$

$$\hat{p} = \hat{b} + \overline{a}\hat{w}. \tag{2.7.3}$$

Combining (2.7.3) with the radiative condition (2.7.1) for wavenumber $K = 2\pi/\lambda$, taking $\overline{\rho N}$ at the top of the model, and eliminating $\hat{p}$, gives

$$\hat{w} = \frac{K\hat{b}}{\overline{\rho N} - \overline{a}K}. \tag{2.7.4}$$

Using a limited-area 2D cosine transform, the forward transform, multiplication and backward transform can be combined into a single operator on the b field to give w_1^{n+1}. Hence

$$w_{IJ} = \sum_{i=I-6}^{I+6} \sum_{j=J-6}^{J+6} \alpha_{ij} b_{ij}, \tag{2.7.5}$$

where we have localized the transform to 13×13 points, and array α can be precalculated and kept constant for the time integration. The elements of α are found from

$$\alpha_{ij} = \sum_{k=0}^{6} \sum_{l=0}^{6} \frac{\delta_i \delta_j \delta_k \delta_l}{36} \cos\frac{2\pi ki}{12} \cos\frac{2\pi lj}{12} f(K), \tag{2.7.6}$$

with $f(K) = \frac{K}{\overline{\rho N} - \overline{a}K}$ and $K = (\hat{k}^2 + \hat{l}^2)^{\frac{1}{2}}$. $\delta = 1$ except for limits of summations where $\delta = \frac{1}{2}$.

Following the suggestion of Klemp and Durran, the finite differencing of pressure gradients and divergences should be taken into account in defining the effective wavenumbers. For a B-grid staggering, the effective wavenumbers can be expressed in terms of the dimensionless wavenumbers, k and l, where

$$\hat{k} = \frac{2}{\Delta x} \sin\frac{k\pi}{12} \cos\frac{l\pi}{12}, \tag{2.7.7a}$$

$$\hat{l} = \frac{2}{\Delta x} \sin\frac{l\pi}{12} \cos\frac{k\pi}{12}, \tag{2.7.7b}$$

and Δx is the grid length.

The scheme is summarized as follows; by the precalculation of parameters $\overline{a}$ and $\overline{\rho N}$ for the model domain, use of (2.7.6) to precalculate coefficients α, then implementation of (2.7.5) during the simulation.

3. The Mesh refinement scheme

The 2-way interactive mesh refinement scheme is constructed to allow for an arbitrary number of overlapping and translating rectangular grids with an arbitrary number of refinement levels. The grids must be aligned with the model coordinates (no rotating meshes), and the mesh refinement ratio of the temporal and spatial grid increments is common for all meshes, and currently set to three. Vital parts of this refinement scheme are the interpolation routines (Smolarkiewicz and Grell, 1992), which are used upon initialization of new nests as well as for defining the boundaries of the fine meshes. If the user can supply his own analysis for the finer grids (or a finer grid), the interpolated fields can be overwritten. In the following section we describe the heart of the scheme, the monotone interpolation routines.

3.1 The monotone interpolation routines

The most vital element of any mesh refinement scheme is an accurate and efficient interpolation procedure. A complaint about traditional polynomial-fitting methods used for interpolating scalar fields defined on a discrete mesh is that they often lead to spurious numerical oscillations in regions of steep gradients of the interpolated variables. In order to suppress computational noise, which is characteristic of quadratic and higher-order interpolation schemes, one often implements a smoothing procedure or increased diffusion. These, however, introduce excessive numerical diffusion that smears out sharp features of interpolated fields. A more advanced approach invokes the so-called shape-preserving interpolation, which incorporates appropriate constraints on the derivative estimates used in the interpolation schemes (see Rasch and Williamson (1990) for a review). In MM5 we consider as an alternate approach a class of schemes derived from monotone advection algorithms (Smolarkiewicz and Grell, 1992). Smolarkiewicz and Grell (1992) show that the interpolation problem becomes identical to the advection problem, when the distance vector is replaced by the velocity vector (see also the end of this section). Here we will describe the implementation of the advection algorithm used in MM5. The interested reader is referred to Smolarkiewicz and Grell (1992) for a detailed derivation of the "advection-interpolation" equivalence.

Since shape preservation and monotonicity are important in the interpolation problem,

we chose the Flux Corrected Transport (FCT) scheme that uses the high-order accurate constant-grid-flux dissipative algorithms developed by Tremback *et al.* (1987). We will first describe, in abbreviated form, a general FCT algorithm, as used in MM5. Given the exactness of the alternate-direction representation of the interpolation algorithm, it is sufficient to consider only one-dimensional FCT schemes. Starting with the one-dimensional advection equation in flux-form

$$\frac{\partial \phi}{\partial t} = -\frac{\partial u\phi}{\partial x}, \tag{3.1.1}$$

where ϕ is a scalar variable advected with a flow field $u(x,t)$, an FCT advection scheme may be compactly written as

$$\phi_i^{n+1} = \Phi_i^{n+1} - (\tilde{A}_{i+1/2} - \tilde{A}_{i-1/2}), \tag{3.1.2}$$

where Φ denotes a low-order, monotone solution to (3.1.1), and $\tilde{A}$ is the antidiffusive flux, limited such as to ensure that the solution (3.1.2) is free of local extrema absent in the low-order solution. Note that

$$\tilde{A}_{i+1/2} = min\left(1, \beta_i^{\downarrow}, \beta_{i+1}^{\uparrow}\right)\left[A_{i+1/2}\right]^{+} + min\left(1, \beta_i^{\uparrow}, \beta_{i+1}^{\downarrow}\right)\left[A_{i+1/2}\right]^{-}, \tag{3.1.3}$$

where

$$A_{i+1/2} \equiv FH_{i+1/2} - FL_{i+1/2}, \tag{3.1.4}$$

with FH and FL denoting fluxes from a high-order and a low-order advection scheme, respectively. $[\ ]^{+} \equiv max(0,\ )$ and $[\ ]^{-} \equiv min(0,\ )$ are the positive- and the negative-part operators, respectively, and

$$\beta_i^{\uparrow} \equiv \frac{\phi_i^{MAX} - \Phi_i^{n+1}}{A_i^{IN} + \varepsilon}\ ;\ \ \beta_i^{\downarrow} \equiv \frac{\Phi_i^{n+1} - \phi_i^{MIN}}{A_i^{OUT} + \varepsilon}, \tag{3.1.5a,b}$$

where A_i^{IN}, A_i^{OUT} are the absolute values of the total incoming and outgoing A-fluxes, (3.1.4), from the i-th grid box, respectively. ε is a small value, e.g. $\sim 10^{-15}$, and allows for efficient coding of β-ratios when A_i^{IN} or A_i^{OUT} vanish. The limiters ϕ_i^{MAX} and ϕ_i^{MIN} define monotonicity of the scheme (i.e., by design $\phi_i^{MIN} \le \phi^{n+1} \le \phi_i^{MAX}$), and they are traditionally specified (Zalesak 1979) as

$$\phi_i^{MAX} = max\left(\phi_{i-1}^n, \phi_i^n, \phi_{i+1}^n, \Phi_{i-1}^{n+1}, \Phi_i^{n+1}, \Phi_{i-1}^{n+1}\right) \tag{3.1.6a}$$

$$\phi_i^{MIN} = min\left(\phi_{i-1}^n, \phi_i^n, \phi_{i+1}^n, \Phi_{i-1}^{n+1}, \Phi_i^{n+1}, \Phi_{i-1}^{n+1}\right). \qquad (3.1.6b)$$

A shape-preserving interpolation scheme requires less restrictive monotonicity constraints than a conservative advection scheme. The minima over β ratios appearing in (3.1.3) ensure that the antidiffusive flux attributed to the $i+1/2$ position on the grid does not contribute to the generation of spurious extrema, either in gridbox i or in gridbox $i+1$. However, monotonicity of the interpolation scheme only requires that $\phi_i^{n+1} = \psi(x_o)$ is free of spurious extrema. Consequently, equation (3.1.3) may be replaced by

$$\tilde{A}_{i+1/2} = min\left(1, \beta_i^{\downarrow}\right)\left[A_{i+1/2}\right]^+ + min\left(1, \beta_i^{\uparrow}\right)\left[A_{i+1/2}\right]^-. \qquad (3.1.3')$$

Furthermore, since the effective flow field is constant, and therefore incompressible, the limiters in (3.1.6) may be simplified to

$$\phi_i^{MAX} = max\left(\phi_{i-1}^n, \phi_i^n, \phi_{i+1}^n, \Phi_i^{n+1},\right) \; ; \; \phi_i^{MIN} = min\left(\phi_{i-1}^n, \phi_i^n, \phi_{i+1}^n, \Phi_i^{n+1}\right), \; (3.1.6'a,b)$$

where the redundant dependence of the limiters on Φ_i^{n+1} has been retained to ensure strictly nonnegative values of the β ratios in (3.1.5) (cf., Section 3.1 in Smolarkiewicz and Grabowski, 1990). Since the low-order solution may always be written as an old value, minus the divergence of fluxes from the low-order scheme, the entire algorithm consisting of (3.1.2), (3.1.3'), (3.1.4), (3.1.5), and (3.1.6') is in the form of a general advection scheme.

The advection schemes used to calculate the high- and low-order fluxes for the above equations are from Tremback *et al.* (1987). They derive as follows. Starting with the flux form of the one-dimensional advection equation (3.1.1) in finite difference form

$$\begin{aligned} \phi_i^{n+1} &= +\phi_i^n + \frac{\Delta t}{\Delta x}[F_{i+1/2} - F_{i-1/2}] \\ &= \phi_i^n + \frac{\Delta x}{\Delta t}\left[\sum_m b_m \phi_{i+1+m}^n - \sum_m b_m \phi_{i+m}^n\right], \end{aligned} \qquad (3.1.7)$$

where

$$F_{i+1/2} = \sum_m b_m \phi_{i+1+m}^n \qquad (3.1.8)$$

and

$$F_{i-1/2} = \sum_m b_m \phi_{i+m}^n \qquad (3.1.9)$$

were used. Following Tremback *et al.* (1987), the solutions for the even-order schemes which are used in the mesh refinement scheme are then given by

$$F_{i+1/2}\frac{\Delta t}{\Delta x} = +\frac{\alpha}{2}(-\phi_i - \phi_{i+1}) + \\ +\frac{\alpha^2}{2}2(-\phi_i + \phi_{i+1}) \tag{3.1.10}$$

for second order accuracy;

$$F_{i+1/2}\frac{\Delta t}{\Delta x} = +\frac{\alpha}{12}(\phi_{i-1} - 7\phi_i - 7\phi_{i+1} + \phi_{i+2}) \\ +\frac{\alpha^2}{24}(\phi_{i-1} - 15\phi_i + 15\phi_{i+1} - \phi_{i+2}) \\ +\frac{\alpha^3}{12}(-\phi_{i-1} + \phi_i + \phi_{i+1} - \phi_{i+2}) \\ +\frac{\alpha^4}{24}(-\phi_{i-1} + 3\phi_i - 3\phi_{i+1} + \phi_{i+2}) \tag{3.1.11}$$

and for fourth order accuracy;

$$F_{i+1/2}\frac{\Delta t}{\Delta x} = +\frac{\alpha}{60}(-\phi_{i-2} + 8\phi_{i-1} - 37\phi_i - 37\phi_{i+1} + 8\phi_{i+2} - \phi_{i+3}) \\ +\frac{\alpha^2}{360}(-2\phi_{i-2} + 25\phi_{i-1} - 245\phi_i + 245\phi_{i+1} - 25\phi_{i+2} + 2\phi_{i+3}) \\ +\frac{\alpha^3}{48}(\phi_{i-2} - 7\phi_{i-1} + 6\phi_i + 6\phi_{i+1} - 7\phi_{i+2} + \phi_{i+3}) \\ +\frac{\alpha^4}{144}(\phi_{i-2} - 11\phi_{i-1} + 28\phi_i - 28\phi_{i+1} + 11\phi_{i+2} - \phi_{i+3}) \\ +\frac{\alpha^5}{240}(-\phi_{i-2} + 3\phi_{i-1} - 2\phi_i - 2\phi_{i+1} + 3\phi_{i+2} - \phi_{i+3}) \\ +\frac{\alpha^6}{720}(-\phi_{i-2} + 5\phi_{i-1} - 10\phi_i + 10\phi_{i+1} - 5\phi_{i+2} + \phi_{i+3}) \tag{3.1.12}$$

for sixth order accuracy; α is defined as

$$\alpha = U\frac{\Delta t}{\Delta x}. \tag{3.1.13}$$

In MM5, equations (3.1.10 - 3.1.12) are used together with (3.1.1), (3.1.3′), (3.1.4), 3.1.5), and (3.1.6′) to solve the interpolation problem. Note that the velocity vector, is replaced by the distance vector, X_d, which, with a mesh-refinement ratio of three, simply becomes 1/3 or 2/3. For interpolating boundary conditions to the finer meshes, fourth order accuracy

is used, while for new nest initialization, sixth order accuracy is used. While the new nest initialization covers the whole domain, boundary interpolation is performed for the outermost 2 rows and columns of the nest. Two rows were necessary to ensure that the same operators were applied to each nested grid-point (including fourth-order diffusion).

3.2 Overlapping and moving grids

The mesh-refinement scheme allows for overlapping grids on the same nest-level. To ensure numerical stability, the solution in the overlap region has to be identical. To accomplish this, after each time-step of the grids in question, the boundary conditions in the overlap regions are provided by the overlapping mesh. It is very important that this procedure be performed at every timestep.

Nests can also be moved at any time in the forecast. This can be done many times, and for any distance (integer number of grid points). The user may also move the nests automatically if he supplies an algorithm to do so. Upon a move, a new nest initialization is performed first. Then all high-resolution information from the previous location of the mesh is used to overwrite the fields of the newly initialized mesh. Therefore, to ensure best use of high resolution information, it is better to move a nest more often and for a smaller distance.

3.3 The feedback to the coarser grids

Since the mesh refinement ratio in MM5 is set to three, a higher resolution mesh has to be integrated three times as often as its "Mother Domain"(MD), where MD means the coarser domain from which it gets its boundary conditions. To keep the solutions in a 2-way interaction from diverging, the meteorological fields have to be fed back from the higher-resolution mesh to its MD. This is done at the end of the three time-step integration. Naturally, when this is done without smoothing or averaging, the solution on the MD will appear somewhat noisy (diluted with small-scale information). To avoid numerical instability, the following methods are supported in MM5 to remove non-resolvable noise from the MD. Note that these smoothers are only applied over an interior area that is completely determined by the higher resolution domain. It is important that input into the nest, and feedback back to the MD does not overlap. The smoother that is used by

the MM5 system in various forms was defined by Shapiro (1970) as

$$\begin{aligned}\bar{\alpha}(i,j) =&\alpha(i,j)\\ &+\frac{\nu}{2}(1-\nu)(\alpha(i+1,j)+\alpha(i-1,j)+\alpha(i,j+1)+\alpha(i,j-1)+4\alpha(i,j))\\ &+\frac{\nu^2}{4}(\alpha(i+1,j+1)+\alpha(i+1,j-1)+\alpha(i-1,j+1)+\alpha(i-1,j-1)-4\alpha(i,j))\end{aligned} \tag{3.3.1}$$

3.3.1 A Nine-point averager

This method was in the original MM4 nested version (Zhang *et al.* 1986). It is a feedback method that averages information for a whole MD grid box (surrounding and centering on the nested grid point). However, it does not take out all non-resolvable information on the MD. It also imposes a severe restriction on the terrain for the hydrostatic model. In case of overlapping and moving nests on several nest levels, it is very elaborate and complicated to apply. It is still an option in the model, because it may be useful for simpler applications (like one coarse and one nested domain). However, care must be taken to create a terrain data set that is consistent with this method. The operator that is applied to the nested grid-points (note that nothing is done to the MD) is defined by using $\nu = 0.5$ in (3.3.1).

3.3.2 A Smoother-Desmoother

The smoother-desmoother is a filter that removes $2\Delta x$ waves and damps short waves, but leaves long waves almost unaffected. It is much more selective than diffusive smoothers. It is applied to the "coarser grid" only in the area where the coarse grid values are overwritten with the nested grid values.

A single pass of the smoother-desmoother involves two steps. Equation (3.3.1) is used first to smooth the fields, then to desmooth the fields. $\nu_1 = 0.50$ is used for the smoothing coefficient, and $\nu_2 = -0.52$ for the desmoothing coefficient. The first step strongly smoothes the field, completely removing the $2\Delta x$ wave, and the second step attempts to restore the other waves to their original amplitudes. There are two passes of the smoother-desmoother applied in the model.

4. Four Dimensional Data Assimilation (FDDA)

The concept of combining current and past data in an explicit dynamical model such that the model's prognostic equations provide time continuity and dynamic coupling among the various fields has become known as four-dimensional data assimilation (FDDA). Current interest in the use of FDDA in mesoscale models, for either model initialization (dynamic initialization) or for use of the model as an analysis/research tool (dynamic analysis), is a logical extension of the traditional link between objective analysis methods and dynamic relationships.

Currently, two major types of FDDA are used operationally and in research. The first is an intermittent process of initializing an explicit prediction model, using the subsequent forecast (typically 3-12 h) as a first guess in a static three-dimensional objective analysis step, and then repeating the process for another forecast cycle. The second is a continuous (every model time step) dynamical assimilation where forcing functions are added to the governing model equations to gradually "nudge" the model state toward the observations. This continuous nudging type of FDDA is used in the PSU/NCAR modeling system. Nudging was first developed and tested at Penn State by Kistler (1974), under Prof. J. Hovermale, and by Anthes (1974), and Hoke and Anthes (1976). See Stauffer and Seaman (1990) for an historical overview of the technique.

Nudging or Newtonian relaxation is a relatively simple but very flexible technique: the data used for nudging can be of any type, measured or derived, analyzed to a grid for assimilation into the model or inserted as individual observations. Gridded analyses of the observations that are assimilated can be obtained by successive correction, variational, or statistical optimal interpolation (OI) techniques, and the weights used when nudging to individual observations can be simple Cressman-type (distance-weighted) functions or more complicated statistical functions based on OI. It can be shown that successive corrections, OI, and variational approaches are all fundamentally related to the "idealized analysis" and thus to each other. In fact, nudging is basically a successive-correction technique which uses a numerical model to include the time dimension.

The method of Newtonian relaxation or nudging relaxes the model state toward the observed state by adding, to one or more of the prognostic equations, artificial

tendency terms based on the difference between the two states. The model solution can be nudged toward either gridded analyses or individual observations during a period of time surrounding the observations. These two techniques, hereafter referred to as "analysis nudging" and "obs nudging", respectively, can be used individually or simultaneously on any MM5 model grid. For guidance in selecting which nudging technique(s) to use for your particular application, as well as suggested parameter specifications, see Stauffer and Seaman (1990), Stauffer et al. (1991) and Stauffer and Seaman (1993).

4.1 Analysis Nudging

The analysis-nudging term for a given variable is proportional to the difference between the model simulation and an analysis of observations calculated at every grid point. The general form for the predictive equation of variable $\alpha(\mathbf{x},t)$ is written in flux form as

$$\frac{\partial p^*\alpha}{\partial t} = F(\alpha,\mathbf{x},t)+G_\alpha \cdot W_\alpha(\mathbf{x},t)\cdot\epsilon_\alpha(\mathbf{x})\cdot p^*(\hat{\alpha}_0-\alpha)+G_{p^*}\cdot W_{p^*}\cdot\epsilon_{p^*}(\mathbf{x})\cdot\alpha(\hat{p}_0^*-p^*) \quad (4.1.1)$$

All of the model's physical forcing terms (advection, Coriolis effects, etc.) are represented by F, where α are the model's dependent variables, $\mathbf{x}$ are the independent spatial variables, and t is time. The second and third terms on the right of (4.1.1) are similar in form and represent the nudging terms for α and p*, respectively. Due to the flux form of the predictive equation, the third term appears in (4.1.1) when nudging pressure in the continuity equation of the hydrostatic version of MM5. (Note that this term is zero in the nonhydrostatic version of MM5 because p^* is computed from the hydrostatic reference state and is constant in time.)

With $G_{p^*} = 0$, or in the nonhydrostatic version of MM5, (4.1.1) simplifies to

$$\frac{\partial p^*\alpha}{\partial t} = F(\alpha,\mathbf{x},t) + G_\alpha \cdot W_\alpha \cdot \epsilon_\alpha(\mathbf{x}) \cdot p^*(\hat{\alpha}_0 - \alpha) \quad (4.1.2)$$

The nudging factor G_α determines the magnitude of the term relative to all the other model processes in F. Its spatial and temporal variation is determined mostly by the four-dimensional weighting function, W, which specifies the horizontal, vertical and time weighting applied to the analysis, where $W = w_{xy}w_\sigma w_t$. The analysis quality factor, ϵ, which ranges between 0 and 1, is based on the quality and distribution of the data used to

produce the gridded analysis. The estimate of the observation for α analyzed to the grid is $\hat{\alpha}_0$.

The nudging factor G_α is defined based on scaling arguments. Because the nudging contribution is artificial, it must not be a dominant term in the governing equations and should be scaled by the slowest physical adjustment process in the model (inertial effects). Thus the G_α is usually defined to be similar in magnitude to the Coriolis parameter, and it must also satisfy the numerical stability criterion, $G_\alpha \leq \frac{1}{\Delta t}$. Typical values of G_α are $10^{-4}s^{-1}$ to $10^{-3}s^{-1}$ for meteorological systems, where values of $G_\alpha = 3 \times 10^{-4}s^{-1}$ to $6 \times 10^{-4}s^{-1}$ are usually "large enough". A value of G_α which is too large will force the model state too strongly toward the observations. This is undesirable because (a) the ability of the model equations to resolve mass-momentum imbalances will be decreased; and (b) the ability of the model to generate its own mesoscale meteorological structures (e.g. fronts, squall lines) will be impaired by heavy insertion of the observed analyses. Such problems arise because the analyses may not resolve these mesoscale structures or may be contaminated by observational and analysis errors. On the other hand, if G_α is too small, the observations will have minimal effect on the evolution of the model state, allowing phase and amplitude errors to grow.

For simplicity, if we drop the physical forcing terms F from (4.1.2), and assume $W(\mathrm{x},t) = 1$, $\frac{\partial p^*}{\partial t} = 0$ and the observational analysis is perfect and time invariant, then

$$\frac{\partial \alpha}{\partial t} = G_\alpha(\hat{\alpha}_0 - \alpha) \tag{4.1.3}$$

which has the solution

$$\alpha = \hat{\alpha}_0 + (\alpha_i - \hat{\alpha}_0)e^{-G_\alpha t} \tag{4.1.4}$$

where α_i is the initial value of α at the start of the nudging period. Therefore, the model state approaches the observed state exponentially with an e-folding time of $T_G = \frac{1}{G_\alpha}$, which is about 0.93 h for $G_\alpha = 3 \times 10^{-4}s^{-1}$. This implies that very high frequency fluctuations in the data, as might be available from wind profilers or Doppler radars (say, every 5 min), would not be retained well unless G_α were much greater; but then the nudging term may not be small compared to some terms of F.

Nudging the vorticity is a alternative method whereby the model's divergent wind is allowed to freely respond in the model's geostrophic adjustment process. Equation 4.1.3 can be modified for u and v such that

$$\frac{\partial u}{\partial t} = G_u \cdot \frac{\partial}{\partial y}(\hat{\zeta}_0 - \zeta) \tag{4.1.5}$$

$$\frac{\partial v}{\partial t} = G_v \cdot \frac{\partial}{\partial x}(\hat{\zeta}_0 - \zeta), \tag{4.1.6}$$

where ζ is the model vorticity and $\hat{\zeta}_0$ is the analyzed observed vorticity. Letting a constant $G = G_u = G_v$ and forming the vorticity equation from (4.1.5) and (4.1.6) we get

$$\frac{\partial \zeta}{\partial t} = G\nabla^2(\hat{\zeta}_0 - \zeta) \tag{4.1.7}$$

Therefore, the model vorticity is diffused toward the observed vorticity. However, the Laplacian in (4.1.7) introduces a scale dependence when nudging vorticity. The model vorticity will be diffused more strongly to small-scale features in the observed vorticity analysis. Thus, when nudging toward large-scale vorticity fields, small-scale features in the model vorticity will be selectively damped. After all factors are considered, it is generally advisable to nudge the u- and v-components of the winds directly whenever possible (see Stauffer and Seaman, 1990).

Although this analysis-nudging technique has been traditionally used to assimilate 3-D analyses based on rawinsonde observations, it can also be used to assimilate 2-D surface analyses within the model PBL (Stauffer et al., 1991).

While the twice daily rawinsonde observations are spaced at about 400 km and number approximately 100 over the U.S., the spatial distribution of the surface data, available at 3-h intervals from the NCAR data archives, is considerably more dense. Depending on the time of day, there are roughly 500- 1200 surface data sites with an average spacing of about 100 km. The greater horizontal and temporal resolution of conventional surface data is especially attractive for mesoscale data assimilation. The surface-level analyses are assimilated in the same manner as the 3-D analyses, except for the vertical extent of their influence. These surface analyses, which are assumed to be representative at 10 m above ground level (AGL), should represent only those scales resolved by the model grid onto

which they are assimilated. This is necessary to avoid difficulties related to the insertion of small-scale divergence patterns (near $2\Delta x$) which might interact adversely with the model's parameterizations (e.g., the moisture-convergence criterion used to determine the existence and intensity of Anthes-Kuo convection).

Effective assimilation of single-level data depends on the equivalent depth over which the data are inserted into the model. Beneficial effects on numerical forecasts can be achieved by distributing single-level data throughout several model layers. This approach requires that the data be applied in a consistent manner such that they are assured to be representative of those layers. For example, the homogenizing effect of vertical mixing during free convective conditions allows us to assume that surface-layer wind and mixing ratio (q) observations can be applied throughout the model PBL according to a conceptual model of boundary-layer structure. Such an idealized conceptual model is given by Garratt et al. (1982) and is based on typical moderate to large instabilities observed at Wangara and Minnesota (Fig. 4.1). However, in this same situation the frequent presence of a shallow superadiabatic layer near the surface makes surface temperature or potential temperature data poorly representative of the boundary layer as a whole, and similarity relationships describing the potential temperature profile become inaccurate. The same is true during nocturnal inversion conditions. These and other factors make assimilation of single-level surface temperature observations unattractive for defining the temperature of the mixed layer above the surface layer. For example, nudging towards an inaccurately diagnosed mixed-layer temperature can cause serious errors in the simulated PBL depth or even lead to a sudden spurious collapse of the unstable PBL structure. This can result from assimilating a surface temperature observation which is cooler than the model-simulated value by only a few tenths of one degree. In general, surface temperature data should not be directly assimilated into the model (see Stauffer et al., 1991).

Figure 4.1 shows the unstable lower troposphere comprised of three distinct layers: a surface layer extending to height h_s, a well-mixed layer from h_s to h_1 and a transition layer extending from h_1 to h_2. With the x-axis defined parallel to the mean wind, Fig. 4.1 suggests that the v component of the wind is zero and there is thus no directional shear through the lower two layers. The surface wind speed analysis, discussed above and

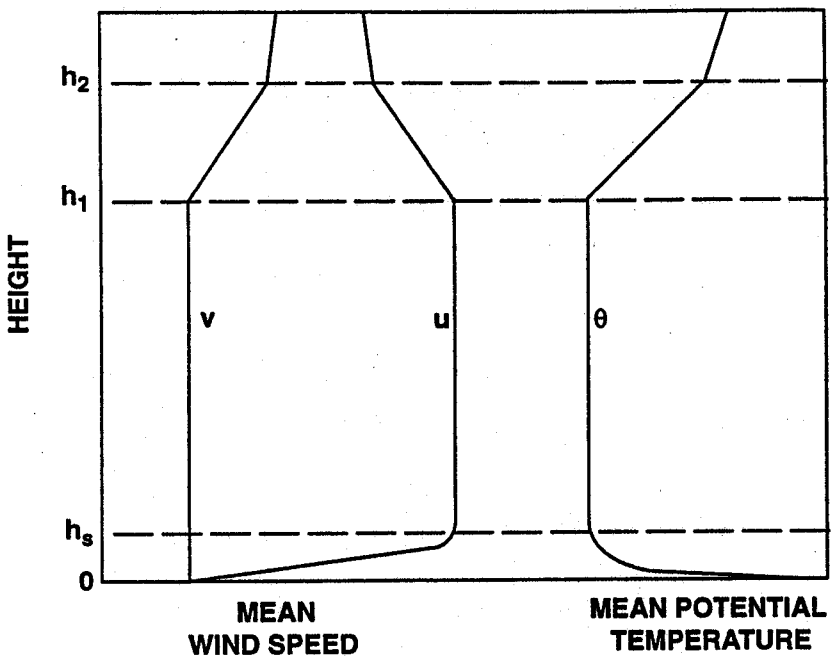

Figure 4.1: Schematic representation of mean wind speed and potential temperature profiles in an idealized conceptual model of the unstable atmospheric boundary layer.

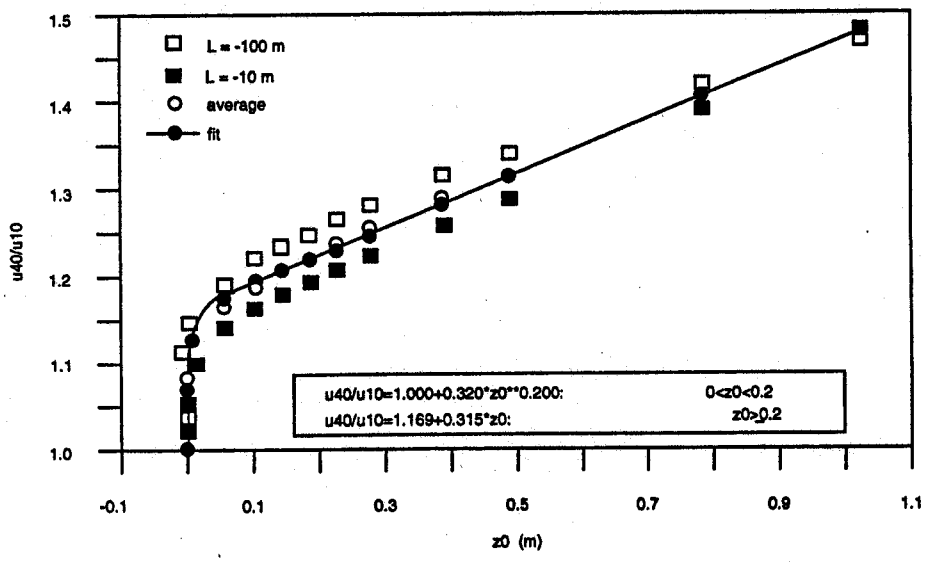

Figure 4.2: Schematic representing the relationship used to adapt the 10-m wind to the 40-m level as a function of roughness length (z_0) and Monin length (L).

assumed to apply at 10 m AGL, can be modified via similarity theory to apply at h_s. This modified wind for h_s is representative of the mean mixed layer up to h_1. These assumptions allow the surface-layer wind information to be applied throughout the model's multilayer PBL rather than at a single level. Similarly, the surface-layer mixing ratio (not shown) is also assumed to be representative of the entire mixed layer, and may be applied over several model layers during free-convective conditions.

The surface-layer wind analyses, however, must be adapted for the depth of the surface layer, h_s, which is assumed to be the height of the lowest model layer under unstable conditions (40 m AGL for $\sigma = 0.995$). Similarity relationships that assume a logarithmic profile of wind with height are used to adjust the 10-m surface wind analysis to the lowest model-layer height. Figure 4.2 shows that this wind adjustment is more strongly dependent on roughness (z_0) than on stability as measured by the Monin length (L); therefore, a "best-fit" relationship is determined for average stability conditions for roughness lengths ranging from 0.0 to 1.0 m. Thus, during free-convective conditions, the mean wind assimilated throughout the model PBL is based on the surface wind analysis modified to account for the model surface-layer height and the grid-box roughness. The surface analysis of mixing ratio is assumed to be representative for the lowest model layer and throughout the mixed layer.

During unstable conditions, the Blackadar scheme may develop a PBL which extends through several model layers. The "nudging correction" to the wind field at the lowest model layer is applied throughout the model PBL to simulate the conceptual model. Because this idealization is also closely reproduced by the PBL scheme (without nudging), the nudging strategy within the PBL is compatible with the boundary-layer physics. The observed surface mixing ratio applied throughout the model mixed layer is adjusted if necessary to remove any supersaturation with respect to the current model-simulated temperature and moisture conditions for a given level and grid point. This prevents the moisture assimilation term from becoming an artificial source of precipitation. During stable conditions, on the other hand, the height of the PBL is defined to be that of the lowest model layer since the boundary layer is largely decoupled from the free troposphere above.

Therefore, the 3-hourly surface-analysis nudging is also given by (4.1.2), but the vertical extent of the nudging is controlled by the model- simulated PBL depth, with $\hat{\alpha}_0$ for wind and moisture adjusted as previously discussed above. The analysis confidence factor, ϵ, for the 3-h surface analyses, is functionally dependent on the spatial distribution of the surface observations used to produce the analysis. Over land it varies from unity at grid boxes within one-half the prescribed radius of influence of a surface observation to 0.2 for grid boxes outside the prescribed radius.

The vertical weighting factor, w_σ, is defined as

$$w_\sigma = w_\sigma^R + w_\sigma^S \leq 1. \tag{4.1.8}$$

where w_σ^R and w_σ^S represent w_σ for assimilation of 3-D rawinsonde and 2-D surface data, respectively, and w_σ^S depends on the model-simulated PBL depth. The surface data are assimilated with full strength ($w_\sigma^S = 1.0$) within the layers defining the PBL and with reduced strength ($w_\sigma^S = 0.9$) one layer above (in the transition layer). The vertical weighting function used to assimilate 3-D rawinsonde data is defined such that $w_\sigma^R = 0.0$ in the PBL, 0.1 in the transition layer and 1.0 aloft. During stable conditions, therefore, the surface data are applied with full strength only in the lowest model layer and with reduced strength one layer above. Both types of analysis nudging generally assimilate temporally interpolated gridded analyses; that is, $\hat{\alpha}_0$ in (4.1.2) is interpolated in time, for example, from either 12-h 3-D analyses or 3-h 2-D surface analyses. Therefore, w_t is usually set to unity, except when decreasing the nudging at the end of a dynamic-initialization period.

4.2 Observational Nudging

This alternative scheme does not require gridded analyses of observations throughout the case study period, and may be better suited for situations with high-frequency asynoptic data (e.g., profilers), especially on the subalpha scales. Its form is similar to (4.1.2) and it uses only those observations which fall within a predetermined time window that is centered about each model time step. The set of differences between the model and the observed state is computed at the observation locations, and analyzed back to the grid in a region surrounding the observations. The tendency for $\alpha(\mathbf{x}, t)$ with $G_{p^*} = 0$ is given

by

$$\frac{\partial p^* \alpha}{\partial t} = F(\alpha, \mathbf{x}, t) + G_\alpha \cdot p^* \frac{\sum_{i=1}^{N} W_i^2(\mathbf{x}, t) \cdot \gamma_i \cdot (\alpha_o - \hat{\alpha})_i}{\sum_{i=1}^{N} W_i(\mathbf{x}, t)}, \tag{4.2.1}$$

where F and G_α are as defined earlier, subscript i denotes the i th observation of a total of N which are within a preset radius of a given grid point, α_o is the locally observed value of α, and $\hat{\alpha}$ is the model's prognostic variable interpolated to the observation location in three dimensions. The observational quality factor,γ , which ranges from 0 to 1, accounts for characteristic errors in measurement systems and representativeness. The four-dimensional weighting function accounts for the spatial and temporal separation of the ith observation from a given grid point at a given time step.

The four-dimensional weighting function for each observation i in (4.2.1) is rewritten as

$$W(\mathbf{x}, t) = w_{xy} \cdot w_\sigma \cdot w_t \tag{4.2.2}$$

The horizontal weighting function, w_{xy}, is a Cressman-type spatial weighting function defined by

$$w_{xy} = \frac{R^2 - D^2}{R^2 + D^2} \qquad 0 \le D \le R \tag{4.2.2}$$

and

$$w_{xy} = 0 \qquad D > R, \tag{4.2.3}$$

where R is the radius of influence and D is the distance from the i th observation location to the grid point. The vertical weighting function, w_σ is also a distance-weighted function defined by

$$w_\sigma = 1 - \frac{|\sigma_{obs} - \sigma|}{R_\sigma} \qquad |\sigma_{obs} - \sigma| \le R_\sigma \tag{4.2.4a}$$

$$w_\sigma = 0 \qquad |\sigma_{obs} - \sigma| > R_\sigma, \tag{4.2.4b}$$

where R_σ is the vertical radius of influence and σ_{obs} is the vertical position of the i th observation. The temporal weighting function is given by

$$w_t = 1 \qquad |t - t_0| < \tau/2 \tag{4.2.5}$$

$$w_t = \frac{\tau - |t - t_0|}{\tau/2} \qquad \tau/2 \le |t - t_0| \le \tau \tag{4.2.6}$$

$$w_t = 0 \qquad\qquad |t - t_0| > \tau, \qquad\qquad (4.2.7)$$

where t is the model-relative time, t_0 is the model-relative time of the ith observation, and τ is the half-period of a predetermined time window over which an observation will influence the model simulation.

For economy, the multi-level observations (soundings) used for obs nudging are usually vertically interpolated to the model sigma surfaces at each observation location prior to each simulation. Although the vertical component of the weighting function, w_σ (4.2.4), is also a distance-weighted function, the vertical radius of influence, R_σ , can be defined to be small (less than the spacing of the model layers) so that each observation above the model surface layer influences only one sigma layer at a given location.

Figure 4.3 illustrates schematically the horizontal and temporal components of W used for nudging to observations. The horizontal weighting function, w_{xy}, is the Cressman function given by (4.2.2) and (4.2.3). As shown in the top of the figure, the horizontal radius of influence varies linearly in the vertical with pressure, from R_s at the surface to the preset value R' at a pressure level p' representing the free atmosphere, where terrain influences are assumed to be small. At pressures less than or equal to this user-defined value, defined by default as 500 mb, the horizontal radius of influence is defined by default as twice the value used in the surface layer, R_s. For example, if $R_s = 100$ km, $R' = 200$ km. For certain situations, such as with upward propagating mountain-induced gravity waves, the assumption of negligible terrain influence within the troposphere is invalid and should be avoided.

As shown in the top of Fig. 4.3, the corrections computed at a given observation site and vertical level above the surface layer (lowest model layer) are spread laterally along a constant pressure level and thus across several sigma layers in regions of sloping terrain. That is, for any given grid point within the horizontal radius of influence, the obs-nudging correction in the horizontal direction is applied to the sigma layer which has a pressure value closest to that of the observation.

Observations within the model surface layer are spread along constant sigma surfaces, but with a modified Cressman function (dashed contours in the middle of Fig. 4.3) which reduces the influence of an observation as a function of the surface pressure (terrain).

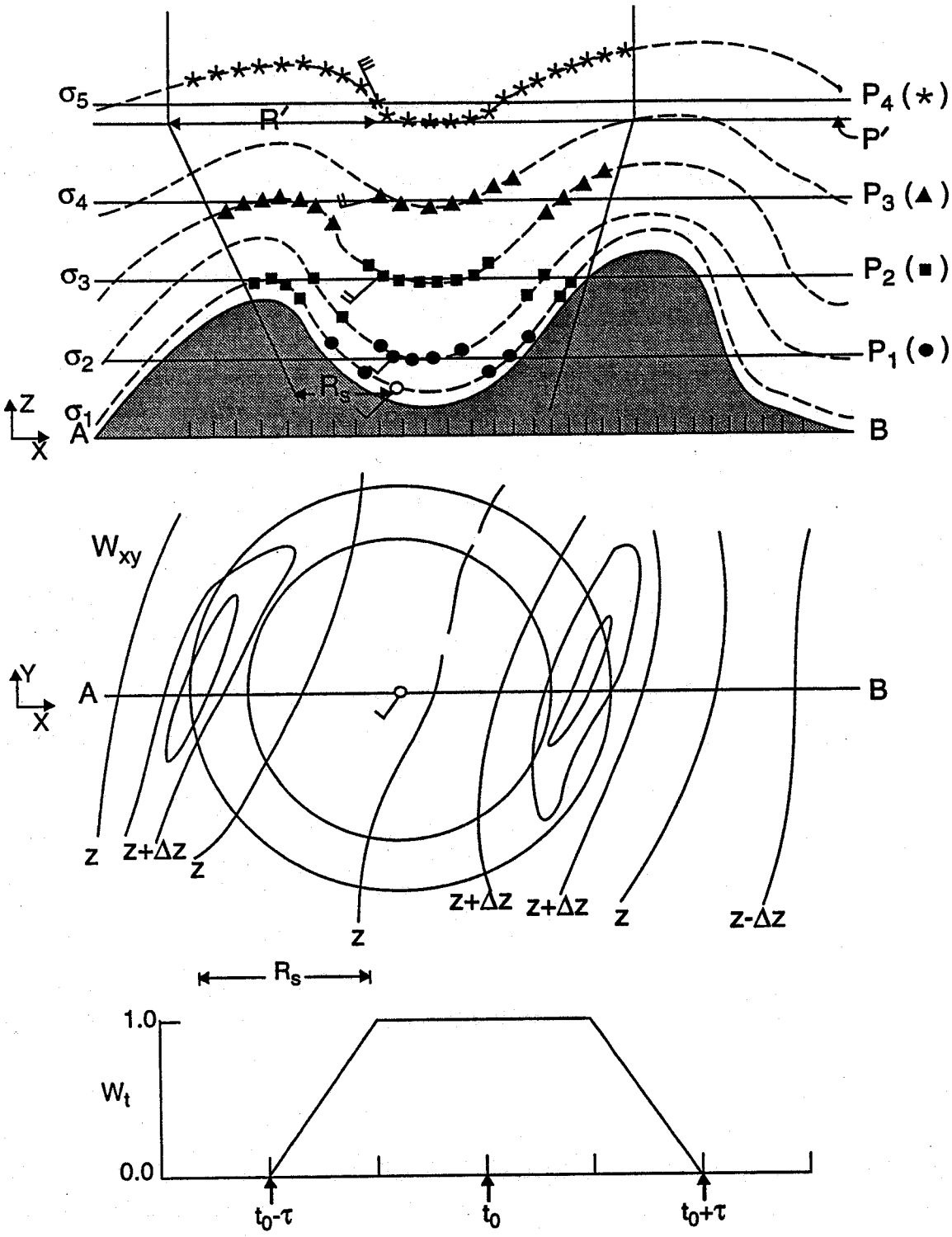

Figure 4.3: Schematic showing the horizontal weighting function, w_{xy}, and the temporal weighting function, w_t, used for obs nudging.

Thus spreading the influence of surface-layer observations along the lowest sigma ensures that the FDDA forcing near the surface in uneven terrain is continuous, and not like a pebble skipping across a pond. For observations in the surface layer, the distance factor D in (4.2.2) is replaced with D_m,

$$D_m = D + R_S C_m^{-1} |p_{s0} - p_s|, \tag{4.2.8}$$

where D is as defined above, C_m is a constant, and p_{s0} and p_s are the surface pressures at the observation location and the grid point, respectively. For example, C_m is typically defined as 75 mb, and R_s is the surface-layer value for the horizontal radius of influence. As the difference in surface pressure between the observation location and the grid point approaches C_m, the second term in (4.2.8) approaches R, and w_{xy} tends to zero faster for a given D. Therefore, the effect of assimilating surface-layer observations in the valley (mountains) on grid point locations in the mountains (valley) will be much reduced. This minimizes the possibility that observations in complex terrain will influence the model solution in areas where they may not be representative. Also, the vertical weighting factor, w_σ, for these surface-layer observations is defined so that the vertical influence of the surface-layer observations decreases linearly through the lowest 3 or so model layers (about 250 m AGL). As mentioned earlier, single-level data are retained better by the model if assimilated through several vertical layers.

The temporal weighting function, w_t (4.2.5-4.2.7), shown in the bottom of Fig. 4.3, is nonzero during a preset time window centered about the observation time, t_0. It determines the time period over which the ith observation can influence the model simulation via (4.2.1). In general, this time window can also be defined as a function of the pressure level of the observation similar to the effect of the horizontal radius of influence, R, in (4.2.2). Thus the final correction to the model solution via obs nudging reflects a weighted average of all observations during the preset time window about the current time step and within some three-dimensional neighborhood of each grid point.

5. Treatment of physical processes

5.1 Horizontal diffusion

Two types of diffusions are used to control nonlinear instability and aliasing. These are a second-order diffusion of the form

$$F_{H2\alpha} = p^* K_H \nabla_\sigma^2 \alpha, \tag{5.1.1}$$

where α is any prognostic variable, and a more scale-selective fourth-order form

$$F_{H4\alpha} = p^* K'_H \nabla_\sigma^4 \alpha, \tag{5.1.2}$$

where

$$K'_H = \Delta s^2 K_H \tag{5.1.3},$$

The second order diffusion is only used in the coarsest domain for the row and column of the grid points next to the lateral boundaries, while the fourth-order form is used in the interior of the coarsest domain as well as in the entire domain of any refinement mesh.

The horizontal diffusion coefficient K_H consists of a background value K_{H0} and a term proportional to the deformation D

$$K_H = K_{H0} + .5k^2 \Delta s_2 D \tag{5.1.4}$$

where k is the von Karman constant and D is given by (Smagorinski *et al.* 1965)

$$D = \left[\left(\frac{\partial u}{\partial x} - \frac{\partial v}{\partial y} \right)^2 + \left(\frac{\partial v}{\partial x} + \frac{\partial u}{\partial y} \right)^2 \right]^{\frac{1}{2}}. \tag{5.1.5}$$

A background value of K_H is a function of grid size and time step, where

$$K_{H0} = 3. \times 10^{-3} \frac{\Delta x^2}{\Delta t}. \tag{5.1.6}$$

Note that the horizontal operators ∇^4 and ∇^2 are applied on constant sigma surfaces. To ensure computational stability, an upper limit of $\frac{\Delta x^2}{64 \Delta t}$ is imposed on K_H

5.2 Dry Convective Adjustment

There may be situations in which super-adiabatic layers are produced in the model atmosphere. When this happens, and there is no call to the Blackadar planetary boundary

layer parameterization, a simple scheme is used to remove any unstable layers. The scheme operates on the entire sounding at once and conserves the vertical integral of internal and potential energy. When the model lapse rate of potential temperature $\frac{\partial\theta}{\partial p}$ exceeds a critical value $\left(\frac{\partial\theta}{\partial p}\right)_c$, the sounding is adjusted so that (1) mass-weighted mean temperature is unchanged, and (2) the potential temperature lapse rate after adjustment equals $\left(\frac{\partial\theta}{\partial p}\right)_c$.

Given n layers in which the model potential temperature lapse rate exceeds the critical value, the first constraint gives

$$(T_n + \Delta T_n)\Delta\sigma_n + (T_{n-1} + \Delta T_{n-1})\Delta\sigma_{n-1} + ... + (T_1 + \Delta T_1)\Delta\sigma_1 = \bar{T}\sum_{i-1}^{n}\Delta\sigma_i, \quad (5.2.1)$$

where T_i are the adjustments to be added to the temperature at layer i, T_i and σ_i are the temperature and thickness of the sigma layers, and $\bar{T}$ is the mass weighted mean temperature. The second constraint gives

$$(T_i + \Delta T_i)\pi_i - (T_{i-1} + \Delta T_{i-1})\pi_{i-1} = \left(\frac{\partial\theta}{\partial p}\right)(p_i - p_{i-1}) \qquad i = 2, ..., n, \qquad (5.2.2)$$

where π_i is the Exner function. There are n equations that can be solved for n variables ΔT_i. The Gaussian elimination method is used to solve the $n \times n$ matrix system. After adjustment, the entire sounding is rechecked for unstable layers.

The moisture in the adjusted layers is assumed constant in the vertical, i.e.,

$$q_{vi} = \bar{q_v} = \frac{\sum_{i=1}^{n} q_{vi}\Delta\sigma_i}{\sum_{i=1}^{n}\Delta\sigma_i} \qquad (5.1.3)$$

5.3 Precipitation physics

MM5 has many different choices to treat precipitation physics. They are usually divided into two different groups: explicit and implicit schemes. Explicit schemes treat resolved precipitation physics while implicit schemes treat the non-resolved precipitation physics. Both may be operating at a grid-point at the same time. A commonly used terminology of "convective" versus "stable" precipitation is generally not acceptable on finer grid-resolutions, where convective precipitation is quite often resolved. Hence in the following subsections we will use resolved/non-resolved and explicit/implicit as common terminologies. As two additional options, MM5 allows for dry runs, where moisture is

treated as a passive variable (no explicit and implicit schemes are applied). Another option is a "fake dry run", where only the effects of the latent heat release are removed. These 2 options do not require any further description and will not be discussed in the following subsections.

5.3.1 Resolvable scale precipitation processes

These schemes are usually activated whenever grid-scale saturation is reached. In other words, they treat resolved precipitation processes. The most simple way that sometimes is still used on larger-scales, is to simply remove super-saturation as precipitation and add the latent heat to the thermodynamic equation. More sophisticated schemes carry additional variables such as cloud and rainwater (subsection 5.3.1.1), or even ice and snow (subsection 5.3.1.2). Both schemes described next are enhancements of MM4's original scheme (Hsie 1984).

5.3.1.1 Explicit treatment of cloudwater, rainwater, snow, and ice

This scheme optionally allows for ice-phase processes below 0 °C, where cloud water is treated as cloud ice and rain is treated as snow (Dudhia 1989). The equations for water vapor, cloud water (ice) and rain water (snow) mixing ratios are given by the following

$$\frac{\partial p^* q_v}{\partial t} = -m^2\left[\frac{\partial p^* u q_v/m}{\partial x} + \frac{\partial p^* v q_v/m}{\partial y}\right] - \frac{\partial p^* q_v \dot{\sigma}}{\partial \sigma} + \delta_{nh} q_v DIV$$
$$+ p^*(-P_{RE} - P_{CON} - P_{II} - P_{ID}) + D_{qv}, \qquad (5.3.1.1.1)$$

$$\frac{\partial p^* q_c}{\partial t} = -m^2\left[\frac{\partial p^* u q_c/m}{\partial x} + \frac{\partial p^* v q_c/m}{\partial y}\right] - \frac{\partial p^* q_c \dot{\sigma}}{\partial \sigma} + \delta_{nh} q_c DIV$$
$$+ p^*(P_{ID} + P_{II} - P_{RC} - P_{RA} + P_{CON}) + D_{qc}, \qquad (5.3.1.1.2)$$

$$\frac{\partial p^* q_r}{\partial t} = -m^2\left[\frac{\partial p^* u q_r/m}{\partial x} + \frac{\partial p^* v q_r/m}{\partial y}\right] - \frac{\partial p^* q_r \dot{\sigma}}{\partial \sigma} + \delta_{nh} q_r DIV$$
$$- \frac{\partial V_f \rho g q_r}{\partial \sigma} + p^*(P_{RE} + P_{RC} + P_{RA}) + D_{qr}, \qquad (5.3.1.1.3)$$

where P_{CON} is condensation (and freezing for $T < 0$ °C) of water vapor into cloud (ice) at water saturation, P_{RA} is accretion of cloud by rain (ice by snow), P_{RC} is conversion of cloud to rain (ice to snow) and P_{RE} is evaporation (sublimation) of rain (snow). Additional ice processes are P_{II}, the initiation of ice crystals, and P_{ID} sublimation/deposition of cloud

ice (Fig. 5.1). The fall speed of rain or snow is V_f. The term δ_{nh} is 1 for nonhydrostatic and 0 for hydrostatic simulations.

In all the relevant processes, Marshall-Palmer size distributions are assumed for rain and snow and droplet fall speeds are taken to be of the form $V(D) = aD^b$, where D is the diameter. For rain, the Marshall-Palmer intercept parameter is $N_0 = 8 \times 10^6$ m^{-4}, $a = 841.99667$ and $b = 0.8$ for V in m s^{-1}and D in meters, while for snow $N_0 = 2 \times 10^7$ m^{-4}, $a = 11.72$ and $b = 0.41$.

The saturated vapor pressure over water (in mb) is taken to be

$$e_{sw} = 6.112\exp\left[17.67\left(\frac{T - 273.15}{T - 29.65}\right)\right], \qquad (5.3.1.1.4)$$

and for ice

$$e_{si} = 6.11\exp\left(22.514 - \frac{6150}{T}\right). \qquad (5.3.1.1.5)$$

The saturated water vapor mixing ratio is then given by

$$q_s = \frac{0.622e_s}{p - e_s}.$$

P_{RC}, the autoconversion term is represented by

$$P_{RC} = \max[k_1(q_c - q_{crit}),\ 0], \qquad (5.3.1.1.6a)$$

for cloud to rain and by

$$P_{RC} = \max[(q_c - M_{max}n_c)/\Delta t,\ 0], \qquad (5.3.1.1.6b)$$

for ice to snow, where $k_1 = 10^{-3}$ s^{-1}, $q_{crit} = 0.5$ g kg^{-1}, $M_{max} = 9.4 \times 10^{-10}$ kg and n_c is given by Fletcher's (1962) formula for the number concentration of ice nuclei (kg^{-1}),

$$n_c = 10^{-2}\exp[0.6(273.15 - T)]/\rho.$$

P_{II}, the initiation of ice crystals is given by

$$P_{II} = \max[(M_0n_c - q_c)/\Delta t,\ 0], \qquad (5.3.1.1.7)$$

as long as sufficient supersaturation over ice exists, where $M_0 = 10^{-12}$ kg.

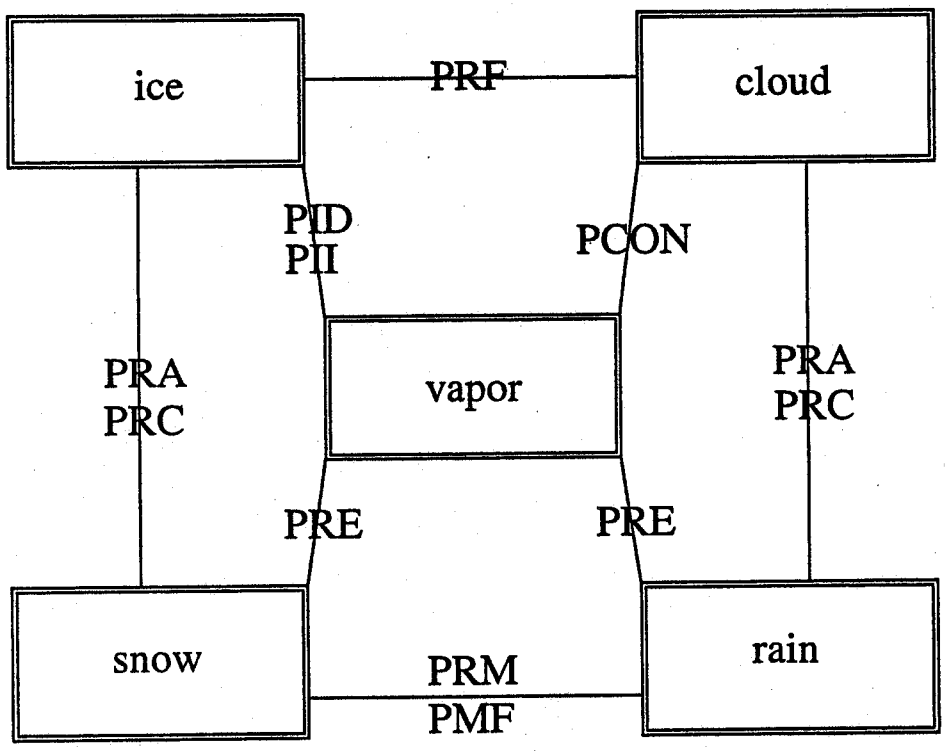

Figure 5.1 Box diagram illustrating the processes in the moisture scheme for ice (crystals), cloud(liquid), snow and rain. PCON, condensation/evaporation of cloud; PRA, accretion; PRC, conversion; PID, deposition onto ice crystals; PRE, evaporation for rain and deposition/sublimation for snow; PMF, melting/freezing due to advection; PII, initiation of ice crystals; and PRM, melting of snow due to fall.

P_{RA}, the accretion rate is given by

$$P_{RA} = \frac{1}{4}\pi\rho a q_c E N_0 \frac{\Gamma(3+b)}{\lambda^{3+b}}, \qquad (5.3.1.1.8)$$

where Γ is the gamma-function, E is the collection efficiency (1 for rain and 0.1 for snow) and λ is given by

$$\lambda = \left(\frac{\pi N_0 \rho_w}{\rho q_r}\right)^{1/4}.$$

Here ρ_w is the mean density of rain or snow particles (1000 and 100 kg m^{-3}, respectively.)

P_{ID}, the deposition onto or sublimation of ice particles is found from

$$P_{ID} = \frac{4D_i(S_i - 1)\rho n_c}{A + B}, \qquad (5.3.1.1.9)$$

where

$$S_i = q_v/q_{si},$$

$$A = \frac{L_s^2 \rho}{K_a R_v T^2}, \quad B = \frac{1}{q_{si}\chi}.$$

L_s is the latent heat of sublimation, K_a is the thermal conductivity of air, R_v is the gas constant for water vapor, and χ is the diffusivity of vapor in air. The mean diameter of ice crystals, D_i, is found from the mean mass, $M_i = q_c/n_c$, and the mass-diameter relation for hexagonal plates from Rutledge and Hobbs (1983), $D_i = 16.3 M_i^{1/2}$ meters.

P_{RE}, the evaporation of rain and sublimation/deposition of snow can be determined from

$$P_{RE} = \frac{2\pi N_0 (S - 1)}{A + B}\left[\frac{f_1}{\lambda^2} + f_2\left(\frac{a\rho}{\mu}\right)^{1/2} S_c^{1/3} \frac{\Gamma(5/2 + b/2)}{\lambda^{5/2+b/2}}\right], \qquad (5.3.1.1.10)$$

with the relevant N_0, a, and b chosen for rain or snow, and $S = S_w$ or S_i. The definition of A and B also change from the above for rain, substituting L_v for L_s and q_{sw} for q_{si}. For snow, 2π is replaced by 4. The values of f_1 and f_2 are 0.78 and 0.32 for rain and 0.65 and 0.44 for snow. The term in brackets represents a distribution-integrated ventilation factor, $F = f_1 + f_2 S_c^{1/3} Re^{1/2}$, with $S_c = \mu/\rho\chi$, the Schmidt number, and $Re = V(D)D\rho/\mu$, the Reynolds number, and μ is the dynamic viscosity of air.

P_{CON}, the condensation is determined as follows. Temperature, water vapor mixing ratio and cloud water are forecast first: these preliminary forecast values are designated by T^*, q_v^* and q_c^*. We define

$$\delta M = q_v^* - q_{vs}^*,$$

where q_{vs}^* is the saturated mixing ratio at temperature T^*,
(1) if $\delta M > 0$ (supersaturation),

$$P_{CON} = \frac{r_1 \delta M}{\Delta t}, \qquad (5.3.1.1.11a)$$

where

$$r_1 = \frac{1}{1 + \frac{L_v^2 q_{vs}^*}{R_v c_{pm} T^{*2}}},$$

(2) if $\delta M < 0$ and $q_c > 0$ (evaporation),

$$P_{CON} = -\min\left[-\frac{r_1 \delta M}{\Delta t}, \frac{q_c^*}{\Delta t}\right], \qquad (5.3.1.1.11b)$$

(3) if $\delta M < 0$ and $q_c = 0$,

$$P_{CON} = 0. \qquad (5.3.1.1.11c)$$

The P_{CON} term is computed diagnostically so no iteration is needed.

Additionally, as snow falls through the 0 °C level, it immediately melts to rain. This process is given by

$$P_{RM} = -\frac{\rho g V_f q_r}{\Delta p}. \qquad (5.3.1.1.12)$$

Advection of ice or snow downwards or of rain or cloud upwards through this level also melts or freezes the particles, where

$$P_{MF} = -\frac{\omega(q_c + q_r)}{\Delta p}. \qquad (5.3.1.1.13)$$

In both cases, the 0 °C isotherm is taken to be at a full model level boundary. Melting occurs at the level immediately below this boundary and freezing above it.

The latent heating is thus

$$\dot{Q} = L(P_{RE} + P_{ID} + P_{II} + P_{CON}) + L_m(P_{RM} + P_{MF}), \qquad (5.3.1.1.14)$$

where $L = L_v$ for $T > 0$ °C and $L = L_s$ for $T < 0$ °C, and $L_m = L_s - L_v$.

The fall speed is mass-weighted and so is determined from

$$V_f = a\frac{\Gamma(4+b)}{6}\lambda^{-b}. \qquad (5.3.1.1.15)$$

The fall term in (5.3.1.1.3), the rain and snow prediction equation, may be calculated on split time-steps, $\Delta t'$, in the explicit moisture routine. This ensures that $V_f \Delta t'/\Delta z < 1$, which is required for numerical stability. The size of $\Delta t'$ is determined independently in each model column based on the maximum value of $V_f \Delta t/\Delta z$ in the column, where Δt is the model time step.

5.3.1.2 Mixed-Phase Ice Scheme

This scheme is based on the simple ice phase scheme described in the previous subsection, but it does not immediately freeze or melt water and ice. Supercooled water can exist below 0°C in this scheme, as can unmelted snow exist above 0°C. Separate arrays are used to store vapor, cloud, rain, cloud ice and snow.

Homogeneous freezing of cloud water to cloud ice occurs immediately below -40°C and cloud ice melts immediately above 0°C. Snow melts according to

$$P_{SM} = -\frac{2\pi N_{0s}}{L_f} K_a (T - T_0) \left[\frac{f_1}{\lambda^2} + f_2 \left(\frac{a\rho}{\mu} \right)^{1/2} S_c^{1/3} \frac{\Gamma(5/2 + b/2)}{\lambda^{5/2+b/2}} \right], \quad (5.3.1.2.1)$$

where $f_1 = 0.78$ and $f_2 = 0.31$ (Rutledge and Hobbs 1984), and the other constants are the ones relevant to snow in subsection (a). Evaporation of melting snow is modified to use the values of A and B for rain as in (5.3.1.1.10).

Heterogeneous freezing of cloud water to cloud ice is also included following Bigg (1953),

$$P_{CI} = B'\{\exp[A'(T_0 - T)] - 1\} \frac{\rho q_c^2}{\rho_w N_c} \quad (5.3.1.2.2)$$

where $A' = 0.66\text{K}^{-1}$, $B' = 100\text{m}^{-3}\text{s}^{-1}$ and the number concentration of cloud droplets per unit volume of air, $N_c = 10^{10}\text{m}^{-3}$.

Sekhon and Srivastava (1970) determined that better comparison against observed snow distributions can be obtained in theoretical studies if the slope intercept value for the size distribution is expressed as

$$N_{0s}(m^{-4}) = 1.05R^{-0.94} \quad (5.3.1.2.3)$$

where, N_{0s} is the slope intercept and R (m s^{-1}) is the snow fall rate. Thus a variable intercept parameter replaces the constant N_{0s} used in the simple ice scheme.

This can be expressed in terms of snow mixing ratio, q_S, as

$$N_{0s} = \left\{ 1.05 \left[\frac{1}{\rho q_S \alpha} \left(\frac{\pi \rho_S}{\rho q_S} \right)^{\frac{b}{4}} \right]^{0.94} \right\}^{\frac{4}{0.94b+4}} \quad (5.3.1.2.4)$$

where, $\alpha^{-1} = \frac{6\rho_w}{a\Gamma(4+b)}$.

5.3.2 Implicit cumulus parameterization schemes

5.3.2.1 The Kuo scheme

In this scheme, the amount of convection is determined by the vertically integrated moisture convergence. The feedback to the larger scale (the vertical distribution of heating and moistening), is determined with the help of the normalized vertical profiles of convective heating ($N_h(\sigma)$) and moistening ($N_m(\sigma)$), and a vertical eddy-flux divergence of water vapor associated with cumulus convection $V_{qf}(\sigma)$. Therefore, equations (2.1.3), (2.2.5) and (5.3.1.1.1) can be rewritten to include the convective-scale fluxes as

$$\frac{\partial p^* T}{\partial t} = -m^2\left[\frac{\partial p^* uT/m}{\partial x} + \frac{\partial p^* vT/m}{\partial y}\right] - \frac{\partial p^* T\dot{\sigma}}{\partial \sigma} + p^*\frac{\omega}{\rho c_p} + p^*\frac{L_v}{c_{pm}}N_h(\sigma)(1-b)gM_t + D_T, \quad (5.3.2.1.1)$$

$$\frac{\partial p^* T}{\partial t} = -m^2\left[\frac{\partial p^* uT/m}{\partial x} + \frac{\partial p^* vT/m}{\partial y}\right] - \frac{\partial p^* T\dot{\sigma}}{\partial \sigma} + T.DIV + \frac{1}{\rho c_p}\left[p^*\frac{Dp'}{Dt} - \rho_0 g p^* w - D_{p'}\right] + p^*\frac{L_v}{c_{pm}}N_h(\sigma)(1-b)gM_t + D_T, \quad (5.3.2.1.2)$$

$$\frac{\partial p^* q_v}{\partial t} = +\delta_{nh} q_v DIV + p^*(-P_{RE} - P_{CON} - P_{II} - P_{ID}) + p^* bgM_t N_m(\sigma) + p^* V_{qf}(\sigma) + D_{qv}, \quad (5.3.2.1.3)$$

where the vertically integrated moisture convergence M_t is

$$M_t = \left(\frac{m^2}{g}\right)\int_0^1 \frac{\nabla p^* \dot{V} q_v}{m} d\sigma. \quad (5.3.2.1.4)$$

A portion $(1-b)$ of M_t is assumed to condense and precipitate, where the remaining fraction b is assumed to moisten the grid column. Following Anthes(1977), b is a function of the mean relative humidity $\overline{RH}$ of the column, where

$$b = 2(1-\overline{RH}) \quad (5.3.2.1.5)$$

for $\overline{RH} \geq 0.5$, and $b = 1$ otherwise.

The vertical profiles of heating and moistening

The normalized, nondimensional functions for the vertical profiles of heating and moistening and the divergence of the vertical eddy flux of water vapor are subject to the constraints

$$\int_0^1 N_h(\sigma)d\sigma = 1, \tag{5.3.2.1.6}$$

$$\int_0^1 N_m(\sigma)d\sigma = 1, \tag{5.3.2.1.7}$$

$$\int_0^1 V_{qf}(\sigma)d\sigma = 0. \tag{5.3.2.1.8}$$

Anthes *et al.* (1987) assume simple relationships for these functions, which are derived from budget studies. For the convective heating profile, N_h, they observe that the convective heating often has a parabolic shape with a maximum in the upper half of the cloud. Hence

$$N_h(\sigma) = a_1x^2 + a_2x + a_3, \tag{5.3.2.1.9}$$

where

$$x = ln\sigma \tag{5.3.2.1.10}$$

with the boundary conditions:

$$N_h(\sigma) = 0, \qquad at \;\; x_b = ln\sigma_b, \;\; and \; x_u = ln\sigma_u \tag{5.3.2.1.11}$$

at cloudbase (σ_b) and cloud top (σ_u), and

$$N_h'(\sigma) = \frac{\partial N_h(\sigma)}{\partial \sigma} = 0 \tag{5.3.2.1.12}$$

at $\bar{x}$, which is defined as

$$\bar{x} = \frac{x_u + x_b}{2}, \tag{5.3.2.1.13}$$

where subscripts u and b stand for the top and the base of the cloud. Using (5.3.2.1.6), a_1 can be shown to be

$$a_1 = \frac{2}{x_u^3 - x_b^3 + x_u^2x_b - x_ux_b^2}. \tag{5.3.2.1.14}$$

The vertical moistening profile, $N_m(\sigma)$, is simply given following Anthes (1977) as

$$N_m(\sigma) = \frac{(1 - RH(\sigma))q_vs(\sigma)}{\int_{\sigma_{htop}}^1 (1 - RH(\sigma'))q_{vs}(\sigma')d\sigma'}. \tag{5.3.2.1.15}$$

Divergence of the Vertical Eddy Flux of Water Vapor $V_{qf}(\sigma)$

The divergence of the vertical eddy flux of water vapor is defined as

$$V_{qf}(\sigma) = \frac{\partial \overline{\dot{\sigma}' q_v'}}{\partial \sigma}. \qquad (5.3.2.1.16)$$

If one assumes a small fraction of convective cloud cover, and the cloud vertical motion $\dot{\sigma}_c$ is much larger than the larger-scale vertical motion, $\dot{\sigma}$ (5.3.2.1.16) can be rewritten as

$$V_{qf}(\sigma) = \frac{a}{1-a}\frac{\partial}{\partial \sigma}[\dot{\sigma}_c(q_{vc} - q_v)], \qquad (5.3.2.1.17)$$

where q_{vc} is the mixing ratio in the cloud.

According to Anthes (1977), the fractional coverage a is calculate using

$$a = \frac{(1-b)gM_t}{\int_0^{p^*}\left(-\omega_c \frac{\partial q_{vc}}{\partial p} + \frac{\partial q_{vc}}{\partial t_e}\right)dp}, \qquad (5.3.2.1.18)$$

which is the ratio between the grid-average condensation rate and that of a single cloud. The term $\frac{\partial q_{vc}}{\partial t_e}$ represents the contribution to the rate of change of cloud-mixing ratio by entrainment (Anthes 1977). Anthes *et al.* (1987) assume a typical value for the denominator of approximately $4.3 \times 10^{-3} cb\ s^{-1}$ and then rewrite (5.3.2.1.17) as

$$V_{qf}(\sigma) = \frac{(1-b)gM_t}{4.3 \times 10^{-3}}\frac{\partial}{\partial \sigma}[\dot{\sigma}_c(q_{vc} - q_v)]. \qquad (5.3.2.1.19)$$

For further simplification, Anthes *et al.* (1987) next assume that $\dot{\sigma}_c$ also has a parabolic shape and can be expressed as

$$\dot{\sigma}_c = c_1 x^2 + c_2 x + c_3, \qquad (5.3.2.1.20)$$

where $x = lnp$, and $\dot{\sigma}_c = 0$ at cloud-top and base. Furthermore, $q_{vc} - q_v$ is assumed to have a parabolic profile with pressure

$$q_{vc} - q_v = b_1 x^2 + b_2 x + b_3 \qquad (5.3.2.1.21)$$

with

$$x = ln[(1-\sigma)(100 - p_t) + p_t]. \qquad (5.3.2.1.22)$$

The procedure

The simple procedure can be summarized as follows:

1. Compute M_t from (5.3.2.1.4)
2. Check whether $M_t \geq 3. \times 10^{-5} kg\ m^{-2}\ s^{-1}$, a critical threshold value.
3. Check the model sounding for convective instability to see if convection is possible.
4. Determine cloud top and base from sounding.
5. Check whether cloud-depth is larger than a critical value ($\Delta\sigma \geq .3$)
6. Calculate the normalized vertical profile functions
7. Calculate $\dot{\sigma}_c$ on the full σ levels from (5.3.2.1.20)
8. Compute $q_{vc} - q_v$ from (5.3.2.1.21)
9. Calculate V_{qf} from (5.3.2.1.19)

5.3.2.2 A modified Arakawa-Schubert scheme

The version of the Arakawa-Schubert scheme used here was developed by Grell (1993). In contrast to the original scheme (Arakawa and Schubert 1974, AS), it includes moist convective-scale downdrafts. Other changes have been implemented to also allow the scheme to be used successfully in mesoscale models in mid-latitudes (Grell *et al.* 1991). To simplify the description we have adapted a terminology originally introduced by Betts (1974), which splits the parameterization problem from the modeling view in three parts: static control, dynamic control, and feedback. The static control includes usually a cloud-model and calculates cloud thermodynamic properties, the dynamic control is what determines the amount and location of the convection, and the feedback determines the vertical distribution of the integrated heating and moistening.

Static control

As with all commonly used one dimensional steady state cloud models (plumes, bubbles, or jets), our AS scheme makes use of the assumption that entrainment occurs over the depth of the buoyant element according to the entrainment hypothesis

$$\mu = \frac{1}{m(z)}\frac{\partial m(z)}{\partial z} \approx \frac{.2}{r}, \tag{5.3.2.2.1}$$

where μ is the total net fractional entrainment rate of the buoyant element, m its mass flux (m_u for updraft, m_d for downdraft), and r its radius. Following AS, the dependence on the radius is not explicitly used. However, implicitly, the radius of the cloud is assumed to be constant. Detrainment was originally only assumed to happen at the cloud top, but this assumption may easily be varied (Houze *et al.* 1979, Lord 1978) by defining a fractional detrainment rate, μ_{ud}, and rewriting (5.3.2.2.1) for the updraft of cloud type λ as

$$\begin{aligned}\mu_u = \mu_{ue} - \mu_{ud} &= \frac{1}{m_u(z)}\frac{\partial m_u(z)}{\partial z} \\ &= \frac{1}{m_u(\lambda,z)}\left(\left(\frac{\partial m_u(\lambda,z)}{\partial z}\right)_{ent} - \left(\frac{\partial m_u(\lambda,z)}{\partial z}\right)_{det}\right)\end{aligned} \tag{5.3.2.2.2}$$

where μ_{ue} is the gross fractional entrainment rate, and μ_u is the total net fractional entrainment rate of the updraft. Subscripts *ent* and *det* indicate changes due to entrainment and detrainment, respectively. Looking at the budget of a thermodynamic

variable in an infinitesimal layer of the updraft we get

$$\frac{\partial m_u \alpha_u}{\partial z} = \left(\frac{\partial m_u}{\partial z}\right)_e \tilde{\alpha} - \left(\frac{\partial m_u}{\partial z}\right)_d \alpha_u + S_u. \tag{5.3.2.2.3}$$

Together with (5.3.2.2.2) this leads to the steady state plume equation

$$\frac{\partial \alpha_u(\lambda, z)}{\partial z} = \mu_{ue}(\tilde{\alpha}(z) - \alpha_u(\lambda, z)) + S_u \tag{5.3.2.2.4}$$

where α is a thermodynamic variable, the tilde denotes an environmental value, and subscript u denots an updraft property. S stands for sources or sinks. Similarly, for the downdraft, we can rewrite equations (5.3.2.2.2) and (5.3.2.2.4) as

$$\begin{aligned} \mu_d = \mu_{de} - \mu_{dd} &= -\frac{1}{m_d(z)} \frac{\partial m_d(z)}{\partial z} \\ &= -\frac{1}{m_d(z)} \left(\left(\frac{\partial m_d(z)}{\partial z}\right)_{ent} - \left(\frac{\partial m_d(z)}{\partial z}\right)_{det} \right) \end{aligned} \tag{5.3.2.2.5}$$

and

$$\frac{\partial \alpha_d(z)}{\partial z} = -\mu_{de}(\tilde{\alpha}(z) - \alpha_d(z)) + S, \tag{5.3.2.2.6}$$

where subscript d denotes a downdraft property. For moist static energy

$$\tilde{h}(z) = C_p \tilde{T}(z) + gz + L\tilde{q}(z), \tag{5.3.2.2.7}$$

equations (5.3.2.2.4) and (5.3.2.2.6) simply become

$$\frac{\partial h_u(\lambda, z)}{\partial z} = \mu_{ue}(\tilde{h}(z) - h_u(\lambda, z)) \tag{5.3.2.2.8}$$

and

$$\frac{\partial h_d(z)}{\partial z} = -\mu_{de}[\tilde{h}(z) - h_d(z)]. \tag{5.3.2.2.9}$$

Next, for the moisture budget of the updraft, we use

$$\alpha_u = q_u(\lambda, z) + q_l(\lambda, z) \tag{5.3.2.2.10}$$

and

$$S_u = -c_0 m_u(\lambda, z) q_l(\lambda, z). \tag{5.3.2.2.11}$$

Here S_u is the total water that is rained out, c_0 is a rainfall conversion parameter and could be a function of cloud size or wind shear, q_l is the suspended liquid water content of the cloud, and q_u is the water vapor mixing ratio inside the updraft. Equation (5.3.2.2.4) can then be rewritten as

$$\frac{\partial(q_u(\lambda,z)+q_l(\lambda,z))}{\partial z}=\mu_{ue}(\tilde{q}(z)-q_u(\lambda,z)-q_l(\lambda,z))+S_u. \qquad (5.3.2.2.12)$$

For the downdraft, the equation for the water vapor reads

$$\frac{\partial q_d(z)}{\partial z}=-\mu_{de}[\tilde{q}(z)-q_d(z)]+S_d. \qquad (5.3.2.2.13)$$

S_d here is a source; namely the evaporation of rain. Assuming saturation in the updraft and downdraft, we can make use of the approximate equation

$$q_c(\lambda,z)=\tilde{q}^*+\frac{\gamma}{1+\gamma}\frac{1}{L}[h_c(\lambda,z)-\tilde{h}^*(z)], \qquad (5.3.2.2.14)$$

where

$$\gamma=\frac{L}{c_p}\left(\frac{\partial\tilde{q}^*}{\partial T}\right)_P \qquad (5.3.2.2.15)$$

the asterisk denotes a saturated value, and h_c here stands for the moist static energy in the cloud (updraft or downdraft), if saturation is assumed. Next, to arrive at a usable closure, the up- and down-draft mass fluxes are normalized by the updraft base ($m_b(\lambda)$) mass flux, and the downdraft base $m_0(\lambda)$ mass flux of a subensemble. Hence, for the updraft,

$$m_u(\lambda,z)=m_b(\lambda)\eta_u(\lambda,z) \qquad (5.3.2.2.16)$$

and

$$\mu_{ue}-\mu_{ud}=\frac{1}{\eta_u(z)}\frac{\partial\eta_u(z)}{\partial z}. \qquad (5.3.2.2.17)$$

Equivalently, for the downdraft we may write

$$m_d(z)=m_0(\lambda)\eta_d(\lambda,z) \qquad (5.3.2.2.18)$$

and

$$\mu_{de}-\mu_{dd}=\frac{1}{\eta_d(z)}\frac{\partial\eta_d(z)}{\partial z}. \qquad (5.3.2.2.19)$$

Here, m_0 is the mass flux at the originating level and η_d, as η_u in equation (5.3.2.2.16), is the normalized mass flux profile.

To leave only one unknown variable, we follow Houze *et al.* (1979) and make the originating mass flux of the downdraft a function of the updraft mass flux and reevaporation of convective condensate. Therefore, the condensate in the updraft

$$C_u(\lambda)d\lambda = m_b d\lambda \left(\int_{z_B}^{z_T} \eta_u(\lambda, z) S_u dz) \right) \equiv I_1 m_b d\lambda \tag{5.3.2.2.20}$$

is apportioned according to

$$C_u(\lambda)d\lambda = (R_c(\lambda) + E_d(\lambda))d\lambda = (\alpha(\lambda) + \beta(\lambda))C_u(\lambda)d\lambda, \tag{5.3.2.2.21}$$

where $\alpha + \beta = 1$ and E_d, the evaporation of condensate in the downdraft for cloud type λ, can be written as

$$E_d d\lambda = m_0(\lambda)d\lambda \left(\int_0^{z_0} \eta_d(\lambda, z) S_d dz \right) \equiv I_2 m_0 d\lambda. \tag{5.3.2.2.22}$$

From equations (5.3.2.2.20-5.3.2.2.22) we see that

$$E_d d\lambda = \beta C_u d\lambda = \beta I_1 m_b d\lambda = I_2 m_0 d\lambda \tag{5.3.2.2.23}$$

and hence

$$m_0(\lambda) = \frac{\beta(\lambda) I_1 m_b(\lambda)}{I_2(\lambda)} = \epsilon(\lambda) m_b(\lambda). \tag{5.3.2.2.24}$$

Here $1 - \beta$ is the precipitation efficiency. Following Fritsch and Chappell (1980), it is made dependent on the windshear.

To solve the above equations we need to specify boundary conditions as well as make some arbitrary assumptions. For the updraft we assume

$$h_u(z_b) = MAX(\tilde{h}(z)), \quad with \quad z \leq z_b, and \tag{5.3.2.2.25}$$

$$h_u(\lambda, z_T) = \tilde{h}^*(z_T), \tag{5.3.2.2.26}$$

where the asterisk denotes a saturation value. Similarly, for the downdraft,

$$h_d(z_0) = MIN(\tilde{h}(z)). \tag{5.3.2.2.27}$$

Physically, for both updraft and downdraft, we allow for maximum buoyancy. The boundary conditions for the updraft are different than in the original scheme, which had a rigid dependence on the planetary boundary layer height. In the original scheme, the mixed layer was assumed to be well mixed, and the cloud base was located on top of the mixed layer. In semi-prognostic tests (Grell *et al.* 1991) large variations of moist static energy profiles were found in very low levels of the troposphere. This was caused by cold downdraft outflow. Naturally, the inflow to an updraft will not be a mixture of downdraft air and the more buoyant air; it is more likely the air with high moist static energy from the layer above the downdraft outflow. Furthermore, compensatory subsidence should only continue to the level from which the updraft draws its air. Compensatory uplifting may be required in very low layers of the troposphere because of the downdraft mass flux.

Feedback

The feedback to the larger-scale environment is expressed in a convenient form as

$$\left(\frac{\partial s}{\partial t}\right)_{cu} = \frac{1.}{\rho}\frac{\partial}{\partial z}F_{s-Ll}, \tag{5.3.2.2.28}$$

$$\left(\frac{\partial q}{\partial t}\right)_{cu} = -\frac{1.}{\rho}\frac{\partial}{\partial z}F_{q+l} - R, \tag{5.3.2.2.29}$$

where s is the dry static energy ($s = c_pT + gz$). The convective-scale fluxes within a grid box are defined as

$$F_{s-Ll} \equiv F_s - LF_l \tag{5.3.2.2.30}$$

$$F_{q+l} \equiv F_q + F_l \tag{5.3.2.2.31}$$

where F_s is the flux of dry static energy, F_q is the flux of water vapor, and F_l is the flux of suspended cloud liquid water. These are defined as

$$\begin{aligned} F_s(z) \equiv &+ \int_\lambda \eta_u(\lambda,z)[s_u(\lambda,z) - \bar{s}(z)]m_b(\lambda)d\lambda \\ &- \int_\lambda \eta_d(\lambda,z)[s_d(\lambda,z) - \bar{s}(z)]m_0(\lambda)d\lambda \end{aligned} \tag{5.3.2.2.32}$$

$$\begin{aligned} F_q(z) \equiv &+ \int_\lambda \eta_u(\lambda,z)[q_u(\lambda,z) - \bar{q}(z)]m_b(\lambda)d\lambda \\ &- \int_\lambda \eta_d(\lambda,z)[q_d(\lambda,z) - \bar{q}(z)]m_0(\lambda)d\lambda \end{aligned} \tag{5.3.2.2.33}$$

$$F_l(z) \equiv \int_\lambda \eta_u(\lambda,z) l(\lambda,z) m_b(\lambda) d\lambda \qquad (5.3.2.2.34)$$

The rainfall (convective-scale sink of cloud water) is defined as

$$\begin{aligned} R(z) \equiv &+ \int_\lambda \eta_u(\lambda,z) c_0(\lambda) l(\lambda,z) m_b(\lambda) d\lambda \\ &- \int_\lambda \eta_d(\lambda,z) q_e(\lambda,z) m_0(\lambda) d\lambda \end{aligned} \qquad (5.3.2.2.35)$$

Here q_e is the amount of moisture that is necessary to keep the downdraft saturated. The second term on the righthand sides is due to downdrafts and is zero above the downdraft-originating level. Below the updraft-air originating level, the first term on the right-hand sides is zero and only downdrafts affect the larger-scale environment. Below the updraft-air originating level, the convective-scale fluxes due to updrafts are zero. Between the updraft-air-originating level and the level of free convection (the LFC), F_l and R are set to zero. Since no liquid water is assumed to be in the environment as the downdraft, the downward flux due to updrafts as well as downdraft fluxes in equation (5.3.2.2.33) are zero. Schubert (1974) showed that convection will not increase the total moist static energy per unit area in a column. In essence, only precipitation can change the dry static energy budget and the total mass of water vapor. All variables in the flux terms can be determined from the equations for the static control, except $m_b(\lambda)$. This is determined in the dynamic control, which incorporates the closure assumption of the scheme and is described next.

Dynamic control

Arakawa-Schubert first introduced the cloud work function, which is an integral measure of the buoyancy force associated with a subensemble. Starting with

$$\frac{dw_u}{dt} = B_u - F_r = \frac{dw_u}{dz}\frac{dz}{dt} = \frac{d}{dt}\frac{d}{dz}\frac{w_u^2}{2} = \frac{1}{w_u}\frac{d}{dt}\frac{w_u^2}{2}, \qquad (5.3.2.2.36)$$

where B_u is the acceleration due to buoyancy and F_r the deceleration due to friction, and multiplying equation (5.3.2.2.36) by $\rho_u(\lambda,z)w_u(\lambda,z)$, gives

$$\frac{d}{dt}\rho_u\frac{w_u^2}{2} = \rho_u w_u(B_u - F_r). \qquad (5.3.2.2.37)$$

Integrating over the depth of the updraft and using $m_u = \rho_u w_u = m_b \eta_u$ yields

$$\frac{d}{dt}\int_{z_b}^{z_T} \rho_u \frac{w_u^2}{2} dz = m_b(\lambda)\int_{z_b}^{z_T} \eta_u B_u dz - D_u, \qquad (5.3.2.2.38)$$

where D is the updraft-scale kinetic energy dissipation. Equation (5.3.2.2.38) can be written in the symbolic form

$$\frac{d}{dt}\overline{KE_u} = A_u(\lambda)m_b(\lambda) - D_u(\lambda), \qquad (5.3.2.2.39)$$

where $A_u(\lambda)$ is a measure of the efficiency of kinetic energy generation inside the cloud and is called the cloud work function. It can also be written as

$$A_u(\lambda) = \int_{z_B}^{z_T} \frac{g}{C_p T(z)} \frac{\eta_u(\lambda, z)}{1+\gamma}(h_u(\lambda, z) - \tilde{h}^*(z))dz, \qquad (5.3.2.2.40)$$

where γ is defined as in equation (5.3.2.2.15). As with equations (5.3.2.2.36-5.3.2.2.38), defining a kinetic energy generation inside the downdraft leads to

$$\frac{d}{dt}\overline{KE_d} = A_d(\lambda)m_0(\lambda) - D_d(\lambda), \qquad (5.3.2.2.41)$$

where A_d, the measure of the efficiency of kinetic energy generation inside the downdraft, can be written as

$$A_d(\lambda) = \int_{z_0}^{z_{sur}} \frac{g}{C_p T(z)} \frac{\eta_d(\lambda, z)}{1+\gamma}(\tilde{h}^*(z) - h_d(\lambda, z))dz. \qquad (5.3.2.2.42)$$

Note that dry static energy instead of moist static energy would have to be used if subsaturation is assumed. We can combine equation (5.3.2.2.39) and (5.3.2.2.41) and then make use of (5.3.2.2.24) to yield

$$\frac{d}{dt}\overline{KE_{tot}} = A_{tot}(\lambda)m_b(\lambda) - D_{tot}(\lambda), \qquad (5.3.2.2.43)$$

where

$$A_{tot}(\lambda) = A_u(\lambda) + \epsilon(\lambda)A_d(\lambda) \qquad (5.3.2.2.44)$$

is the total cloud work function which was redefined as a measure of the efficiency of kinetic energy generation in updrafts as well as downdrafts. Next, AS separated the change of the cloud work function into two parts: One is due to the change in the larger-scale variables

$$\left(\frac{dA_{tot}}{dt}\right)_{LS} \equiv F(\lambda), \qquad (5.3.2.2.45)$$

and one is due to the modification of the environment by the clouds. Since the cumulus feedback on the larger-scale fields is a linear function of m_b, this term can be written in the symbolic form

$$\left(\frac{dA_{tot}}{dt}\right)_{CU} \equiv \int_{\lambda} K(\lambda,\lambda')m_b(\lambda')d\lambda. \qquad (5.3.2.2.46)$$

Therefore

$$\frac{dA_{tot}}{dt} = F(\lambda) + \int_{\lambda} K(\lambda,\lambda')m_b(\lambda')d\lambda, \qquad (5.3.2.2.47)$$

where $K(\lambda,\lambda')$ are the kernels. The kernels are an expression for the interaction between clouds (updrafts and downdrafts). Equation (5.3.2.2.47) is solved with a linear programming method (Lord 1978).

In the original version of the Arakawa-Schubert scheme, the fractional entrainment rate was the parameter which characterized the cloud. In later papers, the cloud-top detrainment level was chosen instead. If a fine vertical resolution is assumed, the second choice will most likely be better numerically, since no interpolation is necessary at the cloud tops. However, in the extremely unstable environment of the mid-latitudes, it is sometimes impossible to calculate "clouds" with cloud tops in the unstable layers. Entrainment rates would have to be extremely large to stop cloud growth. We therefore chose the fractional entrainment rate as the spectral parameter.

The procedure

The cloud base is a function of time and space. However, at a specific grid point the cloud base will be the same for every member of the subensemble. We also distinguish among an updraft-air originating level, z_u, a downdraft-air originating level, z_0, a cloud base level, z_b (the LCL), and a level of free convection, z_{bc} (LFC). Here, z_u is determined from condition (5.3.2.2.25) and determines the thermodynamic properties of the updraft from cloud type i. The air becomes saturated at z_b; condensation will start, but no convection can occur yet because the buoyancy is negative. In some instances this level could be the same as the LFC. The LFC is of great importance since this is the level at which the static control starts the calculations of individual convective elements. Since the air that feeds the cloud originates below the LCL, compensatory subsidence is allowed to reach the originating level of the updraft air.

For the downdraft, the originating level is also a function of time and space. If the downdraft exists, it will always reach the surface.

For updraft and downdraft in layer k the mass budgets are defined as

$$e_u(k,i) - d_u(k,i) = \eta_u(k+.5,i) - \eta_u(k-.5,i) and \tag{5.3.2.2.48a}$$

$$e_d(k,i) - d_d(k,i) = \eta_d(k+.5,i) - \eta_d(k-.5,i), \tag{5.3.2.2.48b}$$

where entrainment for the updraft and downdraft is defined as

$$e_u(k,i) = \mu_{ue}\Delta z_d\, \eta_u(k+.5,i) \tag{5.3.2.2.49a}$$

$$e_d(k,i) = \mu_{de}\Delta z_d\, \eta_d(k-.5,i) \tag{5.3.2.2.49b}$$

and detrainment is defined as

$$d_u(k,i) = \mu_{ud}\Delta z_d\, \eta_u(k+.5,i) \tag{5.3.2.2.50a}$$

$$d_d(k,i) = \mu_{dd}\Delta z_d\, \eta_d(k-.5,i). \tag{5.3.2.2.50b}$$

Combining the above three equations for the updraft and downdraft yields

$$\eta_u(k-.5,i) = \eta_u(k+.5,i)(1. + \mu_{ue}\Delta z_d - \mu_{ud}\Delta z_d) \tag{5.3.2.2.51a}$$

for the updraft and

$$\eta_d(k+.5,i) = \eta_d(k-.5,i)(1. + \mu_{de}\Delta z_d - \mu_{dd}\Delta z_d) \tag{5.3.2.2.51b}$$

for the downdraft. Here we define $\Delta z_d = z(k+.5) - z(k-.5)$. The discretized form for the downdraft moist static energy budget reads

$$\begin{aligned} &e_d(k,i)\tilde{h}(k) - d_d(k,i)\frac{h_d(k+.5,i) - h_d(k-.5,i)}{2} \\ &= \eta_d(k+.5,i)h_d(k+.5,i) - \eta_d(k-.5,i)h_d(k-.5,i) \end{aligned}. \tag{5.3.2.2.52}$$

Using equations (5.3.2.2.48)-(5.3.2.2.51) in equation (5.3.2.2.52) leads to

$$h_d(k+.5,i) = \frac{h_d(k-.5,i)(1. - .5\mu_{dd}\Delta z_d) + \mu_{de}\Delta z_d\,\tilde{h}(k)}{1. + \mu_{de}\Delta z_d - \mu_{dd}\Delta z_d + .5\mu_{dd}\Delta z_d}. \tag{5.3.2.2.53}$$

The moisture budget for the downdraft is developed in several steps. First, the downdraft water vapor mixing ratio before evaporation, but after entrainment, is calculated. This is done using

$$q_d(k,i) = \frac{q_d(k-.5,i)(1.-.5\mu_{dd}\Delta z_d) + \mu_{de}\Delta z_d\,\tilde{q}(k)}{1.+\mu_{de}\Delta z_d - \mu_{dd}\Delta z_d + .5\mu_{dd}\Delta z_d}. \qquad (5.3.2.2.54)$$

Next, equations (5.3.2.2.14) and (5.3.2.2.15) give the mixing ratio, q_{vd}, that the updraft or downdraft would have if saturated. Hence, the amount of moisture that is necessary to keep the downdraft from cloud type i saturated in layer k is

$$q_e(k,i) = -[q_d(k,i) - q_{vd}(k,i)]. \qquad (5.3.2.2.55)$$

Next we check whether the updraft produces enough rain to sustain saturation in the downdraft by requiring that

$$\sum c_0\Delta z(k)\,\eta_u(k-.5,i)q_l(k-.5,i) - \sum \epsilon(i)\Delta z(k)\,\eta_d(k+.5,i)q_e(k,i) > 0. \qquad (5.3.2.2.56)$$

If this is not the case, a downdraft is not allowed to exist.

Having defined the discretized versions of the equations from the static control, we now can describe the procedure.

Using the larger-scale temperature and moisture fields (T_0, q_0) at time t_0, and given a functional or empirical relationship for μ_d, μ_{de}, and μ_{dd}, the equations from the static control are used to calculate $\mu_{ue}, h_u(z,i), h_d(z,i), q_u(z,i), q_d(z,i), \eta_u(z,i)$, and $\eta_d(z,i)$ for cloud type i. These are needed to determine the total cloud work function A_{tot} using

$$A_{tot}(i) = A_u(i) + \epsilon A_d(i). \qquad (5.3.2.2.57)$$

The discretized versions of equations (5.3.2.2.40) and (5.3.2.2.42) that are used to determine the cloud work functions for updrafts and downdrafts are

$$A_u(i) = \sum_{k=LFC}^{k=ktop}\left[\frac{g}{c_p\,T(k-.5)}\eta_u(k-.5,i) * \left(\frac{h_u(k-.5,i) - \tilde{h}^*(k-.5)}{1+\gamma(k-.5)}\right) * (z(k-1) - z(k))\right] \qquad (5.3.2.2.58)$$

and

$$A_d(i) = \sum_{k=z_0}^{k=sur} \left[\frac{g}{c_p\, T(k-.5)} \eta_d(k-.5,i) * \left(\frac{h_d(k-.5,i) - \tilde{h}^*(k-.5)}{1+\gamma(k-.5)} \right) * (z(k) - z(k-1)) \right] \quad (5.3.2.2.59)$$

The kernels of cloud type i are by definition the changes of the cloud work functions due to another subensemble, i'. Thus, following Lord (1978), T_0 and q_0 are modified by an arbitrary amount of mass flux, $m_b' \Delta t'$, from the i' subensemble. This is done for every possible subensemble and can be written in the symbolic form

$$\bar{T}'(k,i) = \bar{T}(k) + \delta_{i'}(\bar{T}(k)) m_b' \Delta t', \quad (5.3.2.2.60)$$

$$\bar{q}'(k,i) = \bar{q}(k) + \delta_{i'}(\bar{q}(k)) m_b' \Delta t'. \quad (5.3.2.2.61)$$

The δ terms, which are changes per unit $m_b(i)$, are easily calculated from budget considerations as in Lord (1978). With the downdraft terms, the moist static energy budget of layer k and cloud type i becomes

$$\begin{aligned} \frac{\Delta p(k)}{g} \delta_{i'}(\tilde{h}(k,i)) = &+ (\eta_u(k-.5,i) - \epsilon(i)\eta_d(k-.5,i))\tilde{h}(k-.5) \\ &- (\eta_u(k+.5,i) - \epsilon(i)\eta_d(k+.5,i))\tilde{h}(k+.5) \\ &- (e_u(k,i) + \epsilon(i) e_d(k,i))\tilde{h}(k) \\ &+ d_u(k,i) \frac{h_u(k+.5,i) + h_u(k-.5,i)}{2} \\ &+ \epsilon(i) d_d(k,i) \frac{h_d(k+.5,i) + h_d(k-.5,i)}{2} \end{aligned} \quad , \quad (5.3.2.2.62)$$

where $e_u(k,i) and d_u(k,i)$ are the entrainment and detrainment for the updraft, and $\Delta p(k)$ is defined by $\Delta p(k) = p(k+.5) - p(k-.5)$. A simple physical interpretation of the terms on the righthand side can be understood by looking at Fig. 5.2. The first term is the subsidence on top of the layer, the second is the subsidence on the bottom of the layer. This subsidence is an environmental compensatory mass flux due to the updraft and downdraft mass fluxes inside the cloud. Note that below z_u the "compensatory subsidence" may be

compensatory uplifting, since in that case only downdrafts exist. The third term represents entrainment into the updraft and downdraft; the fourth term represents detrainment from the edges of the updraft; the fifth term represents detrainment from the edges of the downdraft.

For the moisture budget,

$$\begin{aligned}\frac{\Delta p(k)}{g}\delta_{i\prime}(\tilde{q}(k,i)) = &+ (\eta_u(k-.5,i) - \epsilon(i)\eta_d(k-.5,i))\tilde{q}(k-.5) \\ &- (\eta_u(k+.5,i) - \epsilon(i)\eta_d(k+.5,i))\tilde{q}(k+.5) \\ &- (e_u(k,i) + \epsilon(i)e_d(k,i))\tilde{q}(k) \\ &+ d_u(k,i)\frac{q_u(k+.5,i)+q_u(k-.5,i)}{2} \\ &+ \epsilon(i)d_d(k,i)\frac{q_d(k+.5,i)+q_d(k-.5,i)}{2}\end{aligned} \qquad (5.3.2.2.63)$$

At the cloud top, downdrafts have no effects and updrafts detrain all their mass.

$$\begin{aligned}\frac{\Delta p(ktop)}{g}\delta_{i\prime}(\tilde{h}(ktop,i)) = &- \eta_u(ktop+.5,i)\tilde{h}(ktop+.5) \\ &- e_u(ktop,i)\tilde{h}(ktop) \\ &+ d_u(ktop,i)\frac{h_u(ktop+.5,i)+h_u(ktop,i)}{2} + \eta_u(ktop,i)h_u(ktop,i)\end{aligned} \qquad (5.3.2.2.64)$$

and

$$\begin{aligned}\frac{\Delta p(ktop)}{g}\delta_{i\prime}(\tilde{q}(ktop,i)) = &- \eta_u(ktop+.5,i)\tilde{q}(ktop+.5) \\ &- e_u(ktop,i)\tilde{q}(ktop) \\ &+ d_u(ktop,i)\frac{q_u(ktop+.5,i)+q_u(ktop,i)}{2} + \eta_u(ktop,i)q_u(ktop,i)\end{aligned} \qquad (5.3.2.2.65)$$

Here $\Delta p(ktop) = p(ktop+.5) - p(ktop-.5)$. Note that in the fourth term we have included the detrainment of all the cloud mass at the cloud top. Finally, at the surface

$$\begin{aligned}\frac{\Delta p(ksur)}{g}\delta_{i\prime}(\tilde{h}(ksur,i)) = &- \epsilon(i)\eta_d(ksur-.5,i))\tilde{h}(ksur-.5) \\ &+ \epsilon(i)\eta_d(ksur,i)h_d(ksur,i) \\ &- \epsilon(i)e_d(ksur-.5,i)\tilde{h}(ksur-.5) \\ &+ \epsilon(i)d_d(ksur,i)\frac{h_d(ksur,i)+h_d(ksur-.5,i)}{2}\end{aligned} \qquad (5.3.2.2.66)$$

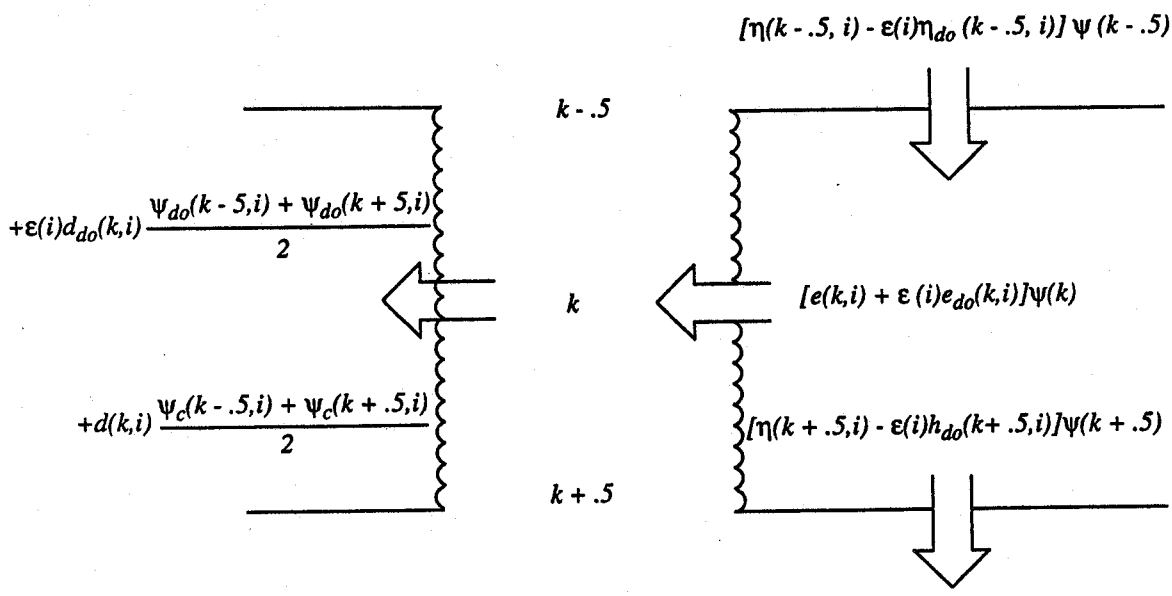

Figure 5.2 Illustration of budget for thermodynamic variable ψ in layer k.

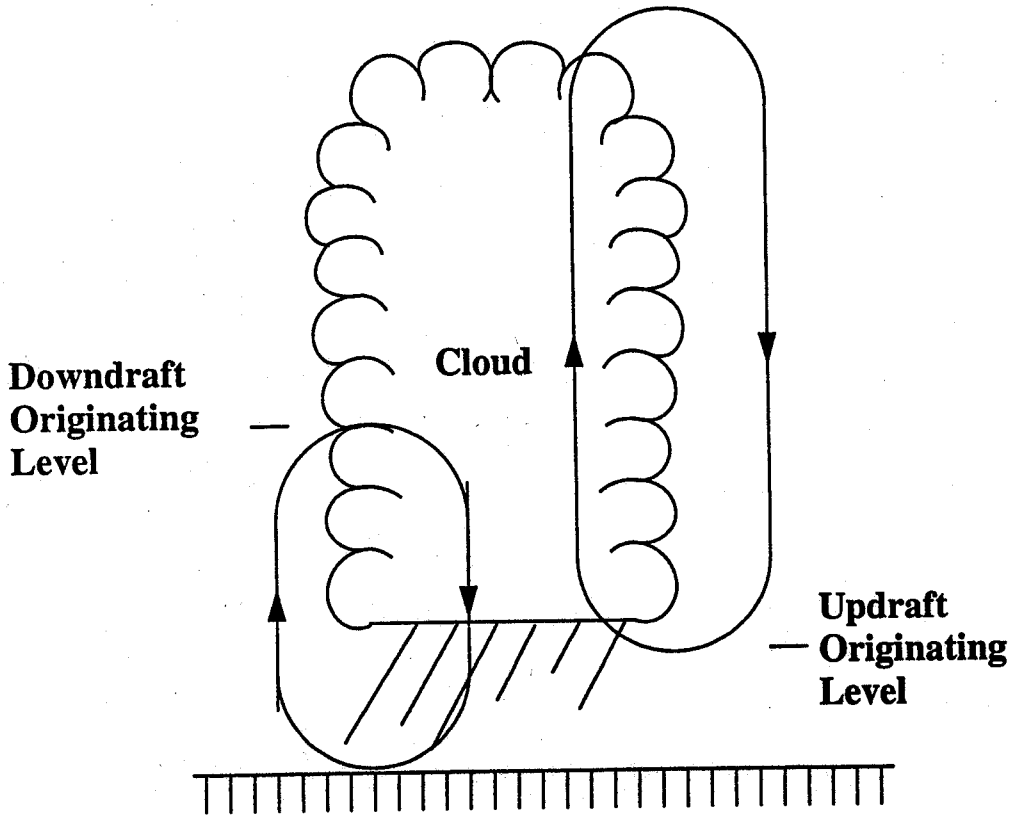

Figure 5.3 Conceptual picture of convection parameterized in Grell scheme.

and

$$\frac{\Delta p(ksur)}{g}\delta_{i,i'}(\tilde{q}(ksur,i)) = -\epsilon(i)\eta_d(ksur-.5,i))\tilde{q}(ksur-.5) + \epsilon(i)\eta_d(ksur,i)q_d(ksur,i) - \epsilon(i)e_d(ksur-.5,i)\tilde{q}(ksur-.5) + \epsilon(i)d_d(ksur,i)\frac{q_d(ksur,i)+q_d(ksur-.5,i)}{2}, \quad (5.3.2.2.67)$$

with $\Delta p(ksur) = p(ksur+.5) - p(ksur-.5)$. Here, the first term is the compensatory environmental mass flux, the second term is the detrainment of all downdraft air at the bottom, the third term is entrainment into the downdraft, and the fourth term is the detrainment of air around the downdraft edges.

The new thermodynamic fields, $T_0{}'(k,i')$ and $q_0{}'(k,i')$, are then used again from the static control to calculate new cloud properties and a new cloud work function, $A'_{tot}(i',i)$. Note that T'_0 and q'_0 are now functions of the subensemble i'. From the definition of the kernel we then can calculate the kernels simply as

$$K(i,i') = \frac{A'_{tot}(i',i) - A_{tot}(i)}{m_b \text{“}\Delta t\text{“}}. \quad (5.3.2.2.68)$$

Next, we go back to the original fields and modify those with the large-scale advective changes to get

$$T\text{“}(k) = T_0 + \left(\frac{\partial T}{\partial t}\right)_{ADV}\Delta t \quad (5.3.2.2.69)$$

and

$$q\text{“}(k) = q_0 + \left(\frac{\partial q}{\partial t}\right)_{ADV}\Delta t, \quad (5.3.2.2.70)$$

where (5.3.2.2.69) and (5.3.2.2.70) are applied over Δt= 30 min. The double prime quantities are then used again by the static control, which will calculate new cloud properties, and so new cloud work functions, $A_{tot}\text{“}(i)$, will be determined. Next, the large-scale forcing (by definition the change of the cloud work function due to large-scale effects only) is calculated using

$$F(i) = \frac{A_{tot}\text{“}(i) - A_{tot}(i)}{\Delta t}. \quad (5.3.2.2.71)$$

The large-scale forcing and the kernels are then both used by the dynamic control to estimate the cloud base mass flux distribution function, m_b, using an IMSL subroutine to solve the linear programming problem. Finally, the feedback to the larger-scale environment is simply given by

$$\left(\frac{\partial T(k)}{\partial t}\right)_{CU} = \sum_{i'=1}^{i'_{MAX}} \delta'_i(T(k)) m_b(i') and \tag{5.3.2.2.72}$$

$$\left(\frac{\partial q(k)}{\partial t}\right)_{CU} = \sum_{i'=1}^{i'_{MAX}} \delta'_i(q(k)) m_b(i'), \tag{5.3.2.2.73}$$

where the precipitation can be calculated using

$$\begin{aligned} P = & \sum_{i'=1}^{i'_{MAX}} \sum_{k=1}^{k=ktop} c_0 \Delta z(k) q_l(k+.5,i) m_u(k+.5,i) \\ & - \sum_{i'=1}^{i'_{MAX}} \sum_{k=1}^{k=ktop} \Delta z(k) q_{ev}(k+.5,i) m_d(k+.5,i) \end{aligned} \tag{5.3.2.2.74}$$

5.3.2.3 The Grell scheme

This is a very simple scheme that was constructed to avoid first-order sources of errors (Grell 1993). The very simplistic conceptual picture of how this parameterization is envisioned to function is shown in Fig. 5.3. Clouds are pictured as two steady-state circulations, caused by an updraft and a downdraft. There is no direct mixing between cloudy air and environmental air, except at the top and the bottom of the circulations. The cloud model that is used to calculate cloud properties in this scheme is formulated with only a few equations. Mass flux is constant with height, and there is no entrainment or detrainment along the cloud edges. We can simply write

$$m_u(z) = m_u(z_b) = m_b \ , and \tag{5.3.2.3.1}$$

$$m_d(z) = m_d(z_0) = m_0 \tag{5.3.2.3.2}$$

for the mass flux of the updraft (m_u) and the downdraft (m_d). Here m_b and m_0 are simply the mass fluxes of the updraft and downdraft at their originating level. If it is assumed that

the conditions at originating levels are given by the environment, for any thermodynamic variable , the budget inside the cloud simply becomes

$$\alpha_u(z) = \tilde{\alpha}(z_b) + S_u(z) \ , and \tag{5.3.2.3.3}$$

$$\alpha_d(z) = \tilde{\alpha}(z_0) + S_d(z), \tag{5.3.2.3.4}$$

where α is a thermodynamic variable, the tilde denotes an environmental value, and S stands for sources or sinks. For moist static energy

$$\tilde{h}(z) = C_p\tilde{T}(z) + gz + L\tilde{q}(z), \tag{5.3.2.3.5}$$

equations (3) and (4) simply become

$$h_u(z) = \tilde{h}(z_b) \tag{5.3.2.3.6}$$

and

$$h_d(z) = \tilde{h}(z_0). \tag{5.3.2.3.7}$$

For the moisture budget of the updraft we can make use of the approximate equations (5.3.2.2.14) and (5.3.2.2.15) to calculate the mixing ratio inside the cloud if saturation is assumed. Together with equations (5.3.2.3.3) and (5.3.2.3.4), this will give us S_u and S_d, the condensation and evaporation. Note also that no cloud water is assumed to exist; all water is converted to rain.

Given boundary conditions, equations (5.3.2.3.1)-(5.3.2.3.7) have two unknowns, m_b, and m_0. In order to leave only one unknown variable, the originating mass flux of the downdraft is made a function of the updraft mass flux and the reevaporation of convective condensate, as in the previous section (see equations (5.3.2.2.20)-(5.3.2.2.24)). Therefore,

$$m_0 = \frac{\beta I_1 m_b}{I_2} = \epsilon m_b. \tag{5.3.2.3.8}$$

Here, $1-\beta$ is the precipitation efficiency. To specify boundary conditions, we assume

$$h_u(z) = h_u(z_b) = MAX(\tilde{h}(z)), \quad with \quad z \leq z_b, and \tag{5.3.2.3.9}$$

$$h_u(z_T) = \tilde{h}^*(z_T), \tag{5.3.2.3.10}$$

where the asterisk denotes a saturation value. Similarly, for the downdraft,

$$h_d(z) = h_d(z_0) = MIN(\tilde{h}(z)). \qquad (5.3.2.3.11)$$

Physically, for both, updraft and downdraft, we allow for maximum buoyancy. For this deep convection scheme, the cloud base for the updraft is not restricted to the boundary layer, but can be anywhere in the troposphere.

Feedback to the larger-scale equations

To avoid zero-order sources of errors, the feedback must include the cooling effects of moist convective downdrafts. Furthermore, lateral mixing should never be excessive, especially if the cloud properties have been calculated with a steady-state cloud model. Keeping in mind the conceptual picture in Fig. 5.3, the feedback for this scheme is entirely determined by compensating mass fluxes and detrainment at cloud top and bottom. Conceptually, no averaging (such as the normally used top-hat or Reynolds averaging methods) is necessary. This does not mean that scale-separation is not required, but for this parameterization it is not necessary to assume that the fractional area coverage is very small. Note, however, that any parameterization can only make sense if a clear scale separation exists. None of the parameterized effects may be resolved by the larger-scale. Assuming that the conceptual picture in Fig. 5.3 happens in only one grid box, we can express the changes caused by the convection as

$$\left(\frac{\partial \tilde{h}(k)}{\partial t}\right)_{CU} = \frac{\partial h_u(z) m_b}{\partial z} - \frac{\partial \tilde{h}(z) m_b}{\partial z} - \frac{\partial h_d(z) m_0}{\partial z} + \frac{\partial \tilde{h}(z) m_0}{\partial z} \qquad (5.3.2.3.12)$$

and

$$\left(\frac{\partial q(k)}{\partial t}\right)_{CU} = \frac{\partial q_u(z) m_b}{\partial z} - \frac{\partial \tilde{q}(z) m_b}{\partial z} - \frac{\partial q_d(z) m_0}{\partial z} + \frac{\partial \tilde{q}(z) m_0}{\partial z}. \qquad (5.3.2.3.13)$$

Because of the simplicity of the static control, these equations can be further simplified to give

$$\left(\frac{\partial \tilde{h}(k)}{\partial t}\right)_{CU} = m_b \frac{\partial \tilde{h}(z)}{\partial z}(1-\epsilon) + m_b\left(\frac{\partial h_u(z)}{\partial z} - \epsilon \frac{\partial h_d(z)}{\partial z}\right) \qquad (5.3.2.3.14)$$

$$\left(\frac{\partial q(k)}{\partial t}\right)_{CU} = m_b \frac{\partial \tilde{q}(z)}{\partial z}(1-\epsilon) + m_b\left(\frac{\partial q_u(z)}{\partial z} - \epsilon \frac{\partial q_d(z)}{\partial z}\right). \qquad (5.3.2.3.15)$$

The rainfall is defined as

$$R \equiv I_1 m_b (1 - \beta). \tag{5.3.2.3.16}$$

The second term on the righthand sides of equations (5.2.2.3.14) and (5.2.2.3.15) are due to downdrafts and are zero above the downdraft originating level. Below the updraft-air originating level, the first term of the right-hand sides are zero and only downdrafts affect the larger-scale environment. All variables in the flux terms can be determined from the equations of the static control, except m_b.

Dynamic control

Because of the simplicity of the above equations, many closure assumptions can be used. The most simple closure is a Kuo-type assumption, which relates the rainfall rate to the moisture convergence. However, more applicable seems to be a stability closure. Again we have two choices. We could assume that the clouds will remove the available buoyant energy as in other mesoscale parameterizations, or that the clouds will stabilize the environment as fast as the larger-scale (or also sub-grid scale) destabilizes it, or even a mixture of both. Although both assumptions are easily implemented, we chose the closure which depends on the rate of destabilization. In this closure the change of the available buoyant energy due to convection offsets the changes due to other effects (larger-scale destabilization as well as sub-grid scale destabilization), yielding

$$\left(\frac{dABE}{dt}\right)_{OTH} = -\left(\frac{dABE}{dt}\right)_{CU}. \tag{5.3.2.3.17}$$

Next, the change due to the convection is normalized in terms of the mass flux to read

$$\left(\frac{dABE}{dt}\right)_{CU} \equiv m_b \left(\frac{dABE}{dt}\right)_{NCU}, \tag{5.3.2.3.18}$$

where subscript NCU denotes the change of the available buoyant energy due to a cloud normalized by the cloud-base mass flux. Equations (5.3.2.3.17) and (5.3.2.3.18) are used to calculate m_b.

The Procedure

This section describes in detail the procedure necessary to calculate the convective feedback. First, we will explain the very simplistic approach to calculate a normalized feedback, then we will describe how the closure assumption determines the mass flux.

Using the larger-scale temperature and moisture fields (T_0, q_0) at time t_0, $h_u(z), h_d(z), q_u(z), q_d(z)$ are simply arrived at (see equations (5.3.2.3.6)-(5.3.2.3.10). The first calculation is the determination of the integrals I_1 and I_2 (calculated as residuals using equations (5.3.2.3.8) and (5.3.2.3.9). The next step is then to estimate the convective changes per unit mass flux (before knowing the actual m_b's). This is done by estimating the net change of a thermodynamic variable α in a layer k by using

$$\frac{\Delta p(k)}{g}\delta(\tilde{\alpha}(k)) = (1-\epsilon)(\tilde{\alpha}(k-.5) - \tilde{\alpha}(k+.5)), \tag{5.3.2.3.19}$$

where $\Delta p(k)$ is defined by $\Delta p(k) = p(k+.5) - p(k-.5)$. This subsidence is an environmental compensatory mass flux due to the updraft and downdraft mass fluxes inside the cloud. Note that below z_u the "compensatory subsidence" may be compensatory uplifting, since in that case only downdrafts exist.

At the cloud top,

$$\frac{\Delta p(ktop)}{g}\delta(\tilde{\alpha}(ktop)) = -\tilde{\alpha}(ktop-.5) + \alpha_u(ktop). \tag{5.3.2.3.20}$$

Here $\Delta p(ktop) = p(ktop+.5) - p(ktop-.5)$. Finally, at the surface (the downdraft tops)

$$\frac{\Delta p(ksur)}{g}\delta(\tilde{\alpha}(ksur)) = -\epsilon(-\tilde{\alpha}(ksur-.5) + \alpha_d(ksur)), \tag{5.3.2.3.21}$$

with $\Delta p(ksur) = p(ksur+.5) - p(ksur-.5)$. Here, the first term is the compensatory environmental mass flux, and the second term is the detrainment of all downdraft air at the bottom. These normalized changes are also used in the calculation of the final feedback (after m_b is determined), which is simply given by

$$\left(\frac{\partial \alpha(k)}{\partial t}\right)_{CU} = \delta(\alpha(k))m_b. \tag{5.3.2.3.22}$$

To calculate the mass flux m_b, we define the buoyant energy which is available to a cloud (updraft and downdraft) as

$$ABE = \sum_{k=LFC}^{k=ktop}\left[\frac{g}{c_p\,T(k-.5)} * \left(\frac{\tilde{h}(kb) - \tilde{h}^*(k-.5)}{1+\gamma(k-.5)}\right) * (z(k-1) - z(k))\right] + \sum_{k=z_0}^{k=sur}\left[\frac{g}{c_p\,T(k-.5)} * \left(\frac{\tilde{h}(k0) - \tilde{h}^*(k-.5)}{1+\gamma(k-.5)}\right) * (z(k) - z(k-1))\right]. \tag{5.3.2.3.23}$$

where γ is defined in equation (5.3.2.2.15). We can calculate ABE (similar to Lord 1982) for the unchanged environment as well as for the environment which has been modified by some arbitrary mass flux $m_b'\Delta t'$. Hence, we can write

$$NA = \left(\frac{dABE}{dt}\right)_{NCU} = \frac{ABE' - ABE}{m_b'\Delta t'}. \tag{5.3.2.3.24}$$

ABE are calculated using T_0 and q_0, while ABE' are calculated after modification of the thermodynamic variables by an arbitrary amount of mass flux, $m_b'\Delta t'$, where

$$\alpha'(k) = \alpha(k) + \delta(\alpha(k))m_b'\Delta t'. \tag{5.3.2.3.25}$$

For a closure which depends on the rate of destabilization, we have to calculate the change in the available buoyant energy due to large-scale or other subgrid-scale effects. We modify the thermodynamic fields with

$$\alpha"(k) = \alpha_0 + \left(\frac{\partial\alpha}{\partial t}\right)_{LS+SUBG}\Delta t, \tag{5.3.2.3.26}$$

where (5.3.2.3.26) is applied at every timestep Δt. These double prime quantities are then used to calculate the changes in the available buoyant energy due to "non-convective" effects. As a result, the equation for the mass flux becomes

$$m_b = \frac{ABE" - ABE}{(ABE' - ABE)m_b'}. \tag{5.3.2.3.27}$$

5.3.3 Parameterization of shallow convection

The shallow convection scheme is constructed to be able to serve two tasks. It parameterizes planetary boundary layer (PBL) forced shallow non-precipitating convection as well as mid-tropospheric shallow convection caused by other sub-grid scale effects (such as cloud top radiational cooling). The first might not be necessary when the parameterization is coupled to a higher order closure PBL scheme. It will transport moisture from inside the boundary layer into the layers just above the boundary layer. This is accomplished by emulating bubbles (forced by surface heat and moisture fluxes only, with strong lateral mixing) which rise without precipitation formation through the top of the boundary layer into the free atmosphere, where they then lose their buoyancy.

Because of the strong lateral mixing, they usually do not rise more than 50-75 mb. The physics involved in describing the second kind of shallow convection is the same, except for the forcing.

To parameterize this type of convection we assume that a "convective element" can be characterized by a bubble which rises through several model layers. It is assumed to be forced by planetary boundary layer fluxes or radiational cooling tendencies. Some of the elements of this parameterization are based on an Arakawa-Schubert type scheme (section 5.3.2.2) and some are based on the simple one-cloud scheme described in section 5.3.2.3. However, the clouds (shallow "convective elements") are characterized by different properties. They usually have large mixing, are non-precipitating, and have no convective-scale downdrafts. They are forced by subgrid-scale processes only. The following description will be focused on differences from the previously described models. Since the sole purpose of this scheme is to represent "very" shallow convection, it is also constructed as a one-cloud scheme. Although it implicitly uses equations (5.3.2.2.1)-(5.3.2.2.4), considerable simplifications can be made by assuming strong lateral mixing (detrainment being equally as strong as entrainment). Equations (5.3.2.2.1) through (5.3.2.2.4) then read

$$\mu = 0, \tag{5.3.3.1}$$

$$\mu_e = \mu_d = \frac{.2}{r}, \tag{5.3.3.2}$$

and

$$\frac{\partial \alpha_c}{\partial z} = \frac{.2}{r}(\tilde{\alpha} - \alpha_c) + S_c, \tag{5.3.3.3}$$

where r in equation (5.3.3.2) is the radius of the element. The parameterization will be sensitive to the choice of r. For this type of convection we assume $r = 50m$. When assuming that no precipitation forms or evaporates, equations (5.3.3.1)-(5.3.3.3), together with initial conditions (5.3.2.2.25) and (5.3.2.2.26), form a simple set of equations to determine the properties of the convective element, if r is given. Without precipitation formation, S_c in equation (5.3.3.3) is zero. For the feedback, equations (5.3.2.2.32)-(5.3.2.2.34) simply

become

$$FS_s(z) \equiv [s_c(z) - \bar{s}(z)]m_c, \tag{5.3.3.4}$$

$$FS_q(z) \equiv [q_c(z) - \bar{q}(z)]m_c, \tag{5.3.3.5}$$

$$FS_l(z) \equiv l(z)m_c = 0. \tag{5.3.3.6}$$

The only unknown in these equations is the mass flux. It is determined in the dynamic control, where we make use of the definition of the cloud work function (5.3.2.2.40) and simply impose

$$\left(\frac{dA(scl)}{dt}\right)_{CU} = -\left(\frac{dA(scl)}{dt}\right)_{SUBG}. \tag{5.3.3.7}$$

Note that since the cloud work function is independent of mass flux (mass flux is constant with height), equation (5.3.2.2.40) for cloud-type *scl* simplifies to

$$A(scl) = \int_{z_B}^{z_T} \frac{g}{C_pT(z)} \frac{1}{1+\gamma}(h_c(z) - \tilde{h}^*(z))dz. \tag{5.3.3.8}$$

Subscript CU refers to the effects due to convection, and $SUBG$ to effects due to sub-grid scale forcing. $A(scl)$ becomes simply the buoyancy which is available for that particular cloud *scl*. Therefore, physically, the change of the efficiency of kinetic energy generation due to cloud *scl* is directly proportional to the buoyancy generation by sub-grid scale forcing. To arrive at a useful closure, the term on the left hand side of equation (5.3.3.7) is normalized by the massflux to yield

$$m_c\left(\frac{dA(scl)}{dt}\right)_{NCU} = -\left(\frac{dA(scl)}{dt}\right)_{SUBG}. \tag{5.3.3.10}$$

Here, the subscript NCU now stands for the change of A due to a unit mass of cloud *scl*. The variables in equation (5.3.3.10) are known, except for m_c. After using (5.3.3.10) to calculate m_c, we can then calculate the feedback. Note that in equation (5.3.3.2), mc is not dependent on height, and is simply the cloud base mass flux. It should be noted here that the above described parameterization will greatly benefit from a high vertical resolution. In some instances it may be of use to allow the shallow convection scheme to be called several times in a column (stacked on top of each other), since different sub-grid-scale forcing mechanisms may act at the same time in one column, but at different levels.

5.4 Planetary boundary layer parameterizations

5.4.1 Surface-Energy equation

Over land, the surface temperature T_g is computed from a surface energy budget that is base on the "force-restore" method developed by Blackadar (Zhang and Anthes 1982). The budget equation is

$$C_g \frac{\partial T_g}{\partial t} = R_n - H_m - H_s - L_v E_s, \tag{5.4.1.1}$$

where C_g is the thermal capacity of the slab per unit area, R_n is the net radiation, H_m is the heat flow into the substrate, H_s is the sensible heat flux into the atmosphere, L_v is the latent heat of vaporization, and E_s is the surface moisture flux. Blackadar (1979) shows that the following formulation enables the amplitude and phase of the slab temperature to be identical to the surface temperature of a real soil layer of uniform thermal conductivity λ and heat capacity per unit volume C_s, with C_g related to these parameters and the angular velocity of the earth Ω by

$$C_g = .95\left(\frac{\lambda C_s}{2\Omega}\right)^{1/2}. \tag{5.4.1.2}$$

The thermal capacity, C_g, is related to a parameter called the thermal inertia, χ, where χ is

$$\chi = (\lambda C_s)^{1/2}. \tag{5.4.1.3}$$

From (5.4.1.2) and (5.4.1.3),

$$C_g = 3.293 \times 10^6 \chi, \tag{5.4.1.4}$$

where χ is specified in the model as a function of land-use characteristic (Appendix 4). The terms on the right hand side of (5.4.1.1) are described as follows:

5.4.1.1 Net radiative flux R_n

Radiation is the driving force of the diabatic planetary boundary layer (PBL) and is the most important component of the slab-energy budget.

$$R_n = Q_s + I_s \tag{5.4.1.5}$$

where Q_s and I_s are the net surface shortwave and longwave irradiances.

a. Clear Sky

For clear sky, the amount of solar radiation absorbed by the slab, including multiple reflection of short waves, is approximated as

$$Q_s = S_0(1-A)\tau cos\psi, \tag{5.4.1.6}$$

where S_0 is the solar constant (1395.6 W m^{-2}), A is the albedo. ψ is the zenith angle, and τ is the short-wave transmissivity. The term $cos\psi$ is given by

$$cos\psi = sin\phi sin\delta + cos\phi cos\delta cosh_0, \tag{5.4.1.7}$$

where ϕ represents the latitude of the location, δ the solar declination, and h_0 the local hour angle of the sun (Sellers. 1974).

The short-wave transmissivity for multiple reflection (Benjamin 1983) is

$$\tau = \frac{\tau_a[\tau_s + (1-\tau_s)(1-b)]}{(1-X_R A)}, \tag{5.4.1.8}$$

where τ_a is the absorption transmissivity, τ_s is the scattering transmissivity, b is the backscattering coefficient, and X_R is the multiple reflection factor

$$X_R = \tau_{ad}(1-\tau_{sd})b_d, \tag{5.4.1.9}$$

where the subscript d denotes diffuse.

All the clear-air transmissivities ($\tau_a, \tau_s, \tau_{ad}, \tau_{sd}$) and backscattering coefficients (b and b_d) are determined as a function of path length and precipitable water from a look-up table from the Carlson and Boland (1978) radiative transfer model. Transmissivities are then adjusted for surface pressure as follows:

$$\tau = \frac{1+(\tau'-1)p_s}{1013.25}, \tag{5.4.1.10}$$

where τ' is the transmissivity from the look-up table (appendix 2) obtained by assuming the surface pressure is 1013.25mb, and p_s is the surface pressure at the location. The net longwave radiation, I_s, is equal to the sum of the outgoing ($I\uparrow$) and downward ($I\downarrow$) longwave radiation. The outgoing longwave radiation is

$$I\uparrow = \epsilon_g \sigma_{SB} T_g^4, \tag{5.4.1.11}$$

where ϵ_g is the slab emissivity, T_g is the ground temperature, and σ_{SB} the Stefan-Boltzmann constant. The downward longwave radiation absorbed at the surface is

$$I\downarrow = \epsilon_g \epsilon_a \sigma_{SB} T_a^4, \tag{5.4.1.12}$$

where T_a is the atmospheric temperature in the layer above the surface, and ϵ_a, the atmospheric longwave emissivity, is given by

$$\epsilon_a = .725 + .17 log_{10} w_p, \tag{5.4.1.13}$$

in which w_p is the precipitable water in centimeters

b. Cloudy skies

For cloudy skies, a cloud parameterization scheme (Benjamin 1983) is used to simulate the effects of clouds on short-wave and downward longwave radiation. Groups of sigma levels are chosen to correspond to low-, middle-, and upper-cloud layers based upon an assumed surface pressure of 1000mb. The clouds below 800mb are designated as low clouds, middle clouds are those between 800mb and 450mb, and upper clouds are those above 450mb.

The attenuation of short-wave radiation by cloud is parameterized with absorption (τ_{ac}) and scattering (τ_{sc}) transmissivities. The transmissivities through the three cloud layers are given by

$$\tau_{ac} = \prod_{i=1}^{3} [1 - (1 - \tau_{ai})] n_i \tag{5.4.1.14}$$

and

$$\tau_{sc} = \prod_{i=1}^{3} [1 - (1 - \tau_{si})] n_i, \tag{5.4.1.15}$$

where $i = 1, 2, 3$ represents low, middle, and high clouds, respectively, n_i is the cloud fraction, and τ_{ai} and τ_{si} are given in table 5.1. The minimum short-wave absorption transmissivity is set at 0.7, and the minimum scattering transmissivity is set at 0.44.

The cloud fraction is based on relative humidity. Cloud fraction at low and middle levels is

$$n = 4.0RH - 3.0, \tag{5.4.1.16}$$

and in the upper atmosphere

$$n = 42.5RH - 1.5, \tag{5.4.1.17}$$

where RH is the maximum relative humidity found in the model layers within the low, middle, or upper cloud layers. The expression for effective short-wave transmissivity under cloudy skies is

$$\tau = \frac{\tau_{ac}\tau_{sc}\tau_a[\tau_s + (1-\tau_s)(1-b)]}{(1 - X_c A)}, \tag{5.4.1.18}$$

where the multiple reflection factor for cloudy skies (X_c) is defined as

$$X_c = \tau_{ad}\tau_{ac}(1 - \tau_{sd}\tau_{sc})\bar{b}_d \tag{5.4.1.19}$$

in which $\bar{b}_d$, the mean backscattering coefficient, is

$$\bar{b}_d = \frac{b_d(1-\tau_{sd}) + (1-\tau_{sc})}{(1-\tau_{sd}) + (1-\tau_{sc})}. \tag{5.4.1.20}$$

The cloud enhancement of long-wave radiation incident on the ground is expressed as

$$I\downarrow' = I\downarrow \left(1 + \sum_{i=1}^{3} c_i n_i\right), \tag{5.4.1.21}$$

where c_i are the enhancement coefficients at different levels (table 5.2).

Table 5.1 Cloud absorption and scattering transmissivities.

Cloud Level	Absorption (τ_{ai})	Scattering (τ_{si})
Low	0.80	0.48
Middle	0.85	0.60
High	0.98	0.80

Table 5.2 Enhancement coefficients c_i on longwave radiation due to clouds.

Cloud Level	Coefficient
Low	0.26
Middle	0.22
High	0.06

5.4.1.2 Heat Flow into the Substrate H_m

The transfer of heat due to molecular conduction is calculated from the equation

$$H_m = K_m C_g (T_g - T_m), \tag{5.4.1.22}$$

where K_m is the heat transfer coefficient expressed as $K_m = 1.8\Omega$, Ω is the angular velocity of the earth, and T_m is the temperature of the substrate, which is presently taken to be a constant value equal to the mean surface-air temperature over the period of simulation. If the model is used in a forecast mode rather than a research mode, T_m may be set equal to the mean surface temperature of the previous day.

5.4.1.3 Sensible-Heat Flux H_s and Surface Moisture Flux E_s

These fluxes are computed in different ways, depending upon what PBL parameterization is used. Details will be described in the next sections.

5.4.2 Bulk-aerodynamic parameterization

The bulk-aerodynamic option of the PBL physics follows Deardorff (1972). It is a very inexpensive choice. The surface-heat fluxes are given by

$$H_s = \rho_a c_{pm} C_\theta C_u (\theta_g - \theta_a) V, \tag{5.4.2.1}$$

where ρ_a and θ_a are density and potential temperature at the lowest model layer, C_θ and C_u are exchange coefficients (Deardorff 1972) defined as

$$C_u = C_{uN} \left(\frac{1 - R_{iB}}{R_{iC}} \right) \tag{5.4.2.2}$$

and

$$C_\theta = C_{\theta N} \left(\frac{1 - R_{iB}}{R_{iC}} \right) \tag{5.4.2.3}$$

for stable conditions ($0 \leq R_{iB} \leq .9R_{ic}$), and

$$C_u = \frac{1}{\frac{1}{C_{uN}} - 25exp(.26\psi - .03\psi^2)} \tag{5.4.2.4}$$

and

$$C_\theta = \frac{1}{\frac{1}{C_{\theta N}} + \frac{1}{C_u} - \frac{1}{C_{uN}}} \tag{5.4.2.5}$$

for the unstable case ($R_{iB} \leq 0$). Here C_{uN} and $C_{\theta N}$ are the neutral values for C_u and C_θ, and are given by

$$C_{uN} = \left[k^{-1} ln \left(\frac{.025h}{z_0}\right) + 8.4\right]^{-1} \tag{5.4.2.6}$$

and

$$C_{\theta N} = \left[0.74k^{-1} ln \left(\frac{.025h}{z_0}\right) + 7.3\right]^{-1}, \tag{5.4.2.7}$$

where $R_{ic} = 3.05$, h is the depth of the lowest model layer, ψ is defined as

$$\psi = log_{10}(-R_{iB}) - 3.5, \tag{5.4.2.8}$$

and the velocity V is given by

$$V = (V_a^2 + V_c^2)^{1/2}. \tag{5.4.2.9}$$

V_a is the wind-speed at the lowest model layer, and V_c is a convective velocity, which is important under conditions of low mean wind-speed and is defined under unstable and neutral conditions as

$$V_c = 2(\theta_g - \theta_a)^{1/2}, \tag{5.4.2.10}$$

while it is zero under stable conditions.

The surface moisture flux is

$$E_s = \rho_a C_\theta C_u M(q_{vs}(T_g) - q_{va})V, \tag{5.4.2.11}$$

where M is the moisture availability parameter which varies from 1.0 for a wet surface to 0.0 for a surface with no potential for evaporation. The moisture availability is specified as a function of land-use category (Appendix 4). The model results are often quite sensitive to the value used for M.

The surface momentum flux is given by

$$\tau_s = \rho_a C_D V^2, \tag{5.4.2.12}$$

where the drag coefficient C_D is defined as

$$C_D = C_D' + 3 \times 10^{-3} \left(\frac{\phi_s}{\phi_s + 9800}\right). \tag{5.4.2.13}$$

The second term in (5.4.2.13), involving the surface geopotential ϕ_s, is a correction for elevated terrain (Bleck,1977). The expression for C'_D follows Deardorff (1972), where

$$C'_D = C_u^2 \tag{5.4.2.14}$$

5.4.3 Blackadar High-resolution model

A revised version of Blackadar's PBL model (Blackadar, 1976, 1979; Zhang and Anthes, 1982) is used to forecast the vertical mixing of horizontal wind (u and v), potential temperature (θ), mixing ratio (q_v), cloud water (q_c), and ice (q_i). The surface heat and moisture fluxes are computed from similarity theory. First the friction velocity, u_*, is computed based on

$$u_* = MAX\left(\frac{kV}{ln\frac{z_a}{z_0} - \psi_m}, u_{*0}\right), \tag{5.4.3.1}$$

where u_{*0} is a background value ($0.1ms^{-1}$ over land and zero over water) and V is given by (5.4.2.9). The surface-heat flux is computed from

$$H_s = -C_{pm}\rho_a k u_* T_*, \tag{5.4.3.2}$$

where

$$T_* = \frac{\theta_a - \theta_g}{ln\frac{z_a}{z_0} - \psi_h}, \tag{5.4.3.3}$$

where z_0 is the roughness parameter, z_a is the height of the lowest σ-level, and ψ_m and ψ_h are nondimensional stability parameters that are a function of the bulk Richardson number R_{iB}, which is given by

$$R_{iB} = \frac{gz_a}{\theta_a}\frac{\theta_{va} - \theta_{vg}}{V^2}, \tag{5.4.3.4}$$

where the subscript v represents virtual potential temperature. There are four cases possible:

a. Stable case

For the stable case, $R_{iB} > R_{ic}$, where the critical Richardson number R_ic is defined as

$$R_{ic} = .2. \tag{5.4.3.5}$$

In this case,

$$u_* = u_{*0}, \tag{5.4.3.6}$$

$$\psi_m = \psi_h = -10ln\frac{z_a}{z_0}, \tag{5.4.3.7}$$

and

$$H_s = Max(-250\ W\ m^{-2}, -c_{pm}\rho_a k u_* T_*). \tag{5.4.3.8}$$

b. Mechanically driven turbulence

For this case $0 \leq R_{iB} \leq R_{ic}$, and we get

$$\psi_m = \psi_h = -5\left(\frac{R_{iB}}{1.1 - 5R_{iB}}\right) ln\frac{z_a}{z_0}. \tag{5.4.3.9}$$

c. Unstable (forced convection)

Here $R_{iB} < 0$ and $\mid h/L \mid \leq 1.5$, where the Monin-Obukhov length, L, is defined as

$$L = -\frac{c_{pm}\rho_a\theta_a u_*^3}{kgH_s} \tag{5.4.3.10}$$

and h is the height of the PBL. In this case, $\psi_m = \psi_h = 0$, and $z_a/L = R_{iB}ln\frac{z_a}{z_0}$.

d. Unstable (free convection)

Here $R_{iB} < 0$ and $\mid h/L \mid > 1.5$. In this case

$$\psi_h = -3.23\left(\frac{z_a}{L}\right) - 1.99\left(\frac{z_a}{L}\right)^2 - 0.474\left(\frac{z_a}{L}\right)^3, \tag{5.4.3.11}$$

and

$$\psi_m = -1.86\left(\frac{z_a}{L}\right) - 1.07\left(\frac{z_a}{L}\right)^2 - 0.249\left(\frac{z_a}{L}\right)^3. \tag{5.4.3.12}$$

where z_a/L is restricted to be no less than -2.0 in this approximation. For z_a/L equal to -2.0, $\psi_h = 2.29$, and $\psi_m = 1.43$.

In the general case, z_a/L is a function of ψ_m and (5.4.3.12) is an implicit equation requiring an iterative solution. To save time, we approximate z_a/L as an explicit function of R_{iB}, such that

$$\frac{z_a}{L} = R_{iB}ln\frac{z_a}{z_0}. \tag{5.4.3.13}$$

The above scheme ensures continuity of ψ_m for all values of R_{iB}. The formulation for the surface moisture flux in the multi-layer case was derived from Carlson and Boland (1978), where

$$E_s = M\rho_a I^{-1}(q_{vs}(T_g) - q_{va}), \tag{5.4.3.14}$$

and

$$I^{-1} = ku_* \left[ln\left(\frac{ku_* z_a}{K_a} + \frac{z_a}{z_l}\right) - \psi_h \right]^{-1}. \tag{5.4.3.15}$$

The quantity z_l is the depth of the molecular layer (0.01 m over land and z_0 over water) and K_a is a background molecular diffusivity equal to $2.4 \times 10^{-5} m^2 s^{-1}$.

Over land, the roughness length z_0 is specified as a function of land-use category (Appendix 4). Over water, z_0 is calculated as a function of friction velocity (Delsol *et al.* , 1971) such that

$$z_0 = 0.032u_*^2/g + z_{0c}, \tag{5.4.3.16}$$

where z_{0c} is a background value of $10^{-4} m$.

The Blackadar scheme considers two different PBL regimes, the nocturnal regime and the free-convection regime. The first three cases (stable, mechanically driven turbulence, and forced convection) are in the nocturnal regime, which is usually stable or at most marginally unstable.

Nocturnal Regime

The first-order closure approach is used to predict model variables. The ground stress is calculated from

$$\tau_s = \rho u_*^2, \tag{5.4.3.17}$$

where u_* is computed from (5.4.3.1). The components of τ_s in the x and y directions are

$$\tau_{sx} = \frac{u}{V_a}\tau_s \tag{5.4.3.18}$$

and

$$\tau_{sy} = \frac{v}{V_a}\tau_s, \tag{5.4.3.19}$$

where V_a is the wind speed at the lowest model level. For surface layer variables, the prognostic equations are

$$\frac{\partial \theta_a}{\partial t} = \frac{-(H_1 - H_s)}{(\rho_a c_{pm} z_1)}, \tag{5.4.3.20}$$

$$\frac{\partial q_{va}}{\partial t} = \frac{-(E_1 - E_s)}{(\rho_a z_1)}, \tag{5.4.3.21}$$

$$\frac{\partial u_a}{\partial t} = \frac{(\tau_{1x} - \tau_{sx})}{(\rho_a z_1)}, \tag{5.4.3.22}$$

$$\frac{\partial v_a}{\partial t} = \frac{(\tau_{1y} - \tau_{sy})}{(\rho_a z_1)}, \tag{5.4.3.23}$$

and

$$\frac{\partial q_{ca}}{\partial t} = \frac{-F_1}{(\rho_a z_1)}, \tag{5.4.3.24}$$

where H_s is the surface heat flux computed from (5.4.3.2), E_S is the surface moisture flux computed from (5.4.3.14), subscript a refers to surface layer variables, subscript 1 refers to the fluxes at the top of the surface layer (Fig. 5.4), and z_1 is the height of the lowest model layer. The fluxes at the full σ levels are computed from K-theory, as described in section (5.6). The prognostic variables above the surface layer are computed from K-theory and an implicit diffusion scheme (Richtmeyer, 1957; Zhang and Anthes, 1982).

Free-Convection Regime

During strong heating from below, large surface heat fluxes and a super- adiabatic layer occur in the lower troposphere. As the buoyant plumes of hot air rise under such unstable conditions, mixing of heat, momentum, and moisture take place at each level. The vertical mixing in this scheme is not determined by local gradients, but by the thermal structure of the whole mixed layer. In the Blackadar PBL model, the vertical mixing is visualized as taking place between the lowest layer and each layer in the mixed layer, instead of between adjacent layers as in K-theory.

In the surface layer, the prognostic variables are solved by the analytic solution

$$\alpha_a^{\tau+1} = \alpha_a^{\tau-1} + \left(\frac{F_s z_1}{\bar{m}h^2} - \frac{F_s}{\bar{m}h} + \frac{F_1}{\bar{m}h}\right) \times \left[exp\left(-\frac{\bar{m}h\Delta t}{z_1}\right) - 1\right] + \frac{F_s \Delta t}{h}, \tag{5.4.3.25}$$

where α represents any prognostic variable, F_s is the surface flux, F_1 is the flux at the top of the surface layer, h is the height of the PBL, Δt is the time-step, and the mixing coefficient is

$$\bar{m} = H_1 \left[\rho_a c_{pm}(1-\epsilon) \int_{z_1}^{h} [\theta_{va} - \theta_v(z')]\, dz'\right]^{-1}. \tag{5.4.3.26}$$

Here ϵ is the entrainment coefficient (0.2) and H_1 is the heat flux at the top of the surface layer computed by the Priestly equation

$$H_1 = \rho_a c_{pm} z_1 (\theta_{va} - \theta_{v2})^{\frac{3}{2}} \left(\frac{2g}{27\theta_{va}}\right)^{\frac{1}{2}} \frac{1}{z_1} \left[z_1^{-\frac{1}{3}} - (2z_2)^{-\frac{1}{3}}\right]^{-\frac{3}{2}}, \qquad (5.4.3.27)$$

where z_1 is the depth of the surface layer and the subscript 2 refers to the second prediction layer above the surface (Fig. 5.4).

For the variables above the surface layer, the prognostic equation is

$$\frac{\partial \alpha_i}{\partial t} = \bar{m}(\alpha_a - \alpha_i), and \qquad \alpha = \theta, q_v, or\ q_c \qquad (5.4.3.28)$$

$$\frac{\partial \alpha_i}{\partial t} = w\bar{m}(\alpha_a - \alpha_i), \qquad \alpha = u, v. \qquad (5.4.3.29)$$

The variable w is a weighting function for reducing mixing near the top of the mixed layer, where

$$w = 1 - \frac{z}{h}. \qquad (5.4.3.30)$$

Care must be taken at the layer where the top of the mixed layer is located because the top of the mixed layer does not necessarily coincide with a model level.

5.4.4 Vertical diffusion

Above the mixed layer, K-theory is used to predict the vertical diffusion of the prognostic variables, such that

$$F_V \alpha = p^* \frac{\partial}{\partial z} K_z \frac{\partial \alpha}{\partial z}, \qquad (5.4.4.1)$$

where the eddy diffusivity, K_z, is a function of the local Richardson number R_i. Specifically,

$$K_z = K_{z0} + l^2\ S^{.5}\ \frac{R_{ic} - R_i}{R_{ic}} \quad and \quad R_i < R_{ic} \qquad (5.4.4.2)$$

$$K_z = K_{z0}, \qquad R_i \geq R_{ic} \qquad (5.4.4.3)$$

where $K_{z0} = 1\ m^2\ s^{-1}$, $l = 40\ m$, $and R_{ic}$ is a critical Richardson number which is a function of layer thickness (m) and is defined as

$$R_{ic} = .257\ \Delta z^{.175}. \qquad (5.4.4.4)$$

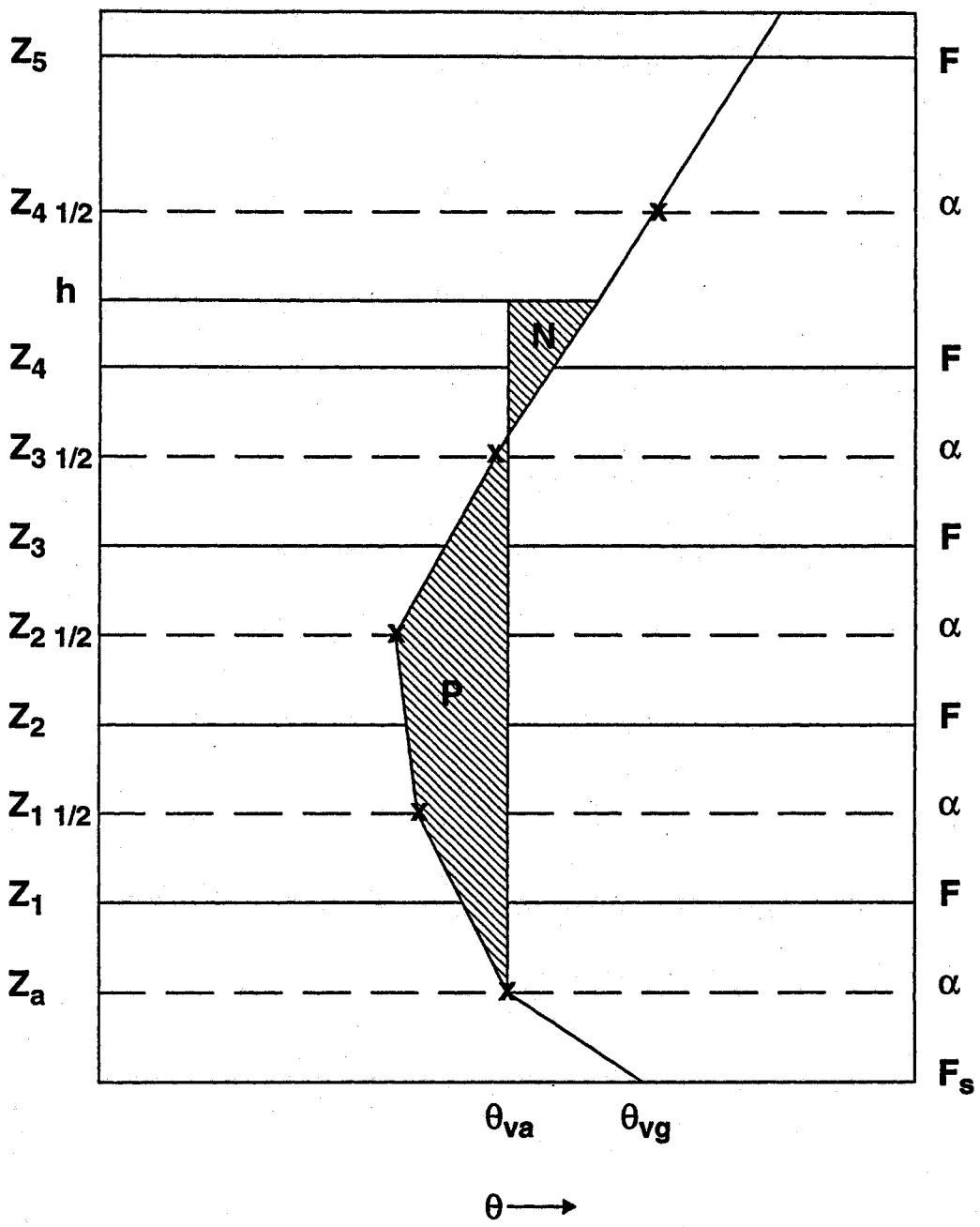

Figure 5.4 Illustration of vertical grid structure for high-resolution (Blackadar) model. The top of the surface layer is z_1; θ_{vg} and θ_{va} are the virtual potential temperatures of the ground surface and lowest model level, respectively; *P* and *N* denote the positive and negative areas associated with a parcel of air originating at z_a and rising to *h*, the top of the PBL.

According to (5.4.4.4), R_{ic} varies from 0.58 for $\Delta z = 100\,m$ to 0.86 for $\Delta z = 1000\,m$. The Richardson number is

$$R_i = \frac{g}{\theta S}\frac{\partial \theta}{\partial z} \tag{5.4.4.5}$$

and S is

$$S = \left(\frac{\partial u}{\partial z}\right)^2 + \left(\frac{\partial v}{\partial z}\right)^2 + 10^{-9}. \tag{5.4.4.6}$$

5.4.5 Moist vertical diffusion

There is an option with explicit moisture of including the effects of moisture on vertical diffusion. Taking into account moist-adiabatic processes in cloudy air (Durran and Klemp 1982), (5.4.4.5) is modified to

$$R_i = (1+\alpha)\left[\frac{g}{\theta S}\frac{\partial \theta}{\partial z} - \frac{g^2 \frac{\chi-\alpha}{1+\chi}}{S c_p T}\right] \tag{5.4.5.1}$$

where

$$\chi = \frac{L_v^2 q_{vs}}{c_p R_v T^2} \tag{5.4.5.2}$$

and

$$\alpha = \frac{L_v q_{vs}}{R_d T}, \tag{5.4.5.3}$$

and this modified value is used in (5.4.4.2) where the cloud amount exceeds 0.1 g kg^{-1}.

5.5 Atmospheric radiation parameterization

The atmospheric radiation option in the model provides a longwave (infra-red) and shortwave (visible) scheme that interact with the atmosphere, cloud and precipitation fields, and with the surface (Dudhia 1989).

5.5.1 Longwave radiative scheme

Longwave absorption by water vapor, the primary clear-air absorber, is strongly spectral in character, and the method employed is the commonly used broadband emissivity method (see Stephens 1984). This involves using a precalculated emissivity function, ϵ, which represents the frequency-integrated absorption spectrum of water vapor, weighted by a suitable envelope function. Rodgers (1967) gives an upward and downward emissivity as a function of water vapor path, u, with a temperature correction term, where u includes a pressure correction factor proportional to $p^{0.86}$. The form of the fitted function is

$$\epsilon(u) = \sum_{i=0}^{i=4}(a_i + \overline{T}b_i)x^i, \qquad (5.5.1.1)$$

where $x = \ln u$ and $\overline{T}$ is a u-weighted T - 250K. For u less than 10 g m^{-2}, the form is

$$\epsilon(u) = \sum_{i=1}^{i=4}(c_i + \overline{T}d_i)y^i, \qquad (5.5.1.2)$$

where $y = u^{1/2}$ and a_i, b_i, c_i and d_i are constants. In the tropics, e-type absorption is an important additional component of the longwave absorption spectrum and is included with a similar fourth-order polynomial in ln (ue) to (5.5.1.1) from Stephens and Webster (1979), where e is the partial pressure due to water vapor. Given the emissivity functions from (5.5.1.1-2) (ϵ_u for upward flux and ϵ_d for downward flux), the upward and downward fluxes at any model level are given by

$$F_u = \int_0^1 B(T)d\epsilon_u, \qquad (5.5.1.3a)$$

$$F_d = \int_0^1 B(T)d\epsilon_d, \qquad (5.5.1.4a)$$

In (5.4.1.3a) the integration is performed downwards through the model layers. The quantity $d\epsilon$ is calculated for each layer using the temperature (T) of the layer and the

frequency-integrated Planck function $B = \sigma_{SB}T^4$, where σ_{SB} is the Stefan-Boltzmann constant. When the surface is encountered, the ground emission F_{bot} is multiplied by $1 - \epsilon$ and added to the integration. In (5.5.1.4a), the integration is performed upwards; the downward longwave flux at the model top, F_{top}, is assumed to result only from CO_2 emission in the stratosphere. Thus (5.5.1.3a-4a) can be expressed as

$$F_u(z) = \int_{z'=z}^{z'=z_{sfc}} B(T)\frac{d\epsilon_u}{dz'}dz' + F_{bot}[1 - \epsilon_u(z, z_{sfc})], and \qquad (5.5.1.3b)$$

$$F_d(z) = \int_{z'=z}^{z'=z_{top}} B(T)\frac{d\epsilon_d}{dz'}dz' + F_{top}[(1 - \epsilon_d(z, z_{top})], \qquad (5.5.1.4b)$$

where

$$\epsilon(z, z_1) = \int_z^{z_1} \frac{d\epsilon}{dz'}dz'. \qquad (5.5.1.5)$$

It can be seen from the formulas that if the emissivity reaches 1 during the integration, the remaining atmosphere makes no contribution to the flux. This is consistent with the idea that an emissivity of 1 corresponds to a "black" layer with respect to longwave radiation.

Following Stephens (1978), the cloud water is assumed to have a constant absorption coefficient which is slightly different for upward and downward radiation. The absorption coefficients are $\alpha_{cu} = 0.130$ m^2 g^{-1} and $\alpha_{cd} = 0.158$ m^2 g^{-1}. To combine these with water vapor absorption, the transmissivities are multiplied since clouds are assumed to be "grey bodies." The net emissivity is then

$$\epsilon_{tot} = 1 - T_v T_c, \qquad (5.5.1.6)$$

with

$$T_v = 1 - \epsilon_{vapor} and \qquad (5.5.1.7)$$

$$T_c = \exp(-\alpha_c u_c), \qquad (5.5.1.8)$$

where u_c is the cloud water path (liquid mass per unit area).

Ice cloud is assumed to be composed of hexagonal plate-like crystals with the diameter-mass relation given in section (5.3.1.1). If the assumption is made that the crystals do not reflect longwave radiation and are sufficiently thick to be "black", it is possible to estimate

an absorption coefficient as an integrated cross-sectional area. Allowing for the random orientation of these crystals and a hemispheric integration factor of 1.66, the absorption coefficient takes a value of $\alpha_i = 0.0735\ \mathrm{m}^2\ \mathrm{g}^{-1}$, or about half that of cloud water. Since this value agrees with some observations, it was applied in the model.

For rain and snow, the size distribution is necessary since the cross section is not proportional to the mass of a particle. The size spectrum changes with precipitation intensity so the absorption coefficient varies with precipitation amount. The effective absorption coefficient is given by

$$\alpha_p = \frac{1.66}{2000}\left(\frac{\pi N_0}{\rho_r^3}\right)^{1/4} \mathrm{m}^2\mathrm{g}^{-1}, \tag{5.5.1.9}$$

where ρ_r is the particle density. For the constants used in the explicit moisture scheme described earlier, the absorption coefficients take values of $2.34 \times 10^{-3}\mathrm{m}^2\mathrm{g}^{-1}$ for snow and $0.330 \times 10^{-3}\mathrm{m}^2\mathrm{g}^{-1}$ for rain. The effective water path for a layer of Δz meters thickness is given by

$$u_p = (\rho q_r)^{3/4}\Delta z \times 1000\mathrm{gm}^{-2}, \tag{5.5.1.10}$$

so that the transmissivity is given by

$$T_p = \exp(-\alpha_p u_p). \tag{5.5.1.11}$$

This transmissivity is multiplied with the others in (5.5.1.6) to give ϵ_{tot}. This is known as an overlap approximation. Rain and snow have less effect on the longwave flux by 2 to 3 orders of magnitude, but still are not insignificant.

Carbon dioxide is less easily treated since it cannot be assumed "grey". That is, its absorption is concentrated in a band of infrared wavelengths. To include its effect, an overlap method is used as discussed by Stephens (1984). In effect, the spectrum is divided into a carbon-dioxide band and a non-carbon-dioxide region. The former requires overlapping of the carbon dioxide transmissivity function while the latter does not. The relative weights of these two regions is slightly temperature dependent, but they add to give the total absorption. A pressure correction factor proportional to $p^{1.75}$ is applied to the carbon dioxide path calculation.

Having obtained the flux profiles, $F_u(z)$ and $F_d(z)$, the radiative heating rate is calculated from

$$\dot{Q}_R = c_p \frac{\partial T}{\partial t} = \frac{1}{\rho}\frac{\partial}{\partial z}(F_d - F_u) = -g\frac{\partial}{\partial p}(F_d - F_u). \qquad (5.5.1.12)$$

In the model, the values of F are defined on the model full sigma-levels. This makes the various integrals and derivatives easier to represent numerically.

5.5.2 Shortwave Radiative Scheme

The downward component of shortwave flux is evaluated taking into account 1) the effects of solar zenith angle, which influences the downward component and the path length; 2) clouds, which have an albedo and absorption; 3) and clear air, where there is scattering and water-vapor absorption. Thus,

$$S_d(z) = \mu S_0 - \int_z^{top} (dS_{cs} + dS_{ca} + dS_s + dS_a), \qquad (5.5.2.13)$$

where μ is the cosine of the zenith angle and S_0 is the solar constant.

As with the longwave scheme, cloud fraction in a grid box is either 0 or 1 because of the assumed stratiform nature of the clouds. The cloud back-scattering (or albedo) and absorption are bilinearly interpolated from tabulated functions of μ and $\ln(w/\mu)$ (where w is the vertically integrated cloud water path) derived from Stephens' (1978) theoretical results. The total effect of a cloud or multiple layers of cloud above a height z is found from the above function as a percentage of the downward solar flux absorbed or reflected. Then at a height $z - \Delta z$, a new total percentage is calculated from the table allowing the effect of the layer Δz to be estimated. However, this percentage is only applied to $\mu S_0 - \Delta S(clear\ air)$; that is, the clear-air effect above z is removed.

Clear-air water vapor absorption is calculated as a function of water vapor path allowing for solar zenith angle. The absorption function is from Lacis and Hansen (1974). The method is a similar integration-difference scheme to that described above for cloud.

Clear-air scattering is taken to be uniform and proportional to the atmosphere's mass path length, again allowing for the zenith angle, with a constant giving 20 percent scattering in one atmosphere. The heating rate is then given by

$$R_T = R_T(longwave) + \frac{1}{\rho c_p} S_{abs}, \qquad (5.5.2.14)$$

where S_{abs} is defined from the absorption part of the S_d integral given in (5.5.2.13), since only cloud and clear-air absorption contribute to solar heating.

The solar and infrared fluxes at the surface, calculated from the atmospheric radiative schemes, are use in the energy budget of the land surface.

Appendix 1. Glossary of Symbols

a	Fraction of convective cloud cover; also constant used in cloud microphysics
ABE	Available buoyant energy
A_T	The forcing terms of the thermodynamic equation that vary on the time-scale of the Rossby-waves
A_u, A_d, A_{tot}	Cloud Work Function for updraft, downdraft, and all of model cloud
A_v	The forcing terms of the v-momentum equation that vary on the time-scale of the Rossby-waves
A_v	The forcing terms of the u-momentum equation that vary on the time-scale of the Rossby-waves
A'	Parameter for heterogeneous freezing (K^{-1})
A	Antidiffusive flux
b	Backscattering coefficient; also fraction of total water vapor convergence used to moisten grid column (section 5.3.2.1); also constant (0.8) used in cloud microphysics computation
B	Planck function
B_u	Acceleration due to buoyancy
B'	Parameter for heterogeneous freezing ($m^{-3}s^{-1}$)
c_0	Rainfall conversion parameter (section 5.3.2.2)

c_m	Constant used in computation of D_m
c_i	Coefficients used in calculation of cloud effect on downward longwave radiation (Table 5.2)
c_p	Specific heat at constant pressure for dry air
c_{pm}	Specific heat at constant pressure for moist air
c^*	Net condensation rate averaged over grid volume
c_c^*	Net condensation rate in cumulus cloud (section 5.3.2.1)
C	Constant (2. m s^{-1} $K^{-1/2}$) used in computing convective velocity
C_g	Thermal capacity of slab per unit area (J m^{-2} K^{-1})
C_s	Heat capacity per unit volume (J m^{-3} K^{-1})
C_θ	Surface exchange coefficient for heat
C_u	Surface exchange coefficient for momentum; also total condensate in updraft (section 5.3.2.2)
C_D	Surface drag coefficient
C_D'	Component of surface-drag coefficient
C_{uN}	Value of surface momentum exchange coefficient under neutral stability conditions

$C_{\theta N}$	Value of surface heat exchange coefficient under neutral stability conditions
D	Mass divergence (hydrostatic split-explicit scheme); also horizontal deformation (section 5.1)
D_f	Diffusivity of water vapor in air
D_u, D_d, D_{tot}	Updraft, downdraft, and total cloud kinetic energy dissipation
	Distance between an observation and a given grid point (section 4)
D_i	Diameter of ice crystal (m)
D_α	Diffusion and PBL tendencies for variable α
D_m	Modified distance between an observation and a given grid point (section 4)
e	Horizontal Coriolis parameter (s^{-1})
e_s, e_{si}, e_{sw}	Saturation vapor pressure, over ice, over water (cb)
E	Efficiency of collection of cloud by precipitation; also vertical flux of water vapor
E_s	Flux of water vapor from surface into atmosphere
f	Coriolis parameter
f_1, f_2	Ventilation coefficients for rain or snow

F	Larger-scale forcing (section 5.3.2.2 and 5.3.2.3); also function of distance from lateral boundary (section 2.6.2)
FH, FL	Flux from high-order and low-order advective scheme
F_{bot}, F_{top}	Longwave radiative flux at bottom, top of model atmosphere (W m^{-2})
F_d, F_u	Downward, upward longwave radiative flux (W m^{-2})
$F_{H\alpha}$	Term representing contribution of horizontal diffusion of a variable α to the temporal rate of change of α
$F_{V\alpha}$	Term representing contribution of vertical diffusion of a variable α to the temporal rate of change of α
F_s	Flux of dry static energy (section 5.3.2.2); also Surface flux of heat, moisture or momentum
F_q	Flux of water vapor (section 5.3.2.2)
F_l	Flux of suspended cloud liquid water (section 5.3.2.2)
F_r	Deceleration
F_1, F_2	Amplitude factors used in computing lateral boundary conditions (section 2.6.2)
g	Acceleration of gravity (9.8 m s^{-2})
h	Moist static energy; also height of planetary boundary layer (m)
h_o	Local hour angle of sun

$\tilde{h}, h_c, h_u, h_d, \tilde{h}^*$	Moist static energy in environment, cloud, updraft, downdraft, and saturation value in environment
H	Vertical flux of sensible heat (W m^{-2})
H_m	Heat flux into substrate (W m^{-2})
H_s	Sensible heat flux from surface into atmosphere (W m^{-2})
I	Function of static stability and surface friction velocity; also horizontal grid-index in y-direction
$IMAX$	Maximum value of grid-index in y-direction
I_s	Net longwave iradiance at surface (wm^{-2})
$I\uparrow$	Outgoing longwave radiation from surface (W m^{-2})
$I\downarrow$	Downward longwave radiation absorbed at surface (W m^{-2}) under clear skies
$I\downarrow'$	Downward longwave radiation absorbed at surface (W m^{-2}) in presence of clouds
I_1	Normalized condensate in updraft (section 5.3.2.2)
I_2	Normalized evaporate in updraft (section 5.3.2.2)
J	Horizontal grid index in x-direction
$JMAX$	Maximum value of grid index in x-direction

k	Dimensionless x-wavenumber for upper radiative scheme; also von Karman constant (0.4)
$\hat{k}$	Dimensionless effective x-wavenumber for upper radiative scheme
k_1	Constant used in formula for computing autoconversion of cloud drops to rain drops
K	Total horizontal wavenmumber (m^{-1}) also Kernels
K_a	Background molecular diffusivity ($2.4 \times 10^{-5} m^2 s^{-1}$); also thermal conductivity of air (J m^{-1} s^{-1} K^{-1})
K_H	Horizontal eddy diffusivity (m^2 s^{-1})
K'_H	Coefficient used in fourth-order diffusion (s^{-1})
K_{HO}	Background value of horizontal eddy diffusivity (m^2 s^{-1})
K_m	Coefficient of heat transfer from ground into substrate (s^{-1})
$KMAX$	Maximum value of index in vertical direction
K_z	Coefficient of vertical diffusivity (m^2 s^{-1})
K_{z0}	Background value of coefficient of vertical diffusivity (m^2 s^{-1})
KE_u, KE_d, KE_{tot}	Kinetic energy for updraft, downdraft, and all of model cloud
L	Hydrostatic term due to liquid water loading; also Monin-Obukhov length
L_m	Latent heat of fusion (0.35×10^6 J kg^{-1})

L_s	Latent heat of sublimation (2.85 $\times 10^6$ J kg^{-1})
L_v	Latent heat of condensation (2.5 $\times 10^6$ J kg^{-1})
l	Dimensionless y-wavenumber for upper radiative scheme; also vertical mixing length
$\hat{l}$	Dimensionless effective y-wavenumber for upper radiative scheme
M_i	Mass of ice crystal (kg)
M_{max}	Maximum mass of ice crystal (kg)
M_0	Initial mass of ice crystal (kg)
m	Mass flux (updraft and downdraft) in convective parameterization cloud (5.3.2.2); also map scale factor
$\bar{m}$	Mixing coefficient used in free-convective regime of high-resolution PBL model
m_b	Cloud base mass flux (section 5.3.2.2)
m_0	Downdraft base mass flux (section 5.3.2.2)
m_u	Updraft mass flux in convective parameterization cloud (5.3.2.2)
m_d	Downdraft mass flux in convective parameterization cloud (5.3.2.2)
M	Surface moisture availability

M_t	Vertical integral of horizontal convergence of water vapor
n	Fraction of cloud
n_0	Cloud microphysics parameter
n_c	Number concentration of ice crystals (kg^{-1})
N	Brunt-Vaisälä frequency (s^{-1})
N_c	Number concentration of cloud droplets per unit volume (10^{10} m^{-3})
N_h	Nondimensional function for vertical profile of convective heating
N_m	Nondimensional function for vertical profile of convective moistening
N_0	Cloud microphysics parameter (8×10^6 m^{-4} for rain 2×10^7 m^{-4} for snow)
p	Pressure (cb)
p_b	Pressure (cb) at convective cloud base
p_s	Surface pressure (cb)
p_t	Pressure (cb) at top of model
p_u	Pressure (cb) at top of convective cloud
p_{LCL}	Pressure (cb) at lifting condensation level

p^*	$p_s - p_t$ (cb)
p_d^*	Dot-point p^* (cb)
p_0	Reference-state pressure
p'	Perturbation pressure (Pa)
	Pressure value representing the free atmosphere, where terrain influences are small (in FDDA)
$\hat{p}$	Fourier transform of p' for upper radiative boundary condition
P_{CON}	Condensation of water vapor or evaporation of cloud drops (kg kg^{-1} s^{-1})
P_{RA}	Accretion of cloud drops by rain drops (kg kg^{-1} s^{-1})
P_{RC}	Autoconversion of cloud drops to rain drops (kg kg^{-1} s^{-1})
P_{RE}	Evaporation of rain drops (kg kg^{-1} s^{-1})
P_{CI}	Heterogeneous freezing of cloud water (kg kg s^{-1})
P_{ID}	Deposition of vapor onto ice crystals (kg kg s^{-1})
P_{II}	Initiation of ice crystals (kg kg s^{-1})
P_{MF}	Melting/freezing of cloud and precipitation due to advection (kg kg s^{-1})

P_{RM}	Melting of falling precipitation (kg kg s^{-1})
P_{SM}	Melting of falling snow (kg kg s^{-1})
$\tilde{q}, q_u, q_d, \tilde{q}^*$	Water vapor mixing ratio in environment, updraft, downdraft, and saturation value in environment
q_c	Mixing ratio of cloud water; also water vapor mixing ratio in cloud (section 5.3.2.2)
q_{c0}	Critical value of mixing ratio of cloud water
q_r	Mixing ratio of rain water
q_l	Suspended liquid water vapor mixing ratio inside updraft
q_v	Mixing ratio of water vapor
q_{vc}	Mixing ratio of water vapor in cumulus cloud
q_{vs}	Saturation mixing ratio of water vapor
Q	Diabatic heating rate per unit mass (J kg^{-1} s^{-1})
Q_s	Net short wave irradiance at the surface (W m^{-2})
R	Rainfall (convective-scale sink of cloud water, 5.3.2.2); also ideal gas constant for dry air (287 J kg^{-1} K^{-1})
RH	Relative humidity
R_i	Richardson number

R_n	Net radiation
R_{iB}	Bulk Richardson number
R_{ic}	Critical value of bulk Richardson number; also critical value of Richardson number
R_v	Gas constant for water vapor (461.5 J kg^{-1} K^{-1})
R_T	Radiative heating rate (K s^{-1})
r	Radius of convective parameterization cloud (sections 5.3.2.2)
S	Supersaturation; also source or sink term (section 5.3.2.2); also square of the vertical wind shear
S_c	Schmidt number
S_o	Solar constant (1395.6 W m^{-2})
S_u	Source or sink term in updraft (section 5.3.2.2)
S_d	Downward solar flux (W m^{-2}); also source or sink term in downdraft (section 5.3.2.2)
S_i	Supersaturation over ice
s	Dry static energy
t	Time (s)

T	Temperature (K)
T_c	Longwave transmissivity due to cloud
T_d	Dewpoint temperature (K)
T_g	Temperature (K) of ground
T_p	Longwave transmissivity due to precipitation
T_v	Virtual temperature (K); also longwave transmissivity due to vapor
T_*	Surface friction temperature (K)
T_0	Reference-state temperature (K)
T'	Perturbation temperature (K)
u	Component of wind velocity in eastward direction ($\mathrm{m\ s^{-1}}$); also water vapor path ($\mathrm{g\ m^{-2}}$)
u_*	Surface friction velocity ($\mathrm{m\ s^{-1}}$)
u_c, u_p	Liquid water path for cloud, precipitation ($\mathrm{g\ m^{-2}}$)
v	Component of wind velocity in northward direction ($\mathrm{m\ s^{-1}}$)
v_t	Mass weighted mean terminal velocity of rain drops ($\mathrm{m\ s^{-1}}$)
V	Fall speed of a precipitation particle ($\mathrm{m\ s^{-1}}$); also modified horizontal wind velocity in PBL

$\mathbf{V}$	Horizontal wind vector
V_a	Horizontal windspeed at lowest model layer
V_c	Convective PBL velocity(m s^{-1})
V_{qf}	Divergence of vertical eddy flux of water vapor due to convective clouds
w	Vertical velocity (m s^{-1}); also weight function for reducing mixing near top of mixed layer
w_n	Weight function for blending model tendencies and large-scale tendencies near lateral boundaries (section 2.6.1)
w_p	Precipitable water (cm)
w_u	Vertical velocity in updraft
$\hat{w}$	Fourier transform of w
x	Horizontal grid coordinate increasing generally eastward
X	Horizontal coordinate on earth surface increasing generally eastward
X_c	Multiple-reflection factor in cloudy air
X_d	Distance vector
X_R	Multiple-reflection factor in clear air

y	Horizontal grid coordinate increasing generally northward
Y	Horizontal coordinate on earth surface increasing generally northward
z	Height above surface (m)
z_a	Height of lowest layer in model (m)
z_b	Height of updraft originating level(section 5.3.2.2) (m)
z_0	Height of downdraft originating level(section 5.3.2.2); also surface roughness length(m)
z_{oc}	Background value of surface roughness length over water (10^{-4}m)
z_l	Depth of molecular layer
z_{LCL}	Height of lifting condensation level (m)
z_T	Height of updraft top (section 5.3.2.2)
α	Coefficient array for upper radiative boundary condition (m s^{-1} Pa^{-1}); also any thermodynamic variable (section 5.3.2.2)
$\tilde{\alpha}$	Any thermodynamic variable in environment
α_u	Any thermodynamic variable in updraft
α_d	Any thermodynamic variable in downdraft
α_c, α_p	Longwave absorption coefficients for cloud, precipitation (m^2 g^{-1})

β	Parameter in sound-wave temporal differencing; also precipitation efficiency parameter in section 5.3.2.2
Γ	Gamma function
Γ_d	Dry adiabatic lapse rate (K m^{-1})
Γ_{dp}	Dewpoint adiabatic lapse rate (K m^{-1})
γ	Ratio of heat capacities (c_p/c_v) for dry air
δ	Solar declination
δM	Supersaturation or undersaturation
Δp	Vertical grid size (Pa)
Δs	Horizontal grid length (m)
Δt	Time step (s)
$\Delta t'$	Short time step for rain fall term (s)
Δx	Horizontal grid length (m)
Δz	Thickness of vertical layer (m)
$\Delta\sigma$	Thickness of model σ levels

$\Delta\sigma_c$	Critical value of convective cloud depth
$\Delta\tau$	Short time step for sound waves (s)
∇^2_σ	Horizontal Laplacian on σ-surfaces
∇^4_σ	Fourth order diffusion operator on σ-surfaces
ϵ	Parameter relating updraft and downdraft mass flux (section 5.3.2.2); also small value; also entrainment coefficient used in high resolution PBL-model (0.2)
ϵ_a	Atmospheric emissivity
ϵ_g	Emissivity of ground
ϵ_u, ϵ_d	Atmospheric longwave emissivity
η_d	Normalized mass flux for downdraft (section 5.3.2.2)
η_u	Normalized mass flux for updraft (section 5.3.2.2)
θ	Potential temperature (K); also angle between y-axis and north for full Coriolis force
θ_a	Potential temperature (K) at lowest layer in model
θ_g	Potential temperature (K) of ground surface
θ_e	Equivalent potential temperature (K)

θ_{es}	Saturation equivalent potential temperature (K)
θ_v	Virtual potential temperature (K)
λ	Longitude; also cloud type (section 5.3.2.2); also thermal conductivity (J m^{-1} s^{-1} K^{-1}); also parameter in raindrop distribution (m^{-1})
μ	Dynamic viscosity of air (kg m^{-1} s^{-1}); also solar zenith angle ; also total net fractional entrainment rate (section 5.3.2.2); also constant in smoother (section 3.3)
μ_u	Total net fractional entrainment rate for updraft (section 5.3.2.2)
μ_{ue}	Gross fractional entrainment rate for updraft (section 5.3.2.2)
μ_{ud}	Gross fractional detrainment rate for updraft (section 5.3.2.2)
ν	Coefficient for Asselin time filter; also for spatial smoother
π	Exner function
ρ	Density of air (kg m^{-3})
ρ_r	Particle density (kg m^{-3})
ρ_u	Density in updraft
ρ_w	Density of water (kg m^{-3})
ρ_0	Reference-state density (kg m^{-3})

ρ'	Perturbation density (kg m^{-3})
σ	Nondimensional vertical coordinate of model
σ'	Dummy variable of integration
$\dot{\sigma}$	Vertical velocity in σ-coordinates (s^{-1})
$\dot{\sigma}_c$	Vertical velocity of convective cloud in σ-coordinates (s^{-1})
σ_{SB}	Stefan-Boltzmann constant (5.67051×10^{-8} J m^{-2} K^{-4} s^{-1})
τ	Half-period of time window of influence of an observation (section 4); also short-wave transmissivity
τ'	Short-wave transmissivity obtained from lookup table
τ_a	Clear air absorption transmissivity
τ_{ac}	Cloudy air absorption transmissivity
τ_s	Clear air scattering transmissivity; also surface stress
τ_{sc}	Cloudy air scattering transmissivity
ϕ	Geopotential; also latitude; also scalar variable in advection equation
ϕ_s	Surface geopotential

Φ	Symbol denoting low-order, monotonic solution to advection equation
χ	Diffusivity of vapor in air ($m^2\ s^{-1}$); also thermal inertia
Ψ	Solar zenith angle; also function of bulk Richardson number
Ψ_m	Nondimensional stability parameter for momentum
Ψ_h	Nondimensional stability parameter for heat and water vapor
ω	Vertical velocity in pressure coordinates (cb s^{-1})
ω_c	Vertical velocity of convective cloud in pressure coordinates (cb s^{-1})
Ω	Angular velocity of earth ($7.2722 \times 10^{-5}\ s^{-1}$)

Appendix 2. Look-up table for transmissivities

precipitable water (cm)

	0.0	0.5	1.0	1.5	2.0	2.5	3.0	3.5	4.0	4.5	5.0
1.0	0.926	0.868	0.855	0.846	0.838	0.832	0.827	0.822	0.818	0.814	0.811
1.2	0.915	0.854	0.840	0.831	0.823	0.817	0.811	0.806	0.802	0.798	0.794
1.4	0.903	0.841	0.826	0.816	0.808	0.802	0.796	0.791	0.787	0.782	0.779
1.6	0.892	0.828	0.813	0.803	0.795	0.788	0.782	0.777	0.772	0.768	0.764
1.8	0.881	0.815	0.800	0.790	0.782	0.775	0.769	0.763	0.758	0.754	0.750
2.0	0.870	0.803	0.788	0.777	0.769	0.762	0.756	0.750	0.745	0.741	0.737
2.2	0.860	0.792	0.776	0.765	0.757	0.750	0.743	0.738	0.733	0.728	0.724
2.4	0.850	0.781	0.765	0.754	0.745	0.738	0.731	0.726	0.7210	0.716	0.712
2.6	0.839	0.770	0.753	0.742	0.733	0.726	0.720	0.714	0.709	0.704	0.700
2.8	0.830	0.759	0.743	0.731	0.722	0.715	0.709	0.703	0.698	0.693	0.689
3.0	0.820	0.748	0.732	0.721	0.712	0.704	0.698	0.692	0.687	0.682	0.678
3.2	0.810	0.738	0.722	0.710	0.701	0.694	0.687	0.681	0.676	0.671	0.667
3.4	0.801	0.728	0.712	0.700	0.691	0.683	0.677	0.671	0.666	0.661	0.656
3.6	0.791	0.719	0.702	0.690	0.681	0.674	0.667	0.661	0.656	0.651	0.646
3.8	0.782	0.709	0.692	0.681	0.671	0.664	0.657	0.651	0.646	0.641	0.636
4.0	0.773	0.700	0.683	0.671	0.662	0.654	0.648	0.642	0.636	0.631	0.627
4.2	0.764	0.691	0.674	0.662	0.653	0.645	0.638	0.632	0.627	0.622	0.618
4.4	0.756	0.682	0.665	0.653	0.644	0.636	0.629	0.623	0.618	0.613	0.608
4.6	0.747	0.673	0.656	0.644	0.635	0.627	0.621	0.615	0.609	0.604	0.600
4.8	0.738	0.665	0.647	0.636	0.626	0.619	0.612	0.606	0.600	0.596	0.591
5.0	0.730	0.656	0.639	0.627	0.618	0.610	0.603	0.597	0.592	0.587	0.582
5.2	0.722	0.648	0.631	0.619	0.610	0.602	0.595	0.589	0.584	0.5790	0.574
5.4	0.714	0.640	0.623	0.611	0.602	0.594	0.587	0.581	0.576	0.571	0.566
5.6	0.706	0.632	0.615	0.603	0.594	0.586	0.579	0.573	0.568	0.563	0.558
5.8	0.698	0.624	0.607	0.595	0.586	0.578	0.571	0.565	0.560	0.555	0.550
6.0	0.690	0.616	0.599	0.588	0.578	0.571	0.564	0.558	0.552	0.547	0.543
6.2	0.683	0.609	0.592	0.580	0.571	0.563	0.556	0.550	0.545	0.540	0.535
6.4	0.675	0.602	0.585	0.573	0.564	0.556	0.549	0.543	0.538	0.533	0.528
6.6	0.668	0.594	0.577	0.566	0.556	0.549	0.542	0.536	0.531	0.526	0.521
6.8	0.661	0.587	0.570	0.559	0.549	0.542	0.535	0.529	0.524	0.519	0.5147
7.0	0.653	0.580	0.563	0.552	0.542	0.535	0.528	0.522	0.517	0.512	0.507
7.2	0.646	0.573	0.556	0.545	0.536	0.528	0.521	0.515	0.510	0.505	0.501
7.4	0.639	0.567	0.550	0.538	0.529	0.521	0.515	0.509	0.503	0.499	0.494
7.6	0.633	0.560	0.543	0.532	0.522	0.515	0.508	0.502	0.497	0.492	0.488
7.8	0.626	0.553	0.537	0.525	0.516	0.508	0.502	0.496	0.491	0.486	0.481
8.0	0.619	0.547	0.530	0.519	0.510	0.502	0.496	0.490	0.484	0.480	0.475
8.2	0.613	0.541	0.524	0.512	0.503	0.496	0.489	0.484	0.478	0.473	0.469
8.4	0.606	0.534	0.518	0.506	0.497	0.490	0.483	0.477	0.472	0.467	0.463
8.6	0.600	0.528	0.512	0.500	0.491	0.484	0.477	0.472	0.466	0.462	0.457
8.8	0.594	0.522	0.506	0.494	0.486	0.478	0.472	0.466	0.461	0.456	0.451
9.0	0.587	0.516	0.500	0.489	0.480	0.472	0.466	0.460	0.455	0.450	0.446
9.2	0.581	0.511	0.494	0.483	0.474	0.467	0.460	0.454	0.449	0.445	0.440
9.4	0.575	0.505	0.488	0.477	0.468	0.461	0.455	0.449	0.444	0.439	0.435
9.6	0.569	0.499	0.483	0.472	0.463	0.456	0.449	0.444	0.438	0.434	0.429
9.8	0.563	0.494	0.477	0.466	0.458	0.450	0.444	0.438	0.433	0.428	0.424
10.0	0.558	0.488	0.472	0.461	0.452	0.445	0.439	0.433	0.428	0.423	0.419

Path length

Appendix 3. Map Projections

Map projections are constructed by projecting the surface of the earth onto a right circular cone, cutting the cone, and flattening it into a plane surface. Three projections are available for the MM4 system – Polar stereographic, Lambert conformal, and Mercator. Polar stereographic is preferred for high-latitude studies, Lambert conformal for middle-latitude studies, and Mercator for low-latitude studies. This appendix summarizes the map scale factors for each projection and gives the equations for converting from latitude and longitude to the x and y positions on the model grid.

Although the grid size $\Delta x = \Delta y = \Delta s$ is constant on the model's grid, the actual distance represented by Δs on the spherical earth varies with location on the grid because the earth is curved. The map scale factor m is defined as the ratio of the distance on the grid to the corresponding distance on the earth's surface

$$m = \frac{distance\ on\ grid}{actual\ distance\ on\ earth} \qquad A.1$$

a. Lambert Conformal

Conformal means that the scale is equal in all directions about a point, so that shapes of geographic features on the earth are preserved. The Lambert conformal grid is true at latitudes 30° and 60°N so that $m = 1.$ at these latitudes. In general,

$$m = \frac{sin\psi_1}{sin\phi}\left[\frac{tan\phi/2}{tan\psi_1/2}\right]^{0.716}, \qquad A.2$$

where $\psi_1 = 30°$ and ψ is the colatitude ($\psi = 90° - \phi$).

It is sometimes necessary to compute the position (x, y) on the grid given the latitude and longitude of a point, or vice versa. The following relations pertain to an $X - Y$ grid with center $X = 0$, $Y = 0$ at latitude ϕ_0 and longitude λ_0. Note that the relationship between (x, y) and (X, Y) is

$$x = X + \frac{JMAX - 1}{2}\Delta s, \qquad A.3$$

$$y = Y + \frac{IMAX - 1}{2}\Delta s, \qquad A.4$$

$$\lambda = any\ longitude$$

$$\lambda_0 = \textit{longitude of } Y \textit{ axis}$$

$$\phi = \textit{any latitude}$$

$$\phi_0 = \textit{latitude along } \lambda_0 \textit{ at which } Y = 0$$

$$\psi = 90° - \phi$$

$$n = .716$$

$$\psi_1 = 30°$$

$$\psi_0 = 90° - \phi_0$$

$$a = 6370km$$

$$r = \frac{a}{n} sin\psi_1 \left[\frac{tan\psi/2}{tan\psi_1/2}\right]^n, \qquad A.5$$

$$C_2 = \frac{a}{n} sin\psi_1 \left[\frac{tan\psi_0/2}{tan\psi_1/2}\right]^n, \qquad A.6$$

$$C_1 = -\lambda_0 - 90°/n, \qquad A.7$$

$$\lambda' = n(\lambda + C_1), \qquad A.8$$

$$X = rcos\lambda', \qquad A.9$$

$$Y = rsin\lambda' + C_2. \qquad A.10$$

The inverse problem to calculate latitude and longitude is done as follows:

$$\lambda' = arctan\left(\frac{Y - C_2}{X}\right), \qquad A.11$$

$$\lambda = \frac{\lambda'}{n} - C_1, \qquad A.12$$

$$r = \frac{X}{cos\lambda'} or \frac{Y - C_2}{sin\lambda'} \qquad A.13$$

$$\psi = 2arctan\left[tan\psi_1/2\left(\frac{nr}{asin\psi_1}\right)^{1/n}\right], \qquad A.14$$

$$\phi = 90° - \psi. \qquad A.15$$

b. Polar Stereographic

For the polar stereographic projection, true at latitude $\phi_1 = 60°N$, the map scale factor is

$$m = \frac{1 + sin\phi_1}{1 + sin\phi} \qquad A.16$$

The relationships between latitude and longitude and X and Y on the polar stereographic grid are calculated as before on the Lambert conformal grid, but now $n = 1$.

$$r = amcos\phi, \qquad A.17$$

$$C_2 = asin\psi_1 \left[\frac{tan\psi_0/2}{tan\psi_1/2}\right], \qquad A.18$$

$$C_1 = -\lambda_0 - 90°, \qquad A.19$$

$$\lambda' = \lambda + C_1, \qquad A.20$$

$$X = rcos\lambda', \qquad A.21$$

$$Y = rsin\lambda' + C_2. \qquad A.22$$

and for the inverse problem

$$\lambda' = arctan\left(\frac{Y - C_2}{X}\right), \qquad A.23$$

$$\lambda = \lambda' - C_1, \qquad A.24$$

$$r = \frac{X}{cos\lambda'} or \frac{Y - C_2}{sin\lambda'} \qquad A.25$$

$$\psi = 2arctan\left[tan\psi_1/2\left(\frac{r}{asin\psi_1}\right)\right], \qquad A.26$$

$$\phi = 90° - \psi. \qquad A.27$$

Note that the signs of $Y - C_2$ and X in (A.23) must be considered to obtain the correct quadrant for λ'.

c. Mercator

For the Mercator grid, $\phi_0(Y = 0)$ corresponds to the equator and the relationships between X and Y and ϕ and λ are relatively simple

$$X = (acos\phi_1)(\lambda - \lambda_0), \qquad A.28$$

$$Y = (a\cos\phi_1)\ln\left[\frac{1+\sin\phi}{\cos\phi}\right], \qquad A.29a$$

$$Y = (a\cos\phi_1)\ln[\tan(45^\circ + \phi/2)]. \qquad A.29b$$

Note that $(\lambda - \lambda_0)$ in (A.28) must be expressed in radians. The latitude ϕ_1 at which the Mercator projection is true is often taken to be 30°.

The reverse problem, to obtain X and Y from ϕ and λ, is also simple

$$\lambda = \lambda_0 + \frac{X}{a\cos\phi_1}. \qquad A.30$$

To solve for ϕ, use (A.29b)

$$\phi = -90^\circ + 2\arctan\left[\exp\left(\frac{Y}{a\cos\phi_1}\right)\right]. \qquad A.31$$

Appendix 4. Land Use Categories

Description of land-use categories and physical parameters for summer (15 April-15 October) and winter (15 October-15 April).

Landuse Integer Identification	Landuse Description	Albedo(%)		Moisture Avail. (%)		Emissivity (% at 9 μ m)		Roughness Length (cm)		Thermal Inertia (cal cm^{-2} k^{-1} $s^{-1/2}$)	
		Sum	Win	Sum	Win	Sum	Win	Sum	Win	Sum	Win
1	Urban land	18	18	5	10	88	88	50	50	0.03	0.03
2	Agriculture	17	23	30	60	92	92	15	5	0.04	0.04
3	Range-grassland	19	23	15	30	92	92	12	10	0.03	0.04
4	Deciduous forest	16	17	30	60	93	93	50	50	0.04	0.05
5	Coniferous forest	12	12	30	60	95	95	50	50	0.04	0.05
6	Mixed forest and wet land	14	14	35	70	95	95	40	40	0.05	0.06
7	Water	8	8	100	100	98	98	.0001	.0001	0.06	0.06
8	Marsh or wet land	14	14	50	75	95	95	20	20	0.06	0.06
9	Desert	25	25	2	5	85	85	10	10	0.02	0.02
10	Tundra	15	70	50	90	92	92	10	10	0.05	0.05
11	Permanent ice	55	70	95	95	95	95	5	5	0.05	0.05
12	Tropical or sub tropical forest	12	12	50	50	95	95	50	50	0.05	0.05
13	Savannah	20	20	15	15	92	92	15	15	0.03	0.03

References

Anthes, R. A., 1972:The development of asymmetries in a three-dimensional numerical model of the tropical cyclone. *Mon. Wea. Rev.*, **100**, 461-476.

—, 1977: A cumulus parameterization scheme utilizing a one-dimensional cloud model. *Mon. Wea. Rev.*, **105**, 270-286.

—, and T. T. Warner, 1978: Development of hydrodynamic models suitable for air pollution and other mesometeorological studies. *Mon. Wea. Rev.*,**106**,1045-1078.

—, E.-Y. Hsie, and Y.H. Kuo, 1987: *Description of the Penn State/NCAR Mesoscale Model Version 4 (MM4).* NCAR/TN-282+STR, National Center for Atmospheric Research, Boulder, CO, 66pp.

Arakawa, A., and W. H. Schubert, 1974: Interaction of a cumulus cloud ensemble with the large scale environment. Part I. *J. Atmos. Sci.*, **31**, 674-701.

—, and V. R. Lamb, 1977: Computational design of the basic dynamical process of the UCLA general circulation model. *Methods in Computational Physics*,**17**, 173-265.

Asselin, R., 1972: Frequency filter for time-integrations. *Mon. Wea. Rev.*,**100**, 487-490.

Benjamin, S. G., 1983: Some effects of surface heating and topography on the regional severe storm environment. Ph.D. thesis, Department of Meteorology, The Pennsylvania State University, 265pp.

Blackadar, A. K., 1976: Modeling the nocturnal boundary layer. *Preprints of Third Symposium on Atmospheric Turbulence and Air Quality*, Raleigh, NC, 19-22 October 1976, Amer. Meteor. Soc., Boston, 46-49.

—, 1979: High resolution models of the planetary boundary layer. *Advances in Environmental Science and Engineering*, 1, No. 1. Pfafflin and Ziegler, Eds., Gordon and Briech Sci. Publ., New York, 50-85.

Betts, A. K., 1974: The scientific basis and objectives of the U.S. subprogram for the GATE. *Bull. Amer. Meteor. Soc.*, **55**, 304-313.

Bleck, R., 1977: Numerical simulation of lee cyclogenesis in the Gulf of Genoa. *Mon. Wea. Rev.*, **105**, 428-445.

Bougeault, P., 1983: A non-reflective upper boundary condition for limited-height hydrostatic models. *Mon. Wea. Rev.*, **111**, 420–429.

Brown, J., and K. Campana, 1978: An economical time-differencing system for numerical weather prediction. *Mon. Wea. Rev.*, **106**, 1125-1136.

Carlson, T. N., and F. E. Boland, 1978: Analysis of urban-rural canopy using a surface heat flux/temperature model. *J. Appl. Meteor.*, **17**, 998-1013.

Davies, H. C., and R. E. Turner, 1977: Updating prediction models by dynamical relaxation: An examination of the technique. *Quart. J. Roy. Meteor. Soc.*, **103**,225-245.

Deardorff, J. W., 1972: Parameterization of the planetary boundary layer for use in general circulation models. *Mon. Wea. Rev.*, **100**,93-106.

—, 1978: Efficient prediction of ground surface temperature and moisture, with inclusion of a layer of vegetation. *J. Geophys. Res.*. **83**, 1889-1903.

Delsol, F., K. Miyakoda, and R. H. Clarke, 1971: Parameterized processes in the surface boundary layer of an atmospheric circulation model. *Quart. J. Roy. Meteor. Soc.*, **97**, 181-208.

Dudhia, J., 1989: Numerical study of convection observed during the winter monsoon experiment using a mesoscale two-dimensional model. *J. Atmos. Sci.*, **46**,3077-3107.

—, 1993: A nonhydrostatic version of the Penn State / NCAR mesoscale model: Validation tests and simulation of an Atlantic cyclone and cold front. *Mon. Wea. Rev.*, **121**, 1493–1513.

Durran, D.R., and J.B. Klemp, 1982: On the effects of moisture on the Brunt-Vaisälä frequency. *J. Atmos. Sci.* **39**, 2152–2158.

Fritsch, J. M., and C. F. Chappel, 1980: Numerical prediction of convectively driven

mesoscale pressure systems. Part I: Convective parameterization. *J. Atmos. Sci.*, **37**, 1722-1733.

Garratt, J.R., J.C. Wyngaard and R. J. Francey, 1982: Winds in the atmospheric boundary layer - prediction and observation. *J. Atmos. Sci.*, **39**, 1307-1316.

Grell, G. A., Y.-H. Kuo, and R. Pasch, 1991: Semi-prognostic tests of cumulus parameterization schemes in the middle latitudes. *Mon. Wea. Rev.*, **119**, 5-31.

__, 1993: Prognostic evaluation of assumptions used by cumulus parameterizations.*Mon. Wea. Rev.*, **121**, 764-787.

Haagenson, P.L., J. Dudhia, G. A. Grell, and D. R. Stauffer, 1994: The Penn State / NCAR mesoscale model (MM5) source code documentation. NCAR Technical Note, NCAR/TN-392+STR, 200pp. [Available from NCAR Information Services, P.O. Box 3000, Boulder, CO 80307.]

Hsie, E.-Y., 1984: Simulations of frontogenesis in a moist atmosphere using alternative parameterizations of condensation and precipitation. *J. Atmos. Sci.*, **41**, 2701-2716.

Hoke, J.E. and R.A. Anthes, 1976: The initialization of numerical models by a dynamical initialization technique. *Mon. Wea. Rev.*, **104**, 1551-1556.

Houze, R. A., C.-P. Cheng, C. A. Leary, and J. F. Gamache, 1979: Diagnosis of cloud mass and heat fluxes from radar and synoptic data. *J. Atmos. Sci.*, **37**, 754-773.

Kessler, E., 1969: On the distribution and continuity of water substance in atmospheric circulation. *Meteorol. Mon. Amer. Meteorol. Soc.*, **10**, 84.

Kistler, R.E., 1974: A study of data assimilation techniques in an autobarotropic primitive equation channel model. M.S. thesis, The Pennsylvania State University, 84 pp. [Available from the Dept. of Meteorology, The Pennsylvania State University, University Park, PA 16802]

Klemp, J.B., and D.R. Durran, 1983: An upper boundary condition permitting internal gravity wave radiation in numerical mesoscale models. *Mon. Wea. Rev.*, **111**, 430–

444.

Klemp, J.B., and R.B.Wilhelmson, 1978: Simulations of three-dimensional convective storm dynamics. *J. Atmos. Sci.*, **35**, 1070–1096.

Kuo, H. L., 1965: On formation and intensification of tropical cyclones through latent heat release by cumulus convection. *J. Atmos. Sci.*, **22**, 40-63.

__, 1974: Further studies of the parameterization of the effect of cumulus convection on large scale flow. *J. Atmos. Sci.*, **31**, 1232-1240.

Lord, S., 1978: Development and observational verification of a cumulus cloud parameterization. Ph. D. dissertation, University of California, Los Angeles, 359pp.

__1982: Interaction of a cumulus cloud ensemble with the large scale environment. Part III: Semi-prognostic test of the Arakawa-Schubert parameterization. *J. Atmos. Sci.*, **39**, 88-103.

Madala, R. V., 1981: Finite-Difference Techniques for Vectorized Fluid Dynamics Calculations. Edited by D. L. Book, Springer Verlag, New York.

Marshall, J. S., and W. M. Palmer, 1948: The distribution of raindrops with size. *J. Meteor.*, **5**, 154-166.

Montieth, J. L., 1961: An empirical method for estimating long wave radiation exchanges in the British Isles. *Quart. J. Roy. Meteor. Soc.*, **87**, 171-179.

Perkey, D. J., and C. W. Kreitzberg, 1976: A time-dependent lateral boundary scheme for limited area primitive equation models. *Mon. Wea. Rev.*, **104**, 744-755.

Richtmeyer, R. D., 1957: *Difference methods for Initial-Value Problems.* Interscience, New York, 283pp.

Schubert, W. H., 1974: Cumulus parameterization theory in terms of feedback and control. Atmos. Sci. Pap. No. 226, Colorado State University, 19 pp.

Sekhon, R.S., and R.C. Srivastava, 1970: Snow size spectra and reflectivity. *J. Atmos. Sci.*, **27**, 299–307.

Shapiro, R., 1970: Smoothing, filtering and boundary effects. *Rev. of Geophys. Space Phy.*,8,359-387.

Skamarock, W.C., and J.B. Klemp, 1992: The stability of time-split numerical methods for the hydrostatic and nonhydrostatic elastic equations. *Mon. Wea. Rev.* **120,** 2109–2127.

Smagorinsky, J., S. Manabe, and J. L. Holloway, Jr., 1965: Numerical results from a nine-level general circulation model of the atmosphere, *Mon. Wea. Rev.*, **93**, 727-768.

Smolarkiewicz, P. K., and G. A. Grell, 1992: A class of monotone interpolation schemes. *J. Comp. Phys.*, **101**, 431-440.

Stauffer, D.R. and N.L. Seaman, 1990: Use of four-dimensional data assimilation in a limited-area mesoscale model. Part I: Experiments with synoptic-scale data. *Mon. Wea. Rev.*, **118**, 1250-1277.

__, N.L. Seaman and F.S. Binkowski, 1991: Use of four- dimensional data assimilation in a limited-area mesoscale model. Part II: Effects of data assimilation within the planetary boundary layer. *Mon. Wea. Rev.*, **119**, 734-754.

__, and N.L. Seaman, 1993: On multi-scale four-dimensional data assimilation. *J. Appl. Meteor.*,**32**, accepted for publication.

Zhang, D.-L., and R.A. Anthes, 1982: A high-resolution model of the planetary boundary layer–sensitivity tests and comparisons with SESAME-79 data.*J. Appl. Meteor.*,**21**,1594-1609.

__,H.-R. Chang, N. L. Seaman, T. T. Warner, and J. M. Fritsch, 1986: A two-way interactive nesting procedure with variable terrain resolution. *Mon. Wea. Rev.*, **114**, 1330-1339.